TUMOR, FAT AND SKELETAL MUSCLE CROSSTALK VIA IL-6R TRANS-SIGNALING MEDIATES PANCREATIC CANCER CACHEXIA

Joseph Emil Rupert

Submitted to the faculty of the University Graduate School
in partial fulfillment of the requirements
for the degree
Doctor of Philosophy
in the Department of Biochemistry and Molecular Biology,
Indiana University

October 2020

Accepted by the Graduate Faculty of Indiana University, in partial fulfillment of the requirements for the degree of Doctor of Philosophy.

Doctoral Committee

Teresa A. Zimmers, Ph.D., Chair

Hal E. Broxmeyer, Ph.D.

July 23, 2020

Mark G. Goebl, Ph.D.

Thomas M. O'Connell, Ph.D.

Lawrence A. Quilliam, Ph.D.

DEDICATION

I dedicate my dissertation to my family and friends, especially my father Brian and my mother Colette for their unfaltering support throughout my academic career.

Joseph Emil Rupert

TUMOR, FAT AND SKELETAL MUSCLE CROSSTALK VIA IL-6R TRANS-SIGNALING MEDIATES PANCREATIC CANCER CACHEXIA

Cachexia, the involuntary loss of fat and muscle is associated with pancreatic ductal adenocarcinoma (PDAC), contributing to its 90% 5-year mortality rate. Elevated Interleukin-6 (IL-6) expression is associated with cachexia severity and reduced survival in patients. IL-6 in cancer is well documented, but IL-6 signaling crosstalk among tissues is not. IL-6 signals by binding membrane-bound IL-6 receptor (IL-6R) (classical signaling) or soluble IL-6R (sIL6R; trans-signaling) produced by shedding of the membrane receptor primarily from muscle, liver and leukocytes. Herein I investigate the role of tumor-derived IL-6 on muscle and fat crosstalk in PDAC. Loss of IL-6 expression in murine KPC PDAC cells was accomplished by CRISPR/Cas9 mutagenesis of the *Il6* gene. Orthotopic KPC IL-6 knockout (KPC-IL-6^{KO}) tumor-bearing mice had reduced cachexia, with attenuated fat loss and no significant muscle loss, and longer survival versus KPC controls. Only KPC tumor-bearing mice had significant myosteatosis, aberrant branched chain amino acid and fatty acid metabolism, and reduced pyruvate entry into the TCA-cycle, determined by increased pyruvate dehydrogenase kinase 4 (PDK4) expression in muscle. Muscle was a main source of sIL6R, and fat a primary contributor of IL-6 in KPC tumor-bearing mice. Myosteatosis leads to activation of lipid-sensitive kinases like protein kinase C theta (PKCθ, gene name *Prkcq*) in muscle. KPC tumor-bearing mice had increased muscle PKCθ activation, and PKCθ is known to

regulate metabolism and inflammation. *Prkcq*$^{-/-}$ KPC tumor-bearing mice had reduced cachexia and maintained muscle mass and force production versus wild type tumor-bearing mice. Together these data implicate progressive signaling mechanisms whereby tumor-derived IL-6 is associated with increased muscle IL6R expression and fat lipolysis, promoting myosteatosis and muscle PKCθ activation, ultimately increasing cachexia severity in PDAC.

Teresa A. Zimmers, Ph.D., Chair

TABLE OF CONTENTS

LIST OF TABLES

LIST OF FIGURES

CHAPTER 1: INTRODUCTION

1.1 Cachexia

Cachexia is a multifactorial syndrome characterized by the involuntary loss of adipose and muscle tissues (Fearon et al., 2011). Cachexia is a long-recognized condition with written descriptions of the disease dating to ancient Greece. While some of the most severe cachectic phenotypes occur with cancer, multiple pathologies are associated with cachexia including sepsis, burn injury, polytrauma, HIV/AIDS, and chronic kidney disease (Argiles, Busquets, Stemmler, & Lopez-Soriano, 2015; Cohen, Nathan, & Goldberg, 2015). Notably, while wasting attributed to caloric restriction such as fasting, anorexia, or starvation can be reversed with feeding, dietary interventions are unsuccessful for improving patients with cachexia (Strohle, Zanker, & Hahn, 2010). This inability to be reversed with feeding categorically separates cachexia as an independent condition from other forms of wasting. Furthermore, ongoing investigation has revealed the important roles of inflammation, tissue dysmetabolism, and the central nervous system play in cachexia (Baracos, Martin, Korc, Guttridge, & Fearon, 2018; Burfeind et al., 2018; Pin, Barreto, Couch, Bonetto, & O'Connell, 2019; VanderVeen, Fix, & Carson, 2017). Collectively, these studies elucidate the complexity of cachexia as an intricate network of tissue crosstalk acting in concert to significantly alter multiple biological processes. Of the multiple inflammatory cytokines expressed during cachexia, IL-6 is one of the most well-known for inciting the severity of the disease. However, the effects of tumor-derived versus host-derived IL-6 in cachexia and the nature of its crosstalk

between affected organs remains unclear. Thus, here I investigate cachexia as it pertains to pancreatic ductal adenocarcinoma (PDAC) and aim to determine the effects of tumor-derived IL-6 on inflammation, skeletal muscle and adipose tissue crosstalk via IL-6 signaling, and alterations in skeletal muscle metabolism.

1.2 The IL-6 Signaling Pathway

IL-6 initiates signal transduction by first binding to either the membrane-bound form of the interleukin-6 receptor (IL6R), also known as glycoprotein 80 (GP80), or its soluble form (sIL6R) (Schaper & Rose-John, 2015). While alternative splicing can produce sIL6R, the predominant source of circulating sIL6R appears to be proteolytic cleavage at the membrane from tissues expressing IL6R, resulting in a 55 kDa extracellular fragment (Schaper & Rose-John, 2015). This activity is mediated in part through intracellular accumulation of phorbol esters, diacylglycerol (DAG), and subsequent activation of protein kinase C theta (PKC-θ) (Mullberg, Schooltink, Stoyan, Heinrich, & Rose-John, 1992). Both complexes, IL-6 with membrane IL6R or with sIL6R, bind the ubiquitously expressed co-receptor IL-6 signal transducer (IL6ST), also known as glycoprotein 130 (GP130). The activity elicited by IL-6 and membrane IL6R is termed classical or cis signaling, while activity instigated by IL-6 with sIL6R is known as trans-signaling. Formation of either complex leads to trans-phosphorylation and activation of Janus kinases (JAKs), which phosphorylate the transcription factor Signal Transducer and Activator of Transcription 3 (STAT3), promoting STAT3 dimerization and translocation to the nucleus (Taniguchi &

Karin, 2014), among other pathways. Unlike GP130, IL6R expression is not ubiquitous across cell types; thus, sIL6R trans-signaling allows for IL-6 signaling in IL6R negative cells (Rosean et al., 2014). Signaling through the membrane receptor is largely beneficial, while trans-signaling is generally pathological (Schaper & Rose-John, 2015). A growing number of studies suggest that neutralization of IL6R could have greater utility versus targeting IL-6 directly (Kraakman et al., 2015).

1.3 The Effects of IL-6 Signaling in Skeletal Muscle

Skeletal muscle consists of multinucleated myofibers organized into fascicles, which are surrounded by the perimysium, a connective tissue layer that maintains fascicle structural integrity while also physically joining fascicles together. Dispersed in the extracellular matrix between myofibers are diverse groups of cells that include resident and infiltrating myeloid cells, fibroblasts, and myogenic stem cells termed satellite cells. Healthy muscle generally undergoes little remodeling; however, injured muscle has the capacity to rapidly regenerate (Ciciliot & Schiaffino, 2010; Dueweke, Awan, & Mendias, 2017; Hardy et al., 2016). Muscle regeneration involves the precise coordination of both myofiber degradation (atrophy) and myofiber enlargement (hypertrophy). IL-6 plays a key role in both muscle hypertrophy and atrophy (Bian et al., 2017; Haddad, Zaldivar, Cooper, & Adams, 2005; Madaro et al., 2018; Mitchell et al., 2013; Munoz-Canoves, Scheele, Pedersen, & Serrano, 2013; Rong, Bian, Hu, Ma, & Zhou, 2018; Washington et al., 2011). The concentration of IL-6 and signaling method

(ie, autocrine vs paracrine) produces very different downstream effects. For instance, exercise induces acute elevations in muscle IL-6 production, subsequently increasing plasma IL-6 levels and influencing paracrine signaling by increasing adipose tissue lipolysis; this autocrine IL-6 signaling on muscle is beneficial for muscle hypertrophy and reestablishing metabolic homeostasis after exercise (Ikeda et al., 2016; Knudsen et al., 2017; Peake, Della Gatta, Suzuki, & Nieman, 2015; Pedersen, Steensberg, & Schjerling, 2001). In contrast, chronic, high levels of plasma IL-6 like those observed during inflammation have detrimental effects on muscle and are largely associated with atrophy (Byun, Cho, Chang, Ahn, & Kim, 2017; de Sire et al., 2018; Hu et al., 2019; Passey, Bozinovski, Vlahos, Anderson, & Hansen, 2016; Szychlinska et al., 2019; Zhu et al., 2017).

The pleiotropic effects of IL-6 are likely a result from the different effects of IL-6 signaling within these various cell populations residing within muscle. Particularly IL-6 has different downstream effects in satellite cells versus myofibers. Satellite cells are perhaps the most important muscle cell type since they are crucial for muscle repair, regeneration, and adaptability to exercise (Brack & Rando, 2012; Chang & Rudnicki, 2014; Kuang & Rudnicki, 2008; Shamim, Hawley, & Camera, 2018; Zammit, Partridge, & Yablonka-Reuveni, 2006). Quiescent satellite cells can become activated and reenter the cell cycle to differentiate into myoblasts, which can then further differentiate into myotubes (in vitro) or myofibers (in vivo) (Konigsberg, 1963; Snow, 1977; Yaffe, 1969). Myoblasts isolated from rat, murine and human skeletal muscle have been used

to generate stable myogenic clones for cell culture, with the most well-known being the rat L6 myoblasts, the murine C2C12 myoblasts, and the human HSkM myoblasts (Yaffe & Saxel, 1977). Via a combination of experiments utilizing myoblasts in vitro and murine genetic knockout models in vivo, the myogenic regulatory factors (MRFs) comprised of Myf5, Myod, Mrf4, Myogenin (Molkentin & Olson, 1996; Sabourin & Rudnicki, 2000; Tapscott, 2005) and the family of myocyte enhancer-binding factor 2 (Mef2) proteins consisting of Mef2a, 2b, 2c, and 2d (Black & Olson, 1998; McKinsey, Zhang, & Olson, 2002) were found to be critical transcription factors regulating myogenesis. In satellite cells, transient exposure to low levels of IL-6 activates STAT3, which directly interacts with Myod (Yang et al., 2009) and is associated with increased satellite cell proliferation (K. Wang, Wang, Xiao, Wang, & Wu, 2008) and satellite cell-mediated myofiber repair and myofiber hypertrophy (Cantini et al., 1995; Serrano, Baeza-Raja, Perdiguero, Jardi, & Munoz-Canoves, 2008; Steyn, Dzobo, Smith, & Myburgh, 2019; Tierney et al., 2014; Toth et al., 2011).

Myofiber hypertrophy is regulated in large part by anabolic signaling and activation of the insulin receptor substrate 1 (IRS-1)/phosphatidylinositol-3-kinase (PI3K)/protein kinase B (Akt)/mammalian target of rapamycin (mTOR) protein synthesis pathway, where mTOR activation is a well-known mechanism of protein synthesis (Egerman & Glass, 2014; Laplante & Sabatini, 2013). When activation of Akt is decreased or inhibited, Akt can no longer repress the fork head box O (FOXO) transcription factors, which have important roles in muscle atrophy including activation of the ubiquitin proteasome pathway through

expression of skeletal muscle specific ubiquitin ligases, including Fbxo32/MAFbx/Atrogin-1 and Trim63/MuRF-1 (Milan et al., 2015; Schiaffino, Dyar, Ciciliot, Blaauw, & Sandri, 2013).

As in satellite cells, IL-6 activates the JAK/STAT signaling pathway in mature myotubes and myofibers, where STAT3 is likely the most (Bonetto et al., 2011) studied of the STAT family of transcription factors (Narsale & Carson, 2014; Strassmann, Fong, Kenney, & Jacob, 1992). Neutralization of IL-6 signaling or STAT3 in muscle attenuates muscle atrophy (Bonetto et al., 2012; Cramer et al., 2018; Puppa, Gao, Narsale, & Carson, 2014; Silva et al., 2015; Tang et al., 2012; Verstovsek et al., 2010; C. Wu et al., 2019). More specifically, inhibition of STAT3 in muscle decreased activation of the ubiquitin-proteosome pathway (Silva et al., 2015). Furthermore, activation of STAT3 induces expression of suppressor of cytokine signaling 3 (SOCS3), the negative regulator of IL-6/STAT3 signaling (Carow & Rottenberg, 2014). SOCS3 has binding affinity for IRS-1, which results in repressed function of IRS-1 and decreased activation of the PI3K/Akt/mTOR protein synthesis pathway (Al-Shanti & Stewart, 2012; Yaspelkis, Kvasha, & Figueroa, 2009; L. Zhang et al., 2009; Zolotnik, Figueroa, & Yaspelkis, 2012), providing another mechanism of STAT3 mediated muscle atrophy.

Thus, these findings directly implicate the IL-6/STAT3 signaling pathway in both muscle protein synthesis and protein degradation. It also suggests that targeting IL-6 signaling in specific cell niches within tissues may be more effective than neutralizing IL-6 in circulation in the treatment of muscle wasting.

1.4 The Effects of IL-6 Signaling in Adipose Tissue

In addition to muscle, fat is a highly metabolic tissue and a primary source of IL-6 during systemic inflammation (Sindhu et al., 2015). The role of fat as an energy storage depot via the storage of triacylglycerol is crucial during times of nutrient deprivation and intense exercise. However, mechanisms governing hydrolysis of triacylglycerol, commonly referred to as lipolysis, can become abnormal during pathological conditions, such as observed in diabetes, obesity, and cancer. The relationship between IL-6 and adipose tissue has been investigated in detail and stoutly implicates IL-6 signaling, particularly adipocyte-derived IL-6, as a driver of inflammation and lipolysis (M. S. Han et al., 2020).

Lipolysis can occur through multiple signaling pathways culminating in the activation of the lipolytic enzymes hormone sensitive lipase (HSL) and adipose triglyceride lipase (ATGL), concomitantly with the phosphorylation of perilipin. Phosphorylation of perilipin causes its dissociation from the lipid droplet surface allowing activated HSL and ATGL access to TG stores and the subsequent breakdown of TG into fatty acids and glycerol (Zechner et al., 2012). In concert with muscle, IL-6 activates STAT3 in fat, which has been linked to increased lipolysis (Pendharkar, Singh, & Petrov, 2018; S. Sun et al., 2017) and reduced expression of the pro-adipogenic transcription factors proliferator-activated receptor gamma (PPARγ) and CCAAT/enhancer-binding protein alpha (C/EBPα) in adipocytes (Almuraikhy et al., 2016; Cortez, Carmo, Rogero, Borelli, & Fock, 2013). Chronic lipolysis increases plasma fatty acids, which profoundly affects systemic tissue metabolism. Skeletal muscle is categorically affected by elevated

plasma fatty acids, which causes excessive lipid accumulation known as myosteatosis. Myosteatosis is associated with insulin resistance and dysmetabolism in muscle. Therefore, it is necessary to consider role of IL-6 mediated lipolysis when investigating muscle wasting and altered metabolism in cachexia.

1.5 Muscle Metabolism

Atrophy and hypertrophy increase the energy demand of muscle since both processes rely on the use of adenosine triphosphate (ATP). Muscle can use both glucose and fatty acids to generate ATP. The generation of ATP in muscle can occur using either aerobic or anaerobic respiration and the amount of ATP generated between the two types of respiration differs greatly. Aerobic respiration metabolizes glucose into pyruvate via glycolysis and pyruvate is then oxidized by the pyruvate dehydrogenase complex (PDH) to form acetyl-CoA, which is used to begin the tricarboxylic acid (TCA) cycle generating NADH and $FADH_2$ to fuel the electron transport chain (ETC) and generate 36 ATP molecules. In contrast, anaerobic respiration generates 2 ATP and 2 NADH molecules during glycolysis and NADH then protonates pyruvate to form lactic acid and NAD+, where NAD+ is again protonated to NADH during glycolysis to continue anaerobic respiration.

Muscle metabolism differs among fiber type isoforms. There are numerous such isoforms, however the most common in skeletal muscle are Type I, IIa, IIx and IIb in rodents and Type I, IIa and IIx in humans (Sciote & Rowlerson, 1998; Toniolo et al., 2005). Type I fibers have a slower shortening velocity and

predominantly generate ATP through aerobic respiration, while Type II fibers have a more rapid shortening velocity and generate ATP through anaerobic respiration (Schiaffino & Reggiani, 2011; Sciote & Rowlerson, 1998; Toniolo et al., 2005). Fibers can also use a combination of aerobic and anaerobic respiration such as observed in the Type IIa and IIx fibers, both of which have capacities for aerobic respiration (Schiaffino & Reggiani, 2011; M. Y. Zhang, Zhang, & Medler, 2010). Because Type I fibers contract more slowly and usually have smaller fiber cross-sectional areas (CSA) compared to Type II fibers, Type I fibers generate less force production than the faster and larger Type II fibers (Schiaffino & Reggiani, 2011).

Glucose uptake into myofibers for use in glycolysis requires the presence of glucose transporters (GLUT) within the plasma membrane. There are more than twelve GLUT transporters and GLUT4 is the most expressed isoform at the muscle membrane after insulin stimulation (Navale & Paranjape, 2016). Insulin signaling directly regulates glucose uptake in muscle. Insulin binds the alpha-subunit on the insulin receptor (IR), which induces autophosphorylation of the IR beta-subunit and promotes downstream phosphorylation and activation of insulin receptor substrates (IRS) (Eckstein, Weigert, & Lehmann, 2017). IRS-1 is the predominant isoform in muscle and activation of IRS-1 leads to downstream activation of the PI3K/Akt/mTOR pathway, where Akt phosphorylates and activates downstream substrates important for the trafficking of GLUT4 to the plasma membrane (Guo et al., 2019). Thus, intact insulin signaling in muscle is important for both regulation of muscle hypertrophy and glycolysis.

During hypoglycemia and depletion of muscle glycogen stores, muscle can use fatty acids as a fuel source (Margolis et al., 2019). Fatty acids can be directly taken up by myofibers through fatty acid transporters or generated from lipid stores within muscle from TAG hydrolysis (Shang et al., 2019; Turcotte et al., 2000). Fatty acid oxidation (FAO) in muscle can occur through various mechanisms, but beta-oxidation occurring within the mitochondria is perhaps the most common. Beta-oxidation of FA is the breakdown of longer FA into fatty acyls containing two carbons (acetate), which is then combined with co-enzyme A (CoA) to form acetyl-CoA. Acetyl-CoA can then be used in the TCA cycle, to generate intermediates for use in the ETC and generation of ATP as described previously. Furthermore, to prioritize FAO, pyruvate entry into the TCA cycle for oxidation is slowed or halted by activation of pyruvate dehydrogenase kinase (PDK), which inhibits the function of PDH (Harris, Bowker-Kinley, Huang, & Wu, 2002). In muscle, PDK4 is the predominate isoform and is transcriptionally regulated by FOXO1 (Bowker-Kinley, Davis, Wu, Harris, & Popov, 1998; Furuyama, Kitayama, Yamashita, & Mori, 2003). This regulation relates impaired insulin signaling or reduced glucose availability with decreased activation of Akt and subsequent de-repression of FOXO1 and downstream activation of PDK4. Thus, creating a link between impaired glucose metabolism and increased reliance on FAO while also activating key regulators important in muscle wasting.

1.6 Myosteatosis and Bioactive Lipid Signaling in Muscle

When presented with chronically high levels of plasma FA, muscle can increase FA uptake and oxidation. However, if FA uptake outpaces FAO then muscle accumulates triacylglycerol in the form of lipid droplets, which can become pathological and known as myosteatosis. Myosteatosis is not a novel research question per se; however, our understanding of the specific mechanisms and downstream effects of myosteatosis on muscle size and metabolism is lacking. Myosteatosis is reported in multiple chronic inflammatory diseases and may be a suitable target for restoring muscle size and metabolism homeostasis.

Muscle commonly acquires plasma fatty acids during non-pathological conditions like exercise and fasting, which results in acute increases in muscle lipid followed shortly by their oxidation and clearance from the muscle (Daemen, van Polanen, & Hesselink, 2018; Dotzert et al., 2018). However, during chronic inflammation and lipid mobilization from fat stores, lipid accumulation surpasses lipid oxidation in muscle and results in synthesis and storage of triacylglycerol (TAG) in muscle (Daemen et al., 2018). Myosteatosis negatively impacts muscle in a number of ways. First, it alters muscle metabolic homeostasis by increasing insulin resistance and reactive oxygen species (ROS) due to increased endoplasmic reticulum (ER) and mitochondrial stress (J. Han & Kaufman, 2016; Jung et al., 2018; Morales, Bucarey, & Espinosa, 2017; Y. Wang et al., 2019). Next, this aberrant metabolism inhibits anabolic pathways such as the PI3K/Akt/mTOR pathway while also activating the ubiquitin proteosome pathway,

resulting in muscle atrophy (Fukawa et al., 2016; Pellegrinelli et al., 2015; Woodworth-Hobbs et al., 2017).

Myosteatosis-induced insulin resistance largely occurs from activation of lipid sensitive signaling molecules as a result of the increased accumulation of bioactive lipids. Diacylglycerols (DAG) are among the most characterized bioactive lipids. DAGs are commonly synthesized in healthy muscle and are essential for plasma membrane formation, signaling pathways and energy storage (Massart & Zierath, 2019). DAGs are comprised of two fatty acid chains bonded to a glycerol backbone and can be generated at multiple subcellular compartments including the ER, Golgi apparatus, lipid droplets and the plasma membrane. Generation of DAGs can be both catabolic and anabolic, occurring during the hydrolysis of TAG as well as *de novo* synthesis of TAG using fatty acids, acyltransferases and phosphohydrolases. DAGs plays a crucial role in inflammatory and metabolic diseases through their interactions with downstream signaling mediators, especially the protein kinase C (PKC) family of kinases (Massart & Zierath, 2019).

PKC activation is important in a variety of biological functions including T-cell activation (Altman, Isakov, & Baier, 2000; Isakov & Altman, 1987), cell cycle and differentiation (Carter et al., 2013; Nitti et al., 2010; Poli et al., 2018; Ye et al., 2019), cell survival (Cardoso et al., 2018; L. Liu et al., 2018; J. Zhang et al., 2018), inflammation (Ali & Sarna, 2002; Xu et al., 2010; J. Yang et al., 2013), and metabolism (Greene et al., 2014; Kim et al., 2004; Mayr et al., 2004; Ramzy et al., 2006; Tsuru et al., 2002). Activated PKC isozymes, especially DAG sensitive

cPKCs and nPKCs, have a well-documented role in inflammation, insulin resistance, and alterations in tissue metabolism homeostasis, implicating this family of kinases as an important signaling node in myosteatosis-induced muscle wasting and dysmetabolism.

Yasutomi Nishizuka family of serine/threonine kinases within bovine and rat brain in 1979(Kishimoto, Kajikawa, Shiota, & Nishizuka, 1983; Takai et al., 1979) . There are now multiple PKC isozymes categorized into three subfamilies, conventional (cPKC) including PKCα, β_I, β_{II} and γ, novel (nPKC) including PKCδ, ε, η, and θ, and atypical (aPKC) including PKCι and ζ (Lipp & Reither, 2011; Marrocco et al., 2019). Each PKC isozyme contains a C-terminal catalytic kinase region and a N-terminal regulatory region joined by a middle hinge region. Activation of PKC requires three specific phosphorylation events within the C-terminus of the kinase. The first phosphorylation event occurs at a threonine residue located within the activation loop and is trans-phosphorylated by phosphoinositide-dependent protein kinase-1 (Pdk1) causing the kinase to become catalytically competent (Dutil, Toker, & Newton, 1998; Y. Liu, Graham, Li, Fisher, & Shaw, 2002). Next, two autophosphorylation events occur within the C-terminus, one at a threonine residue acting to further stabilize the catalytically active kinase (Newton, 1995) and the second at a serine residue, which promotes the release of the mature PKC into the cytosol (Newton, 1995). The specific positions of the residues to be phosphorylated are isozyme dependent. Interestingly, phosphorylated cytosolic PKC maintains a pseudo-substrate in its catalytic region preventing it from phosphorylating downstream substrates.

Phosphorylated PKC must be trans located to the plasma membrane and anchored there by phosphatidylserine for removal of the pseudo-substrate, a process that is regulated in cPKCs and nPKCs by the secondary messengers calcium (Ca^{2+}) and diacylglycerol (DAG). Translocation regulation in the aPKCs remains less understood but likely occurs through interaction with the phosphoinositide-3 kinase (PI3K) pathway(Farese, Sajan, & Standaert, 2005)□. Within the regulatory domain, the cPKC and nPKC subfamilies contain two C1 domains (C1A and C1B) critical for DAG binding and one C2 domain important for Ca^{2+} binding (Evans, Murray, Leslie, & Falke, 2006; Farah & Sossin, 2012; Nalefski & Falke, 1996; Sutton, Davletov, Berghuis, Sudhof, & Sprang, 1995; G. Zhang, Kazanietz, Blumberg, & Hurley, 1995). In cPKCs, the C1 domain (DAG binding) precedes the C2 domain (Ca^{2+} binding) making this subfamily sensitive to both Ca^{2+} and DAG. Translocation occurs through the binding of calcium with the C2 domain, increasing the affinity of the C2 domain for phosphatidylserine, while accumulation of DAG at the plasma membrane binds with the C1 domain (Ayo, Radnik, Garoni, Troyer, & Kreisberg, 1991; Huang, 1989). In nPKCs, the C1 domain is insensitive to Ca^{2+} and follows the C2 domain in the structural order within the regulatory region. While insensitive to calcium, the C1 domain of nPKCs is thought to possess a basal affinity for phosphatidylserine through alterations in domain structure (Nalefski & Falke, 1996), making nPKC translocation to the plasma membrane only sensitive to DAG (Bell & Burns, 1991; Konno, Ohno, Akita, Kawasaki, & Suzuki, 1989; Mellor & Parker, 1998; Newton, 2001; Nishizuka, 1992; Ron & Kazanietz, 1999). The aPKCs lack a C2

domain and contain a DAG insensitive C1 domain, which has an affinity for ceramides and downstream products of the PI3K pathway such as phosphatidylinositol (3,4,5)-triphosphate promoting its translocation to the plasma membrane (Sanchez, De Carcer, Sandoval, Moscat, & Diaz-Meco, 1998). Once positioned on the cytosolic side of the plasma membrane, the conformation of the activated kinase allows for degradation of the pseudo-substrate and PKC is able to phosphorylate downstream targets.

1.7 Pancreatic Ductal Adenocarcinoma-Associated Cachexia and IL-6

Pancreatic ductal adenocarcinoma (PDAC) is one of the deadliest cancers with a five-year mortality rate of >91% (Siegel, Miller, & Jemal, 2019). Cachexia affects over 80% of patients with PDAC and leads to increased morbidity and mortality (Hendifar et al., 2018; L. Sun, Quan, & Yu, 2015; von Haehling, Anker, & Anker, 2016). Both cancer and cachexia are associated with systemic inflammation affecting multiple organ systems (Argiles, Stemmler, Lopez-Soriano, & Busquets, 2018; Onesti & Guttridge, 2014). While various cytokines, chemokines, and growth factors are changed in PDAC, Interleukin-6 (IL-6) specifically has been positively correlated with PDAC presence (Holmer, Goumas, Waetzig, Rose-John, & Kalthoff, 2014), disease progression (Ramsey et al., 2019), mortality (Babic et al., 2018; Suh et al., 2013), and cachexia (Okada et al., 1998) (Ebrahimi, Tucker, Li, Abbruzzese, & Kurzrock, 2004) (Martignoni et al., 2005). Although circulating IL-6 levels are not always detectable in early PDAC nor always correlated with cachexia severity (Ramsey et al., 2019; Talbert

et al., 2018), higher tumor staining for IL-6 is associated with PDAC cachexia (Martignoni et al., 2005) and induction of monocyte IL-6 is predictive of survival in PDAC (Moses, Maingay, Sangster, Fearon, & Ross, 2009), suggesting that the serum levels of this short-lived cytokine might not be an inappropriate measure of tissue activity. Functional data also support a role for IL-6 in PDAC tumor development (Lesina et al., 2011), progression (Y. Zhang et al., 2013), metastasis (Razidlo, Burton, & McNiven, 2018), anti-tumor immunity (Flint et al., 2016), and response to chemotherapy (Long et al., 2017). IL-6 levels are high in PDAC models with weight loss (Flint et al., 2016) and IL-6 is also functionally linked to cachexia in murine C26 colon adenocarcinoma and other models of cancer cachexia (Baltgalvis et al., 2008; Bonetto et al., 2012; Bonetto et al., 2011; Narsale & Carson, 2014). Moreover, IL-6 is sufficient to induce cachexia in mice (Baltgalvis et al., 2009; J. L. Chen et al., 2016; Tsujinaka et al., 1996) as well as lipolysis and atrophy in cultured adipocytes (Trujillo et al., 2004) and myotubes (Bonetto et al., 2012), respectively.

CHAPTER 2: TUMOR, SKELETAL MUSCLE AND ADIPOSE TISSUE CROSSTALK IN PDAC

2.1 Overview

Given its various roles in PDAC, lipolysis and muscle wasting, here I investigated the effects of IL-6 emanating from PDAC tumor cells on tissue crosstalk and cachexia using isolated mouse PDAC cells deleted for IL-6 (KPC IL-6^{KO}) in a mouse model of pancreatic cancer cachexia. Furthermore, I used this approach to characterize fat and muscle crosstalk via IL-6 signaling and myosteatosis in pancreatic cancer cachexia. Specifically, I evaluate the effects of tumor cell-derived IL-6 on muscle atrophy in vitro by treating C2C12 myotubes with KPC and KPC IL-6^{KO} cell conditioned media and in vivo, using orthotopic implantation of KPC and KPC IL-6^{KO} cells. I also report changes to global gene expression in skeletal muscle and adipose tissue associated with deletion of tumor-derived IL-6 using RNA-sequencing. Furthermore, I determined skeletal muscle to be the primary contributor of sIL6R in plasma and adipose tissue as the primary contributor of circulating IL-6. I also observed significant myosteatosis only in KPC tumor-bearing mice suggesting a potential role for tumor IL-6 and dysmetabolism in muscle. Collectively, my results suggest a feed-forward signaling loop between tumor-derived IL-6, myosteatosis and muscle sIL6R trans-signaling with adipose tissue IL-6 production working in concert to exacerbate dysmetabolism and atrophy in skeletal muscle in PDAC.

2.2 Materials and Methods

A detailed list of cell lines, mouse strains, equipment and reagents is provided in Table 2.1

2.2.1 Immunohistochemistry (IHC) Performed on Human and Mouse Tumors

Formalin-fixed human pancreatic ductal adenocarcinoma (PDAC) tumor arrays were obtained from US Biomax (PA1001a, Rockville, MD, USA) and consisted of 100 core samples from 50 patients. Twenty-eight core samples consisting of normal pancreas tissue or tumor samples having no reactivity for IL-6 were excluded. The final sample population was made up of 72 core samples and included 21 males and 15 females ranging in age from 40-78 years of age. Tumor samples varied in stage from IB (maximum tumor diameter greater than four centimeters) to IV (metastases in four or more regional lymphnodes) as defined by the 8th edition of AJCC cancer staging manual. Sections were deparaffinized with xylenes and rehydrated using deionized water (dH_2O). Antigen retrieval was performed by incubating the sections in a sodium citrate buffer (10 mM sodium citrate, 0.05% Tween 20, pH 6.0) at 95° C for 10 minutes and allowing them to cool to room temperature for 30 minutes. Sections were washed using dH_2O and endogenous peroxidase was quenched using 3% hydrogen peroxide (S25360, Thermo Fisher; Waltham, MA, USA). Sections incubated with blocking buffer which was comprised of 8% FBS (SH3007103HI, Thermo Fisher; Waltham, MA USA) in PBS (21040CV, Corning; Corning, NY, USA) for one hour and incubated overnight in a humid chamber at 4° C with an

anti-IL-6 monoclonal antibody (mAb) (ab6672, Abcam; Cambridge, MA, USA) diluted 1:400 in blocking buffer. Detection and visualization of the anti-IL-6 mAb was done using ImmPACT DAB Peroxidase (HRP) Substrate kit from Vector Laboratories (SK-4105, Burlingame, CA, USA). Sections were counter stained with hematoxylin for one minute, dehydrated and cleared using sequential incubations (3 minutes each) of dH_2O, 70% ethanol, 95% ethanol, 100% xylenes and then cover slips applied.

2.2.2 In Vitro Cell Culture

C2C12 mouse myoblasts were purchased from ATCC (CRL-1772; Manassas, VA, USA). 3T3 fibroblasts were purchased from Zen Bio (SP-LF-1, Zen Bio; Research Triangle Park, NC, USA). KPC tumor cells were a gift from Dr. David Tuveson, who isolated them from a pancreatic tumor from a male LSL-**K**rasG12D: LSL-Tr**p**53R172H:Pdx1-**C**re (KPC) mouse on a C57BL/6 background (Hingorani et al., 2005) and we used these cells to generate the KPC IL-6^{KO} cells (RRID: CVCL_UR56).

2.2.3 C2C12 Mouse Myoblast Cell culture and Differentiation into Myotubes

Frozen murine C2C12 myoblasts (2 X 10^6 cells) were thawed in a 37°C water bath and then seeded in flasks (130191, Thermo Scientific; Waltham, MA, USA) containing 20 mL of growth media (GM), which consisted of DMEM base media (10013CV, Corning; Corning, NY, USA), 10% fetal bovine serum (FBS) (SH30071.03, GE Healthcare Life Sciences; Pittsburgh, PA, USA) and 0.1%

penicillin and streptomycin (15140122, ThermoFisher Scientific, Waltham, MA, USA;) and maintained in a humidified incubator at 37°C with 5% CO_2 until 70% confluent (~2 days). The GM was aspirated, the cells were washed with PBS and adherent cells dislodged using 3 mL of 0.25% trypsin (25053CL, Corning; Corning, NY, USA). Cells were then seeded 0.3 X 10^6 cells per well in 6-well plates (140685, Thermo Scientific; Waltham, MA, USA) with growth media (GM) and maintained at 37°C with 5% CO_2 until 90% confluent. The GM was then aspirated, cells were washed with PBS and 2 mL per well of differentiation media (DM) consisting of DMEM base media (10013CV, Corning; Corning, NY, USA), 2% horse serum (26050-088, Life Technologies; Carlsbad, CA, USA) and 0.1% penicillin and streptomycin (15140122, Gibco; Dublin, Ireland) was added and cells maintained at 37°C with 5% CO_2. The DM was replaced every 48 hours and C2C12 myoblasts were fully differentiated into myotubes after 5-6 days in DM.

2.2.4 3T3 Fibroblast Cell Culture and Differentiation into 3T3 Adipocytes

Frozen 3T3 fibroblasts (0.5 X 10^6) were thawed and seeded in flasks with preadipocyte media (PM-1-L1, Zen Bio; Research Triangle Park, NC, USA) at 37°C with 5% CO_2 in a humidified incubator until 70% confluent. Adherent cells were then dislodged using 0.25% trypsin and seeded 0.3 X 10^6 cells per well in six well plates with preadipocyte media and placed in the incubator. Cells were allowed to become 100% confluent, at which time cells were maintained at 100% confluence in preadipocyte media for an additional 48 hours to ensure growth arrest, refreshing the preadipocyte media every 48 hours. Cells were then

washed with PBS and differentiation media (DM-2-L1, Zen Bio; Research Triangle Park, NC, USA) was added to the wells and cells placed back into the incubator. Cells were cultured for three days in differentiation media. Cells were then washed with PBS and adipocyte maintenance media (AM-1-L1, Zen Bio; Research Triangle Park, NC, USA) was added to the wells and cells placed back into the incubator. Cells were cultured in maintenance media for ten days refreshing the maintenance media every 48 hours. At ten days, fully differentiated 3T3 adipocytes were produced.

2.2.5 Generation of KPC and KPC IL-6^{KO} Tumor Cell Lines

Frozen KPC cells were thawed and cultured flasks with GM as described for C2C12 myoblasts. When cells reached 70% confluence adherent cells were removed using trypsin (per C2C12 methods) and plated 0.3 X 10^6 cells per well in two separate 6-well plates. Once cells were 70% confluent, Lipofectamine 3000 (L3000008, Invitrogen; Carlsbad, CA, USA) was used to transfect one plate of KPC cells with a CRISPR/Cas9 non-targeting pCMV-Cas9-GFP (CRISPR06-1EA, Sigma Aldrich; St. Louis, MO, USA) as a control. The additional plate was transfected with a CRISPR/Cas9 U6-gRNA:CMV-eCas9-2a-tRFP plasmid (MM0000468506, Sigma Aldrich; St. Louis, MO, USA) targeting the *mll6* gene. Cells were incubated for 48 hours with the lipofectamine and CRISPR plasmids. Cells were removed from the wells using trypsin and sorted one GFP-positive cell (control) or one RFP-positive cell (IL-6^{KO}) per well into separate 96-well plates (167008, Thermo Fisher; Waltham, MA, USA) using fluorescence-activated cell

sorting (FACS). One 96-well plate contained cells transfected with the non-targeting control plasmid and the other plate contained cells transfected with the plasmid targeting *Il6*. Single cell cultures were maintained in GM and expanded into colonies over ~4 weeks. Colonies transfected with the plasmid targeting *mIl6* were screened for loss of *Il6* mRNA expression using RT-PCR. The selected clone with loss of *Il6* mRNA expression was designated KPC IL-6^{KO}. Colonies transfected with the non-targeting control plasmid were screened using RT-PCR for *Il6* mRNA expression similar to that of the non-transfected parental cell line (KPC-P) and the control clone selected was designated KPC.

2.2.6 Proliferation Assay of KPC Cells

Comparison of *in vitro* proliferation between non-transfected KPC cells (KPC-P), KPC cells transfected with a null CRISPR/Cas9 plasmid (KPC) and the mutant KPC IL-6^{KO} cells was performed using the xCELLigence Real-Time Cell Analysis (RTCA) assay (ACEA Biosciences; San Diego, CA). Cells were plated in GM at 2,000 cells per well in triplicate in an Eplate 16 (ACEA Biosciences; San Diego, CA). Cell growth was measured each hour for 100 hours.

2.2.7 In Vivo Mouse Experiments

Experiments that included mice were approved by and performed in accordance with the Indiana University School of Medicine Institutional Animal Care and Use Committee. Seven-week-old male C57BL/6J mice (000664, Jackson Laboratory; Bar Harbor, Maine, USA) mice were group-housed in a

barrier facility with ad libitum access to autoclaved food (Envigo: Huntingdon, Cambridgeshire, United Kingdom), sterile water, maintained on a 12hr light/dark cycle and allowed to acclimate to the facility for one week.

2.2.8 Orthotopic Implantation of KPC and KPC IL-6^{KO} Cells into Mice

Eight-week-old, male C57BL/6J mice were anesthetized using 4% isoflurane in an induction chamber within a biosafety cabinet. Mice were subcutaneously injected with buprenorphine (4202317005, PAR Pharmaceuticals; Chestnut Ridge, NY, USA) at 0.5 mg/kg in 0.1 mL sterile PBS prior to surgery and then every 12 hours from the first injection for 48 hours.

The abdomen was shaved, and mice were placed in lateral recumbency with the right side against a heated surgical platform and the left side facing upward. From this point forward aseptic technique was maintained. A sterile drape was placed over the abdomen and a hole cut in the drape to reveal the abdominal skin. The skin was prepped using three alternating scrubs of Betadine (6761815117, Purdue Products; Stamford, CT, USA) and 100% isopropanol. An incision (~1 cm) was made through both skin and muscle into the left middle quadrant of the abdomen directly above the spleen using scissors. The pancreas was retracted using ring tip forceps by gripping the spleen (which is loosely connected with the pancreas) and retracting both the spleen and pancreas onto the sterile drape. The pancreas was injected with 5 x 10^4 KPC or KPC IL-6^{KO} cells in 50μl GM of cells using a 1 mL syringe with a 26G needle (329652, Becton, Dickinson and Co.; Franklin Lakes, NJ, USA) over a period of thirty

seconds. The spleen and accompanying pancreas were gently laid back into the abdominal cavity using the ring tip forceps. The incision was closed by suturing the abdominal wall musculature using absorbable 4.0-vicryl suture (33227, Butler Schein Animal Health; Dublin, OH, USA) and the skin flap closed using stainless steel wound clips (500346, World Precision Instruments; Sarasota, FL, USA).

2.2.9 Euthanasia and Tissue Excision from Animal Models

All mice were euthanized when any group exhibited average body weight loss >10% or total fat mass <5% via EchoMRI. Euthanasia under general anesthesia (4% isoflurane) was done by exsanguination via cardiac puncture followed by cervical dislocation. Prior to euthanasia, blood was collected in EDTA tubes (366643, Becton, Dickinson and Co.; Franklin Lakes, NJ, USA) via cardiac puncture after anesthetizing the mice. The plasma was separated using centrifugation of the blood at 3,500 rpm at 4°C and stored at -80°C. Immediately following euthanasia tissues were excised and weighed. Sections of tissues were either placed into 2 mL cryogenic storage vials (82050-208, VWR; Radnor, PA, USA) and snap frozen in liquid nitrogen. Additionally, sections of tumor were placed into tubes containing 10% neutral buffered formalin (NBF) and sections of epididymal fat were placed into tubes containing Bouin's solution 23-005-69, Thermo Fisher; Waltham, MA USA) for 24 hours. Fixed tumor and fat tissues were washed twice with PBS and transferred to new tubes containing 70% ethanol and stored at 4°C. Sections of the quadriceps muscle were mounted to cork discs, keeping the muscle fascicles perpendicular to the disc, by using

Tissue plus O.C.T. compound (23-730-571, Thermo Healthcare; Waltham, MA USA). The muscle blocks were snap frozen by submerging the mounted muscle for 45 seconds in isopentane (2-methylbutane) (03551-4, Fisher Chemical; Waltham, MA USA) cooled to -150°C in a bath of liquid nitrogen and then stored at -80°C.

2.2.10 RNA Isolation, Library Preparation, Sequencing and Quantitative PCR (qPCR)

RNA was isolated from ~50 mg of snap frozen tissue or from cells cultured in 6-well plates via the miRNeasy Mini Kit (217004, Qiagen; Fredrick, MD USA). The concentration and quality of total RNA samples was first assessed using Agilent 2100 Bioanalyzer. A RIN (RNA Integrity Number) of six or higher was required to pass the quality control. Isolated RNA from quadriceps and epididymal fat pads was taken from four animals per group (i.e. No tumor, KPC tumor and KPC IL-6^{KO} tumor mice) and subjected to next generation sequencing. For adipose tissue, 500 nanograms (ng) of RNA per sample were used to prepare dual-indexed strand-specific cDNA library using TruSeq Stranded mRNA Library Prep Kit (Illumina; San Diego, CA, USA). For skeletal muscle, 100 ng of RNA per sample were used to prepare single-indexed strand specific cDNA library using TruSeq Nano DNA Library Prep kit.

The resulting libraries were assessed for quantity and size distribution using a Qubit and Agilent 2100 Bioanalyzer. 200 picomolar pooled RNA libraries were utilized per flow cell for clustering amplification on cBot using HiSeq

3000/4000 PE Cluster Kit and sequenced with 2×75bp paired-end configuration on HiSeq4000 (Illumina; San Diego, CA, USA) using the HiSeq 3000/4000 PE SBS Kit. A Phred quality score (Q score) was used to measure the quality of sequencing. More than 95% of the sequencing reads reached Q30 (99.9% base call accuracy) for both muscle and adipose tissues.

The sequencing data were first assessed using FastQC (Babraham Bioinformatics, Cambridge, UK) and then all sequenced libraries were mapped to the mm10 mouse genome using STAR RNA-seq aligner (Dobin et al., 2013). Uniquely mapped sequencing reads were assigned to mm10 UCSC reference genome. The data were normalized using the TMM (trimmed mean of M values) method. One muscle sample from the No Tumor group was identified as an outlier and removed from further analyses. Differential expression analysis was performed using edgeR (McCarthy, Chen, & Smyth, 2012; Robinson, McCarthy, & Smyth, 2010) and the false discovery rate (FDR) was computed from p-values using the Benjamini-Hochberg procedure. Differentially expressed genes were determined as having a fold change of ≥1.5 and an FDR of ≤ 0.05. Ingenuity Pathway Analysis (Qiagen; Fredrick, MD USA) was used for secondary analysis of RNA sequencing results. Data are deposited into GEO Datasets under series record GSE123310.

For qPCR analyses, 100 ng of isolated RNA was reverse transcribed into cDNA using the VERSO cDNA Synthesis Kit (AB1453B, Thermo Fisher; Waltham, MA USA). Taqman Universal Master Mix II (4440038, Thermo Fisher; Waltham, MA, USA) and gene specific Taqman probes (see Table 2.1) were

used to measure gene expression using cDNA in Light Cycler 480 96-well plates (04729692001, Roche; Indianapolis, IN, USA) on a Light Cycler 96 (Roche; Indianapolis, IN USA). For each sample, TATA binding protein (*Tbp)* gene expression was used to normalize the expression of the target gene. Each well contained one PCR reaction and reactions for each sample of cDNA were performed in triplicate for both target and control genes. Results from qPCR analyses were analyzed using the $2^{-\Delta\Delta CT}$ method and reported as fold change.

2.2.11 Western Blotting

Tissue protein lysates were made by homogenizing snap frozen tissue in ice cold RIPA buffer (Harlow & Lane, 2006) using a Polytron PT 10/35 homogenizer with PCU 11 controller (Kinematica; Luzern, Switzerland). Protein lysate concentration was measured using the Pierce™ BCA Protein Assay Kit (PI23228, Thermo Scientific; Waltham, MA USA). Protein lysate was then added 1:1 to 2X sample buffer (125 mM Tris; pH 6.8, 4% (w/v) SDS, 20% glycerol, 100 mM DTT, 0.02% (w/v) bromophenol blue) and heated at 95˚C for five minutes. Proteins were then separated via SDS-PAGE by loading 30 μg of protein from each sample into wells on a 4-15% Criterion™ TGX™ gel (5671084, Bio-Rad; Hercules, CA, USA) in running buffer (25 mM Tris, 192 mM glycine, 0.1% SDS) at 140 volts for one hour using a Power Pac HC (Bio-Rad; Hercules, CA, USA). The proteins were transferred to 0.2μm nitrocellulose membranes (1620233, Bio-Rad; Hercules, CA, USA) in ice-cold transfer buffer (25 mM Tris, 192 mM glycine, 20% (v/v) methanol, pH 8.3) at 100 volts for thirty minutes. Membranes were

blocked using Sea Block (37527, Thermo Scientific; Waltham, MA USA) for one hour at room temperature on a shaker table. Proteins were detected using antigen specific primary antibodies (see Table 2.1) diluted in Sea block with 0.1% Tween 20 (BP337-500, Fisher Scientific; Waltham, MA USA) and incubated with the membranes overnight at 4°C. Membranes were then washed twice with PBS and primary antibodies were visualized using florescent DyLight™ secondary antibodies (Cell Signaling; Danvers, MA, USA) with specificity against the primary antibodies and imaged on an Odyssey CLx (LiCor; Lincoln, NE, USA). The quantification of target proteins was done by normalizing target protein expression to the loading control protein expression (α tubulin for muscle, β-actin for adipose tissue) specific to each membrane using Image Studio version 4.0 (LiCor; Lincoln, NE, USA). Normalized protein expression was then presented as fold-change versus no tumor bearing mice.

2.2.12 Muscle Histology

For Oil Red O (ORO) staining, succinate dehydrogenase (SDH) reaction and IF performed on muscle, snap frozen mounted muscle blocks were serial sectioned (10 µm thickness) at -20˚C on a Leica CM1860 cryostat (Buffalo Grove, IL, USA) and muscle cross-sections mounted to Superfrost Plus microscope slides (12-550-15, Thermo Scientific; Waltham, MA USA).

2.2.13 Oil Red O Staining

ORO staining solution was prepared by dissolving 0.7 g of ORO (00625-25G, Sigma Aldrich; St. Louis, MO, USA) with 100 mL of 100% propylene glycol (398039, Sigma Aldrich; St. Louis, MO, USA) for five minutes at 100˚C. The ORO staining was then maintained at 60˚C until needed. Muscle cross-sections were post fixed in 10% NBF for 10 minutes at room temperature. Sections were washed for 15 minutes in running tap water, and then submerged in two separate bathes of 100% propylene glycol for five minutes each. Sections were then incubated in ORO staining solution for ten minutes with gentle shaking, washed in 85% propylene glycol for three minutes and rinsed using distilled water for three minutes. Sections were counterstained with Harris Modified Hematoxylin (SH26-500D, Fisher Chemical; Waltham, MA USA), rinsed with running tap water for ten minutes, rinsed with distilled water for three minutes and then counter slips were mounted using Prolong Gold Antifade Mountant (P36934, Life Technologies; Carlsbad, CA, USA).

2.2.14 SDH Reaction

Glass Coplin jars were prewarmed to 37˚C in an incubator prior to beginning the reaction. Succinic acid solution was made by adding 0.4 g of succinic acid (6106-21-4, Acros Organics; New Jersey, USA), 0.04 g nitroblue tetrazolium (N8129, Sigma Aldrich; St. Louis, MO, USA) and 0.001 g of phenazine methosulfate (P9625, Sigma Aldrich; St. Louis, MO, USA) to 40 mL of 0.1M Tris buffer and pH equilibrated to 7.01. The succinic acid solution was

warmed to 37˚C and the muscle sections were submerged in the solution for 30 minutes maintaining the temperature at 37˚C in an incubator. Sections were then washed using a series of 30%, 60%, 90%, 60%, 30% acetone (A18-1, Fisher Chemical; Waltham, MA USA) solutions for 5 seconds each and rinsed in distilled water. Coverslips were applied using Prolong Gold Antifade mounting media.

2.2.15 Measurement of C2C12 Myotube Diameter and Quadriceps Muscle Fiber Cross-sectional Area (CSA)

Fully differentiated myotubes were washed with PBS and fixed by incubation with ice-cold acetone and methanol (A412-4, Fisher Chemical; Waltham, MA USA) (1:1) at -20˚C for 15 minutes. Myotubes were washed with PBS twice and blocked using blocking buffer (8% FBS in PBS) at room temperature for one hour. Myotubes were then incubated with an anti-myosin primary mAb (MF 20, DSHB; Iowa City, IA, USA) at a dilution of 1:50 in blocking buffer overnight at 4° C in a humid chamber. Myotubes were washed with PBS and incubated with a florescent secondary antibody (A-11029, Thermo Fisher; Waltham, MA USA) for one hour at room temperature in a humid chamber. Myotubes were washed with PBS, imaged and myotube diameter measured using Image J analysis.

IF was performed on frozen muscle cross-sections that were post-fixed in pre-cooled acetone (-20˚C) for ten minutes and placed at room temperature for 30 minutes. Sections were washed twice in PBS and then blocked by incubating the sections with blocking buffer for one hour at room temperature. The sections

were washed with PBS and incubated with the primary antibodies against IL6R and CD31 (see Table 2.1 for antibody information) diluted in blocking buffer overnight at 4˚C in a humid chamber. Sections were washed and the secondary antibody applied (see Table 2.1 for secondary antibody details) at a dilution of 1:1000 in blocking buffer for one hour at room temperature. Sections were washed and incubated with DAPI (268298, EMD Millipore; Burlington, MA, USA) for 1 minute to visualize nuclei. Sections were washed and cover slips applied using Prolong Gold Antifade mounting media.

To measure muscle fiber CSA using IF, frozen sections of mouse quadriceps muscles were fixed and blocked as described previously and incubated with an anti-dystrophin primary antibody (MANDRA11, DSHB; Iowa City, IA, USA) and detection of the primary antibody was done using a goat anti-mouse AlexaFluor 594 florescent secondary antibody (A-11032, Thermo Fisher; Waltham, MA, USA). Muscle fiber CSA was measured from images taken of the IF dystrophin sections using an ImageJ macro obtained from the Lieber laboratory (Mehlem, Hagberg, Muhl, Eriksson, & Falkevall, 2013; Minamoto et al., 2007).

2.2.16 Mouse Tumor and Adipose Tissue IHC

Tumors were excised from mice and immediately fixed in 10% neutral buffered formalin (NBF) for 48 hours. Tumors were then washed in PBS and stored in 70% ethanol at 4° C until analysis. Tumors were paraffin embedded and cross-sections were cut at 5 μm and mounted to microscope slides.

Deparaffinization, antigen retrieval, endogenous peroxidase neutralization and blocking were performed as previously described for human tumors. After blocking, tumors were incubated with an anti-IL-6 mAb (ab7737, Abcam; Cambridge, MA, USA) at 1:50 dilution in blocking buffer at 4° C overnight in a humid chamber. Detection of the primary mAb, counter staining, clearing and cover slip application were performed as described for the human tumors.

Fixed adipose tissue was washed in PBS and stored in 70% ethanol at 4° C. Fixed adipose tissue was then paraffin embedded and sectioned at 5 μm and mounted to microscope slides. Deparaffinization, antigen retrieval, endogenous peroxidase neutralization and blocking were performed as previously described for human tumors. Sections were then incubated with an anti-IL-6 mAb (ab7737, Abcam; Cambridge, MA, USA) diluted 1:50 in blocking buffer or an anti-F4/80 (NB600-404, Novus Biologicals; Centennial, CO, USA) diluted 1:250 in blocking buffer overnight at 4° C in a humid chamber. Detection of the primary mAb, counter staining, clearing and cover slip application were performed as described for the human tumors.

2.2.17 Plasma Analysis of IL-6, IL6R, Glycerol, and Fatty Acids

Mouse plasma obtained from cardiac puncture (see section 2.2.9) was measured for IL-6 and IL6R protein levels via enzyme-linked immunosorbent assay (ELISA) mouse Quantikine kits (MR600 & M6000B, R&D Systems;

Minneapolis, MN USA). Plasma glycerol and FAs were measured using Glycerol and FA Quantitation Kits (MAK117 & MAK044, Sigma Aldrich; St. Louis, MO USA).

2.2.18 Treatment of C2C12 Myotubes and 3T3 Adipocytes with KPC Conditioned Media (CM) and Measurement of Il6 and Il6ra mRNA

C2C12 myoblasts and 3T3 fibroblasts were cultured separately in six well plates and differentiated into myotubes and adipocytes, respectively (see sections 2.2.2-2.2.4). KPC cells were cultured in GM in flasks until becoming 100% confluent. At that time, the GM was refreshed and 100% confluent KPC cells were maintained for an additional 24 hours. After 24 hours, the CM was collected, centrifuged at 3,500 rpm to pellet unwanted cellular debris and the supernatant collected. Myotubes and adipocytes were treated in triplicate with either 30% GM (control) or 30% KPC CM per well. The treatment media was aspirated, cells were washed and myotubes RNA was isolated at 12 hours, 24 hours and 96 hours after treatment. 3T3 adipocyte RNA was isolated at one hour and three hours post-treatment in the same method used for the myotubes. Myotube and adipocyte expression of *Il6* and *Il6r* mRNA at each timepoint was measured via qPCR using probes for *Il6* (Mm00446190, Applied Biosciences; Beverly Hills, CA, USA) and *Il6r* (Mm01211444, Applied Biosciences; Beverly Hills, CA, USA).

2.2.19 Treatment of Myotubes with IL-6, IL6R and Neutralizing Antibodies

C2C12 myoblasts were differentiated into myotubes in six well plates. Fully differentiated myotubes were then treated in triplicate with either DF media (control), recombinant mouse IL-6 (300 pg/mL) protein (406-ML-005, R&D Systems; Minneapolis, MN USA), recombinant mouse IL6R (25 ng/mL) (P9767-5G, Sigma Aldrich; St. Louis, MO, USA), the combination of IL-6 (300 pg/mL) and IL6R (25 ng/mL) (1830-SR-025, R&D Systems; Minneapolis, MN, USA) or IL-6 (300 pg/mL) in the presence of IL-6 neutralizing antibody (2 mg/mL) (14-7061-85, Thermo Fisher; Waltham, MA, USA) for 48 hours. After 48 hours of treatment, myotubes were washed with PBS and fixed using ice-cold acetone/methanol (1:1) for fifteen minutes at -20° C. Myotubes were then visualized with IF using an anti-myosin antibody (see section 2.2.1) and myotube diameter measured with Image J.

2.2.20 Statistical Analyses

The Student t-test was used for the comparison of means between two datasets while one-way ANOVA with the Tukey's post-hoc test was used for comparison of the means between three or more datasets. The differences between group means was considered statistically different when $P<0.05$. Data are presented as mean $\pm$ SEM. All statistical analyses were performed using Graph Pad Prism version 7.0 (San Diego, CA, USA).

Table 2.1 An all-inclusive list of reagents and equipment used.

REAGENT or RESOURCE	SOURCE	IDENTIFIER
Antibodies (dilution)		
IL-6 (1:500)	Abcam	ab6672
Myosin (1:500)	DSHB Iowa	MF 20
IL-6 (1:200)	Abcam	ab7737
Dystrophin (1:100)	DSHB Iowa	MANDRA11 (8B11)
Ubiquitin (1:1000)	Cell Signaling	3933
LC3BII (1:1000)	Sigma Aldrich	L7543
Beclin-1 (1:1000)	Cell Signaling	3738S
ATF4 (1:1000)	Cell Signaling	11815S
p-Akt (S473) (1:1000)	Cell Signaling	4060L
Akt (1:1000)	Cell Signaling	9272S
p-4EBP1 (T70) (1:1000)	Cell Signaling	9455S
4EBP1 (1:1000)	Cell Signaling	9644S
p-mTOR (S2448) (1:1000)	Cell Signaling	5536
mTOR (1:1000)	Cell Signaling	2983
PGC1-α (1:500)	Abcam	ab54481
PGC1-β (1:500)	Abcam	ab130741
UCP2 (1:1000)	Cell Signaling	89326S
UCP3 (1:500)	Novus Bio	NBP2-24608SS
α-tubulin (1:1000)	DSHB Iowa	12G10
IL-6Rα (1:500)	Abcam	ab83053
p-STAT3 (Y705) (1:1000)	Cell Signaling	9145S
STAT3(1:1000)	Cell Signaling	4904S
F4/80 (1:250)	Novus Bio	NB600-404
Pdk4 (1:1000)	Abcam	ab110336
p-PKCθ (1:1000)	Cell Signaling	9377
PKCθ (1:1000)	Cell Signaling	13643
IL-6 Neutralizing Antibody	Thermo Fisher	MP5-20F3
IL6R Neutralizing Antibody	R&D Systems	AF1830
Chemicals and Recombinant Proteins		
Sodium Citrate	Sigma Aldrich	W302600-1KG
Bovine Serum Albumin	Fisher Bioreagents	BP1600-100
Tween-20	Fisher Bioreagents	BP337-500
Hydrogen Peroxide	Thermo Fisher	S25360
Phosphate Buffered Saline (PBS)	Corning	21040CV
Lipofectamine 3000	Invitrogen	L3000008
Betadine	Purdue Products	6761815117
Bouin Solution	Thermo Fisher	23-005-69
Tissue Plus O.C.T. Compound	Fisher Healthcare	23-730-571
Isopentane (2-methylbutane)	Fisher Chemical	03551-4
10% Neutral Buffered Formalin	VWR	95042-908
Sodium Palmitate	Sigma Aldrich	P9767-5G
Tris	Fisher Chemical	BP152-5
Glycine	Fisher Chemical	BP381-5
Sodium Dodecyl Sulfate (SDS)	Fisher Bioreagents	BP166-100
Glycerol	Acros Organics	15892-0010
DTT	Promega	PR-V3151
Sea Block	Thermo Scientific	37527
Oil Red O	Sigma Aldrich	00625-25G

Table 2.1 An all-inclusive list of reagents and equipment used. (Continued)

Propylene Glycol (1,2-Propanediol)	Sigma Aldrich	398039-500ML
Harris Modified Hematoxylin	Fisher Chemical	SH26-500D
Prolong Gold Antifade Mountant	Invitrogen	P36934
Succinic Acid	Acros Organics	6106-21-4
Nitroblue Tetrazolium	Sigma Aldrich	N8129
Phenazine Methosulfate	Sigma Aldrich	P9625
Acetone	Fisher Chemical	A18-1
Methanol	Fisher Chemical	A412-4
DAPI	EMD Millipore	268298
Recombinant Mouse Interleukin 6 (rIL-6)	R&D Systems	406-ML-005
Recombinant Mouse Interleukin 6 Receptor (rIL6R)	R&D Systems	1830-SR
Mouse Strains, Cell Lines and Tissue Arrays		
C57BL/6J Mice	The Jackson Laboratory	000664
B6.ABJ-*Prkcq-rpea1*/Boc (PKC theta knockout)	The Jackson Laboratory	004658
Mouse PDAC Tumor Cells (KPC)	Dr. David Tuveson	N/A
Mouse PDAC Tumor Cells IL-6 Deleted (KPC IL-6 K	Dr. Teresa Zimmers	RRID: CVCL_UR56
C2C12 Mouse Myoblasts	ATCC	CRL-1772
3T3-L1 Preadipocytes	Zen Bio	SP-L1-F
Human Pancreatic Cancer Tissue Array	US Biomax	PA1001a
Cell Culture		
0.25% Trypsin	Corning	25053CI
DMEM	Corning	10013CV
Fetal Bovine Serum (FBS)	GE Healthcare Life Scienc	SH30071.03HI
Penicillin/Streptomycin (10,000 U/mL)	Gibco	15140122
6-well Cell Culture Treated Dishes	Thermo Scientific	140685
Biolite Cell Culture Treated Flasks	Thermo Scientific	130191
Horse Serum	Life Technologies	26050-088
96-well Cell Culture Treated Dishes	Thermo Scientific	167008
3T3 L1 Preadipocyte Media	Zen Bio	PM-1-L1
3T3 L1 Adipocyte Differentiation Media	Zen Bio	DM-2-L1
3T3 L1 Adipocyte Maintenance Media	Zen Bio	AM-1-L1
Oligonucleotides and CRISPR Plasmids		
Il6	Life Technologies	Mm00446190
Il6r	Life Technologies	Mm01211444
Trim63 (Murf1)	Life Technologies	Mm01185221
Fbxo32 (Atrogin-1)	Life Technologies	Mm00499523
TATA binding protein (Tbp)	Life Technologies	Mm01277042
CRISPR/Cas9 Plasmid Targeting *Il6*	Sigma Aldrich	MM0000468506
CRISPR/Cas9 Negative Control Plasmid	Sigma Aldrich	CRISPR06-1EA
Commercial Assay kits		
Immpact DAB Peroxidase (HRP) Substrate	Vector Laboratories	SK-4105
miRNeasy Mini Kit (50)	Qiagen	217004
Verso cDNA Kit	Life Technologies	AB1453B
Taqman Universal Master Mix II, with UNG	Applied Biosystems	4440038
Pierce BCA Protein Assay	Thermo Scientific	PI23228

Table 2.1 An all-inclusive list of reagents and equipment used. (Continued)

Mouse IL-6 Quantikine ELISA Kit	R&D Systems	M600B
Mouse IL-6R alpha Quantikine ELISA Kit	R&D Systems	MR600
Free Fatty Acid Quantitation Kit	Sigma Aldrich	MAK044-1KT
Glycerol Assay Kit	Sigma Aldrich	MAK117-1KT
Computer Programs		
Ingenuity Pathway Analysis	Qiagen	N/A
Prism 7.0	Graph Pad	N/A
Image J	N/A	N/A
Other Materials		
Superfrost Plus Microscope Slides	Thermo Scientific	12-550-15
4-15% Criterion TGX Gel	Bio Rad	5671084
Nitrocellulose Filter Paper Sandwiches	Bio Rad	1620233
1 mL Syringe	Becton, Dickinson and Co.	329652
4-0 Coated Vicryl Suture	Butler Schein Animal Healt	33227
Stainless Steel Wound Clips	World Precision Instrument	500346
EDTA Coated Collection Tubes	Becton, Dickinson and Co.	366643
2 mL Cryo Vials	VWR	82050-208
Normal Mouse Chow	Envigo	2018SX
Buprenorphine	PAR Pharmaceuticals	4202317005

2.3 Results

2.3.1 Human PDAC Tumor Cells are Heterogeneous for IL-6 Expression

Immunohistochemistry on human PDAC tumors obtained at surgery revealed stromal IL-6 staining in all tumors tested (Figure 2.1 A) as previously reported (Mace et al., 2018). However, IL-6 staining in tumor epithelial cells was also observed. Of 72 tumor samples, 32 demonstrated weak intensity IL-6 staining (Figure 2.1 A, top and 2.1 B, left) and 40 samples strong intensity staining (Figure 2.1 A, bottom and 2.1 B, right). Expression profiling of human PDAC cell lines also confirmed a range of *IL6* expression from high (PSN-1, Panc03.27, PANC-1) to low (MIA PaCA, AsPC-1, HuPT4) (Figure 2.2). The importance of tumor cell-derived IL-6 was further investigated using human tumors in a murine xenograft model. Mice implanted with human PDAC tumors had a negative correlation when comparing murine IL-6 expression in plasma and survival (Figure 2.1 C), loss of quadriceps mass and survival (Figure 2.1 D), and a positive correlation between loss of quadriceps mass and plasma IL-6 (Figure 2.1 E). These results indicate that PDAC epithelial cells are a source of IL-6 in the tumor micro- and macro environment and significantly contribute to cachexia and survival.

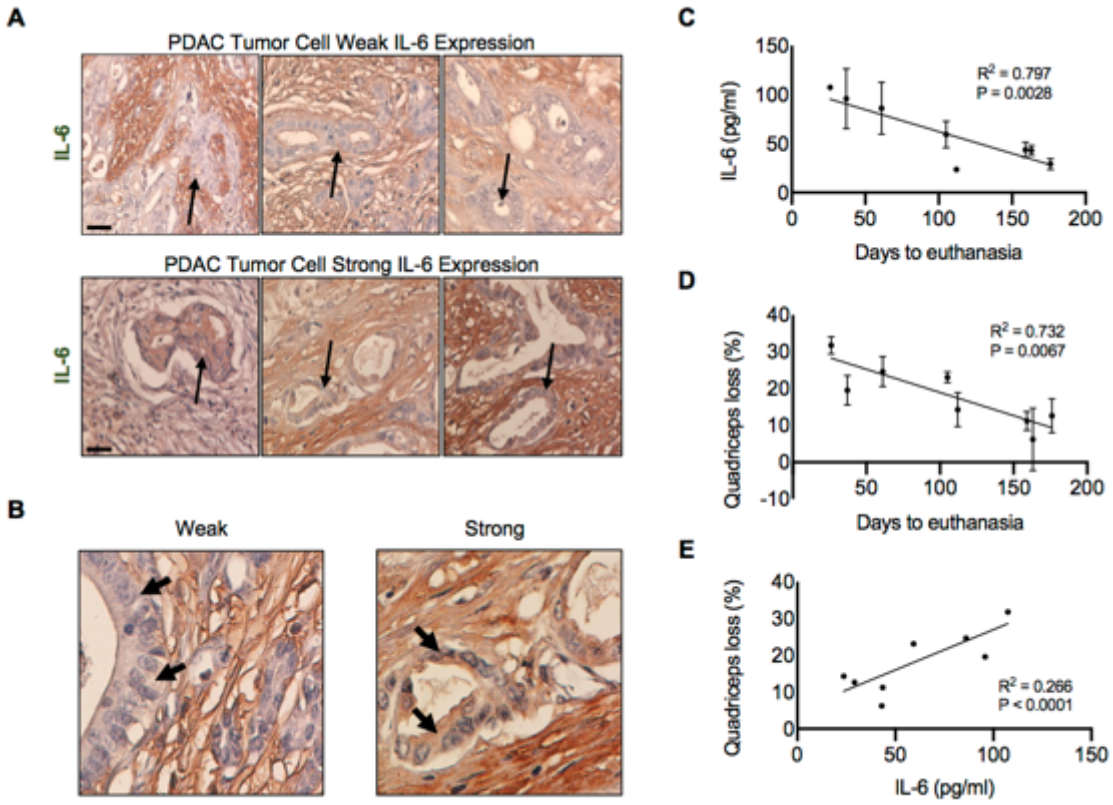

Figure 2.1. IL-6 protein expression is heterogeneous in human PDAC tumors and is associated with increased mortality and muscle wasting. Human PDAC tumors obtained were reacted for IL-6 immunohistochemistry (IHC)**.** Tumor sections were classified as having either high or low expression of IL-6 specifically in tumor epithelial cells (arrows) **(A)**. Of the 72 tumors, 40 had low tumor-cell IL-6 expression and 32 had high tumor-cell IL-6 expression. Images using increased magnification to show PDAC tumor cell IL-6 expression (**B**). Xenograft implantation of human tumors into mice showed correlations between human IL-6 and mortality (**C**), muscle loss and mortality (**D**), and human IL-6 and muscle loss (**E**). Scale bar = 40 μm.

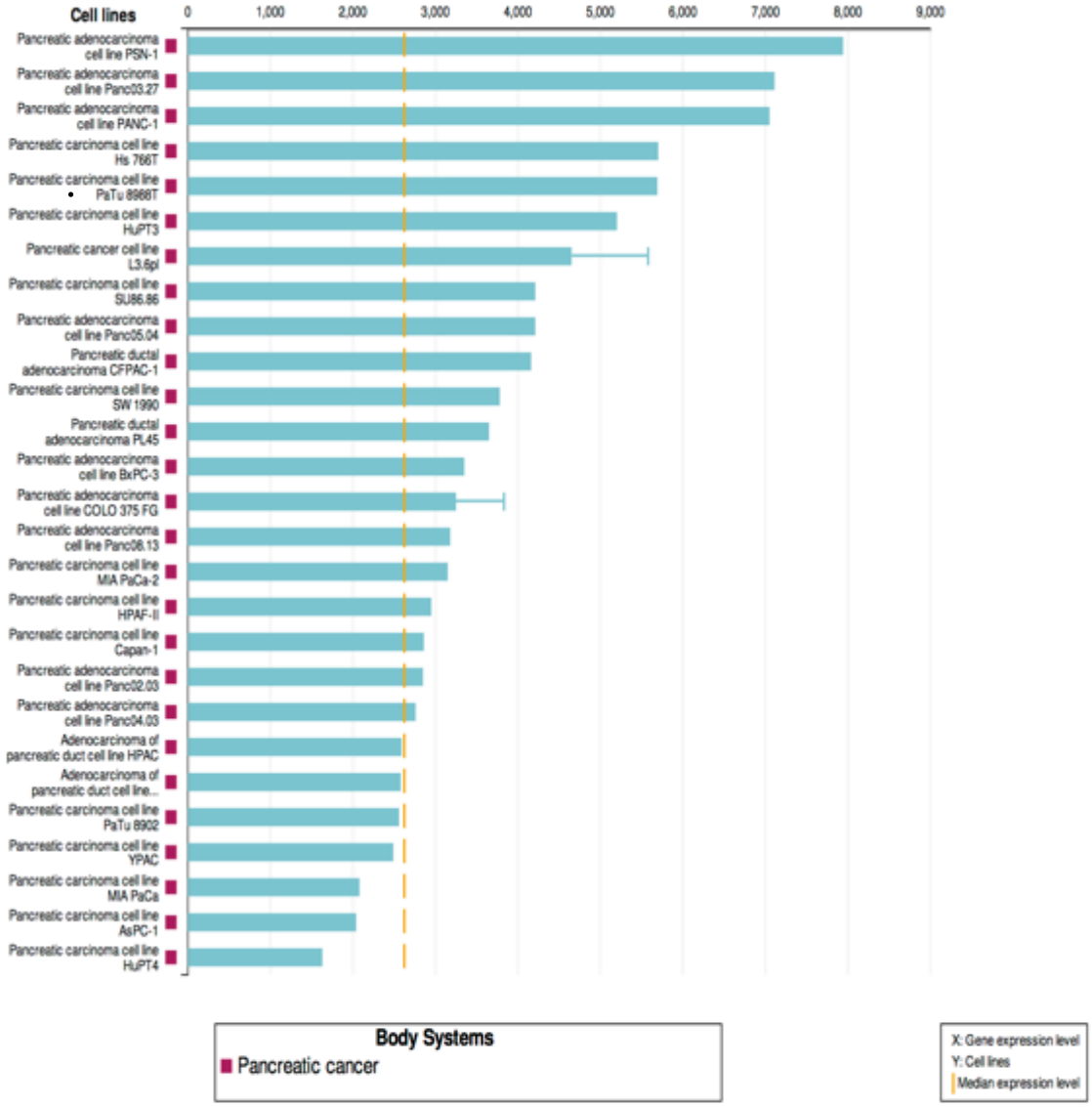

Figure 2.2. Expression of IL6 RNA in human pancreatic cancer cell lines. Expression levels of *IL6* mRNA across multiple human pancreatic cancer cell lines from Illumina BaseSpace Correlation Engine illustrating heterogeneity in *IL6* expression.

2.3.2 PDAC-induced Cachexia and Mortality are Significantly Improved by Deletion of IL-6 from Tumor Cells

To evaluate the effects of tumor cell-derived IL-6 in PDAC cachexia I used CRISPR/Cas9 to edit the *Il6* gene in a cell line isolated from an autochthonic tumor arising in a C57BL/6 male KPC mouse. A similarly transfected clone not exposed to gRNAs was used as a control (KPC). *Il6* mRNA was detected in the parental KPC cell line (KPC-P) and the control KPC line, but not in the KPC-IL6^{KO} line (Figure 2.3 A); loss of expression was due to an insertional mutation (Figure 2.4). Both control and knockout lines exhibited similar growth characteristics in vitro (Figure 2.3 B), indicating that autocrine IL-6 was not required for proliferation.

Deleting IL-6 also abolished muscle-wasting activity associated with KPC tumor cell conditioned media. Muscle growth and wasting is often modeled by manipulation or treatment of myotubes differentiated from C2C12 myoblasts (Figure 2.3 C). IL-6 itself induces atrophy of C2C12 myotubes via a STAT3-dependent mechanism (Bonetto et al., 2012). Here, conditioned media from KPC cells induced STAT3 phosphorylation (Figure 2.3 D). Myotubes were visualized using immunofluorescence for MHC (Figure 2.3 E) and myotube diameter was measured resulting in a 25% reduction of myotube diameter in those treated with KPC media (Figure 2.3 F). An increase in STAT3 phosphorylation and a reduction in myotube diameter were absent in KPC-IL6^{KO}CM treated myotube. To determine if the deletion of IL-6 from KPC IL-6^{KO} CM attenuating myotube atrophy, IL-6 was added back to KPC IL-6^{KO} CM media

as well as neutralized in KPC CM and KPC IL-6^{KO} + IL-6 CM. Myotubes were again visualized using immunofluorescence for MHC (Figure 2.3 G) and diameters measured. The addition of IL-6 (300 pg/mL) to KPC IL-6^{KO} CM induced myotube atrophy (Figure 2.3 H), while the addition of IL-6 neutralizing antibody (2 mg/mL) to KPC CM and KPC IL-6^{KO} + IL-6 CM was sufficient to attenuate myotube atrophy (Figure 2.3 H). Next, the effects of deleting tumor cell-derived IL-6 in vivo were investigated. Orthotopic tumors from mice bearing KPC or KPC IL-6^{KO} tumors were reacted for IL-6 expression and positive IL-6 expression in KPC cells (Figure 2.3 I, left) and negative IL-6 expression in KPC IL-6^{KO} tumor cells (Figure 2.3 I, right) was confirmed. Finally, the deletion of tumor cell-derived IL-6 increased the survival of KPC IL-6^{KO} tumor mice compared to KPC tumor mice (Figure 2.3 J).

Figure 2.3

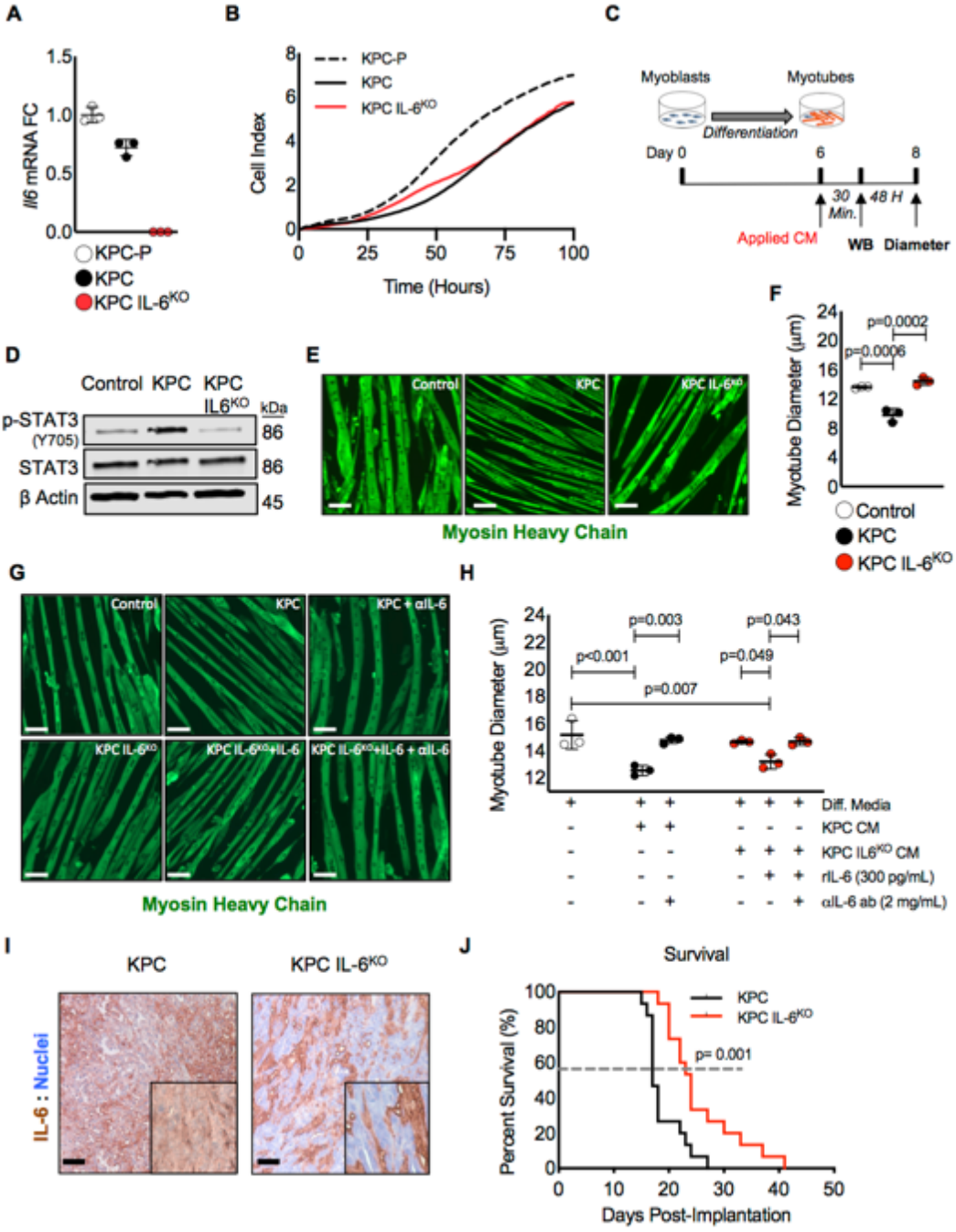
A
Il6 mRNA FC
KPC-P
KPC
KPC IL-6KO
B
Cell Index
Time (Hours)
KPC-P
KPC
KPC IL-6KO
C
Myoblasts
Myotubes
Differentiation
Day 0
6
8
30 Min.
48 H
Applied CM
WB
Diameter
D
Control
KPC
KPC IL6KO
kDa
p-STAT3 (Y705)
STAT3
β Actin
86
86
45
E
Control
KPC
KPC IL-6KO
Myosin Heavy Chain
F
Myotube Diameter (μm)
p=0.0002
p=0.0006
Control
KPC
KPC IL-6KO
G
Control
KPC
KPC + αIL-6
KPC IL-6KO
KPC IL-6KO+IL-6
KPC IL-6KO+IL-6 + αIL-6
Myosin Heavy Chain
H
Myotube Diameter (μm)
p=0.003
p=0.043
p<0.001
p=0.049
p=0.007
Diff. Media
KPC CM
KPC IL6KO CM
rIL-6 (300 pg/mL)
αIL-6 ab (2 mg/mL)
I
KPC
KPC IL-6KO
IL-6 : Nuclei
J
Survival
KPC
KPC IL-6KO
p= 0.001
Percent Survival (%)
Days Post-Implantation

Figure 2.3. Deletion of IL-6 from KPC cells prevented muscle wasting in vitro and increased survival in mice. Targeted mutagenesis of the *Il6* gene was performed and *Il6* mRNA expression in a transfection control clone (KPC) and an *Il6* ablated clone (KPC IL-6^{KO}) were compared to non-transfected KPC parental cells (KPC-P) and selected for use in downstream experiments (**A**). The parental cell line (KPC-P) was used as a positive control for selection of clones (**A**). To determine if deletion of IL-6 affected tumor cell growth a proliferation assay was performed comparing the clones (**B**). Myoblasts were differentiated into myotubes and treated with 30% CM from clones to measure effects on myotube atrophy and STAT3 activation (**C**). Western blotting using myotube protein lysates were performed to measure STAT3 phosphorylation (**D**). Myotubes were visualized using florescent immunocytochemistry with an anti-myosin heavy chain antibody (**E**) and myotube atrophy measured (**F**). To verify atrophy was due to IL-6, myotubes were treated with KPC IL-6^{KO} CM plus recombinant IL-6 with and without the presence of an anti-IL-6 neutralizing antibody and the anti-IL-6 neutralizing antibody was also used to treat the KPC CM; myotubes were visualized with MHC IF and atrophy measured (**G and H**). KPC tumor cells were orthotopically implanted into mice, tumors were excised, sectioned and reacted with anti-IL-6 IHC to verify tumor cell IL-6 deletion (**I**). Survival was measured in mice orthotopically implanted with KPC and KPC IL-6^{KO} tumor cells (**J**). Scale bar = 20 μm; Error bars are standard deviation and significant differences are shown in the charts.

Figure 2.4. Characterization of KPC-IL-6^{KO} cells. DNA sequencing was performed at the CRISPR/Cas9 target site (green line) within the murine *Il6* gene showing an insertion mutation of 45 nucleotides (red line) into the KPC IL-6^{KO} mutant sequence. Asterisks indicate point mutations.

2.3.3 Muscle Wasting is Spared in KPC IL-6^{KO} Tumor-bearing Mice

Apart from the survival study, two separate cohorts were analyzed for effects on cachexia, euthanizing mice when one group reached specified humane endpoints. Cachexia was prominent in the KPC group, with 11% to 26% wasting of limb muscles and heart (Figure 2.5 A), with significant loss of body weight (Figure 2.6 A) and loss of carcass mass (Figure 2.6 B). In contrast, muscle weights in the KPC-IL6^{KO} group were unchanged versus tumor-free control mice (Figure 2.5 A) with no change in body weight or carcass mass (Figure 2.6 A and 2.6 B). KPC tumor-bearing mice also had wasting of the liver (Figure 2.6 C) and increased splenomegaly versus KPC IL-6^{KO} tumor-bearing mice (Figure 2.6 D), although KPC IL-6^{KO} tumor-bearing mice had splenomegaly when compared to tumor-free mice (Figure 2.6 D). This degree of wasting would be considered severe cachexia.

The quadriceps muscles were sectioned, and individual muscle fibers were visualized using immunofluorescence for dystrophin (Figure 2.5 B). Muscle from mice with KPC-IL6^{KO} tumors showed normal dystrophin expression, not the reduced expression described in murine cachexia (Acharyya et al., 2005; Stephens et al., 2015) and observed in mice with KPC tumors (Figure 2.5 B). Mice with KPC-IL6^{KO} tumors were also spared the myofiber atrophy observed in quadriceps of mice with control KPC tumors (Figure 2.5 C and 2.5 D). Mice bearing the KPC tumor had larger tumor mass than mice with KPC IL-6^{KO} tumors (Figure 2.5 E). Therefore, to investigate if tumor size was affecting muscle loss, a regression analysis was performed comparing tumor mass versus normalized

muscle mass. There were no correlations between tumor mass and quadriceps mass (Figure 2.5 F) and tumor mass and heart mass (Figure 2.5 G). Tumor mass was also compared to the remaining skeletal muscles (Figure 2.6 E and 2.6 F) and epididymal fat pad mass (Figure 2.6 G) with no correlations observed. To determine if deletion of IL-6 was playing a role in tumor grade and subsequently affecting the severity of cachexia, tumors were blindly scored in two independent evaluations. There was no difference in tumor grade between KPC and KPC IL-6^{KO} tumor-bearing mice (Figure 2.6 H). Collectively, these results are consistent with IL-6 as a KPC-derived mediator of cachexia and mortality.

Figure 2.5

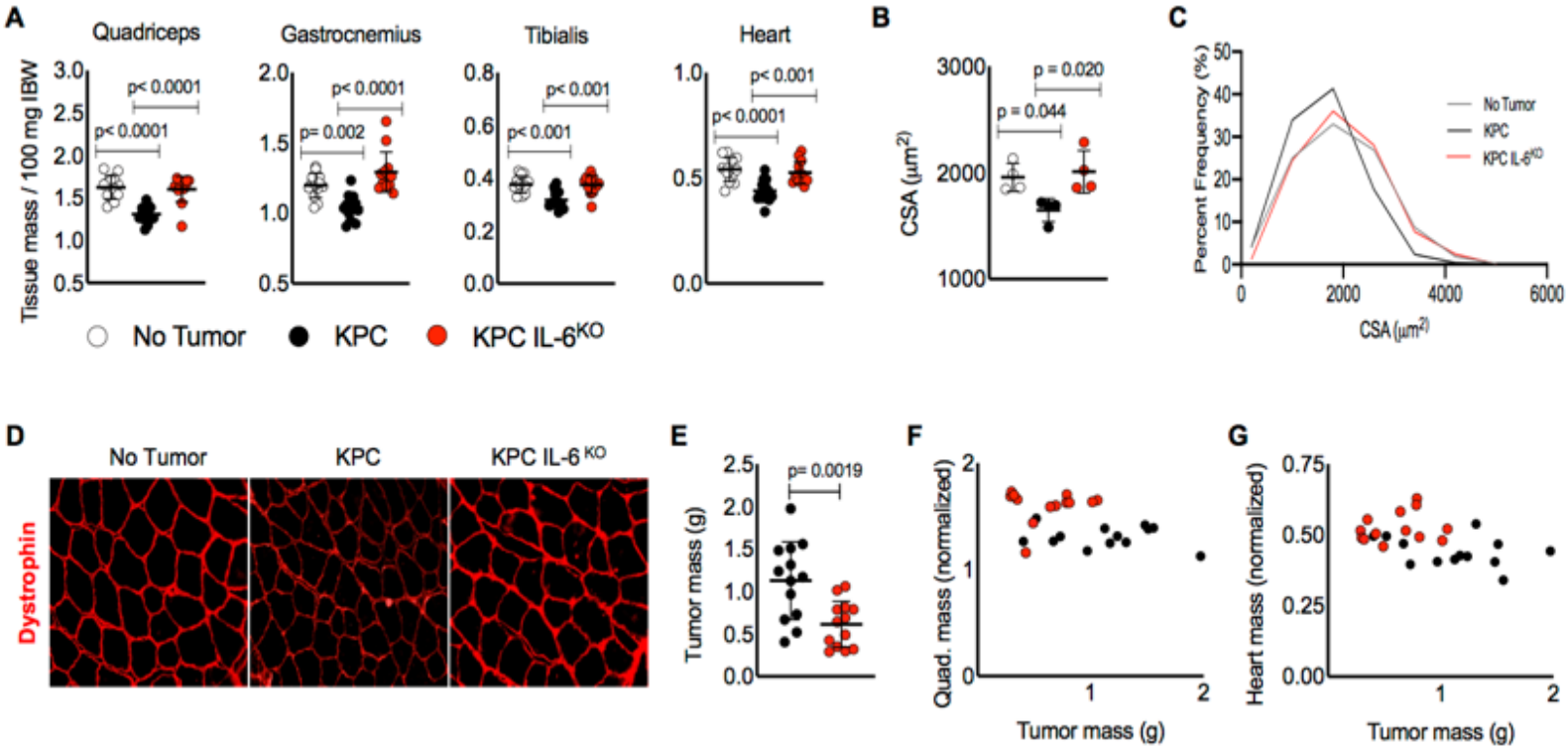
A
Quadriceps
Gastrocnemius
Tibialis
Heart
Tissue mass / 100 mg IBW
p< 0.0001
p< 0.0001
p= 0.002
p< 0.0001
p< 0.001
p< 0.001
p< 0.001
p< 0.0001
No Tumor
KPC
KPC IL-6KO
B
CSA (μm2)
p = 0.044
p = 0.020
C
Percent Frequency (%)
CSA (μm2)
No Tumor
KPC
KPC IL-6KO
D
No Tumor
KPC
KPC IL-6 KO
Dystrophin
E
Tumor mass (g)
p= 0.0019
F
Quad. mass (normalized)
Tumor mass (g)
G
Heart mass (normalized)
Tumor mass (g)

Figure 2.5. Deletion of tumor cell IL-6 attenuates muscle wasting. Mice were euthanized 17 days after injection due to severe cachexia in the KPC group and reaching humane endpoints. Skeletal muscles and the heart were excised at euthanasia and weighed and normalized to initial body weight (IBW) (**A**). Evaluation of muscle fiber CSA was done using sections from excised quadriceps muscles reacted for dystrophin expression (**D**) and mean fiber CSA measured (**B**). Cumulative fiber CSA values were organized based on percent distribution of fiber CSA and plotted to observe shifts in distribution (**C**). KPC IL-6^{KO} excised tumor mass was smaller than KPC tumor mass (**E**) thus, tumor mass was compared with muscle mass to determine if any correlation ns were present (**F and G**). Scale bar = 50 μm; Error bars are standard deviation and significant differences shown in charts.

Figure 2.6

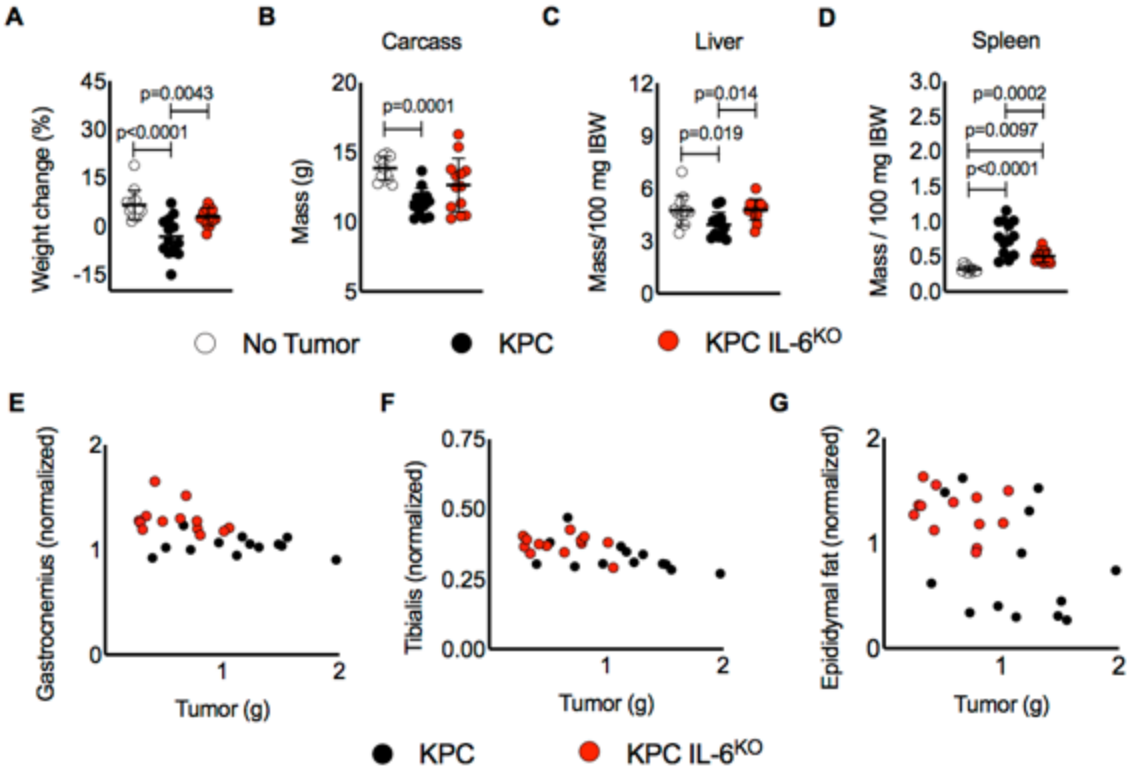

H

KPC Tumors	% Necrosis	% Inflammation	Mitotic Figures	Apoptotic Bodies	Adenocarcinoma	Grade
1	None	None	Yes	Yes	Yes	3
2	10%	None	1-2	Yes	Yes	3
3	20%	None	Yes	Yes	No (solid)	3
4	15%	N/A	N/A	Yes	Yes	3
5	20%	10%	2-3	2-3	Yes	3

KPC IL-6KO Tumors	% Necrosis	% Inflammation	Mitotic Figures	Apoptotic Bodies	Adenocarcinoma	Grade
1	None	Chronic	Yes	Yes	Yes	3
2	10%	10%	3	3	Yes	3
3	None	None	2	2	Yes	3
4	None	None	4	Yes	Yes	3
5	10%	None	4	Yes	Yes	3

Figure 2.6. Deletion of tumor cell-derived IL-6 is associated with reduced weight loss, carcass and liver wasting, and splenomegaly in mice with PDAC. Tumor free final body weight was measured at euthanasia (**A**) and tissue weights for the carcass (**B**), liver (**C**) and spleen (**D**) were also recorded. No correlation was observed between tumor mass and gastrocnemius (**E**), tibialis (**F**), and epididymal fat pad (**G**) masses. Sections of excised KPC and KPC IL-6^{KO} tumors were stained with H&E and blindly scored by two separate pathologists to determine any differences in tumor grade (**H**). Error bars are standard deviation and statistical differences re reported in the charts.

2.3.4 Tumor Cell Deletion of IL6 Reduces Muscle Atrophy Pathway Activation

Muscle of mice with KPC-IL6^{KO} tumors also demonstrated reduced activation of atrophy pathways, including those involved in ubiquitin-proteasome mediated proteolysis, autophagy, translation repression, and mitochondrial function. Quadriceps muscles from mice with KPC tumors demonstrated increased total protein ubiquitination, as commonly observed in conditions of muscle catabolism, while total protein ubiquitination in mice with KPC IL-6^{KO} tumors was no different from controls (Figures 2.7 A and 2.7 B). Corroboratively, RNA levels for the atrophy-associated skeletal muscle E3 ubiquitin ligases *Fbxo32/Atrogin-1/MAFbx* and *Trim63/Murf1,* were only increased in KPC and not KPC-IL6^{KO} muscles (Figure 2.7 B, right). Autophagy and endoplasmic reticulum (ER) stress are also triggered in muscle atrophy marked by LC3B-II and Beclin-1, proteins with important roles in autophagosome formation (Sandri, 2016) and Atf4, which is increased by ER stress and the unfolded protein response (Bohnert et al., 2016). LC3B-II and ATF4 protein were increased in the muscle of KPC but not KPC IL-6^{KO} tumor-bearing mice (Figure 2.7 C and 2.7 D). While Beclin-1 was unchanged in muscle of mice with KPC tumors, it was actually decreased in muscle of mice with KPC IL-6^{KO} tumors (Figure 2.7 B and 2.7 D). Effects of these KPC tumors on protein synthesis markers in quadriceps were subtle, with no significant change in anabolic pAKT/AKT and p-mTOR/mTOR (Figure 2.7 E and 2.7 F). A significant decrease in p-4EBP1 in KPC muscle was suggestive of de-repression of translation (Figure 2.7 E and 2.7 F). There was no difference across groups in the master regulators of mitochondrial biogenesis,

PGC1A and PGC1B (Figure 2.7 G and 2.7 H). While there was no difference in the mitochondrial uncoupling protein UCP2, an increase in UCP3 was observed in mice with KPC tumors, but not in those with KPC-IL6^{KO} tumors (Figure 2.7 G and 2.7 H). These results indicated that deletion of IL-6 from tumor cells largely abolished activation of muscle wasting pathways, especially those involved in the ubiquitin-proteasome and autophagy, in mice with PDAC tumors.

Figure 2.7

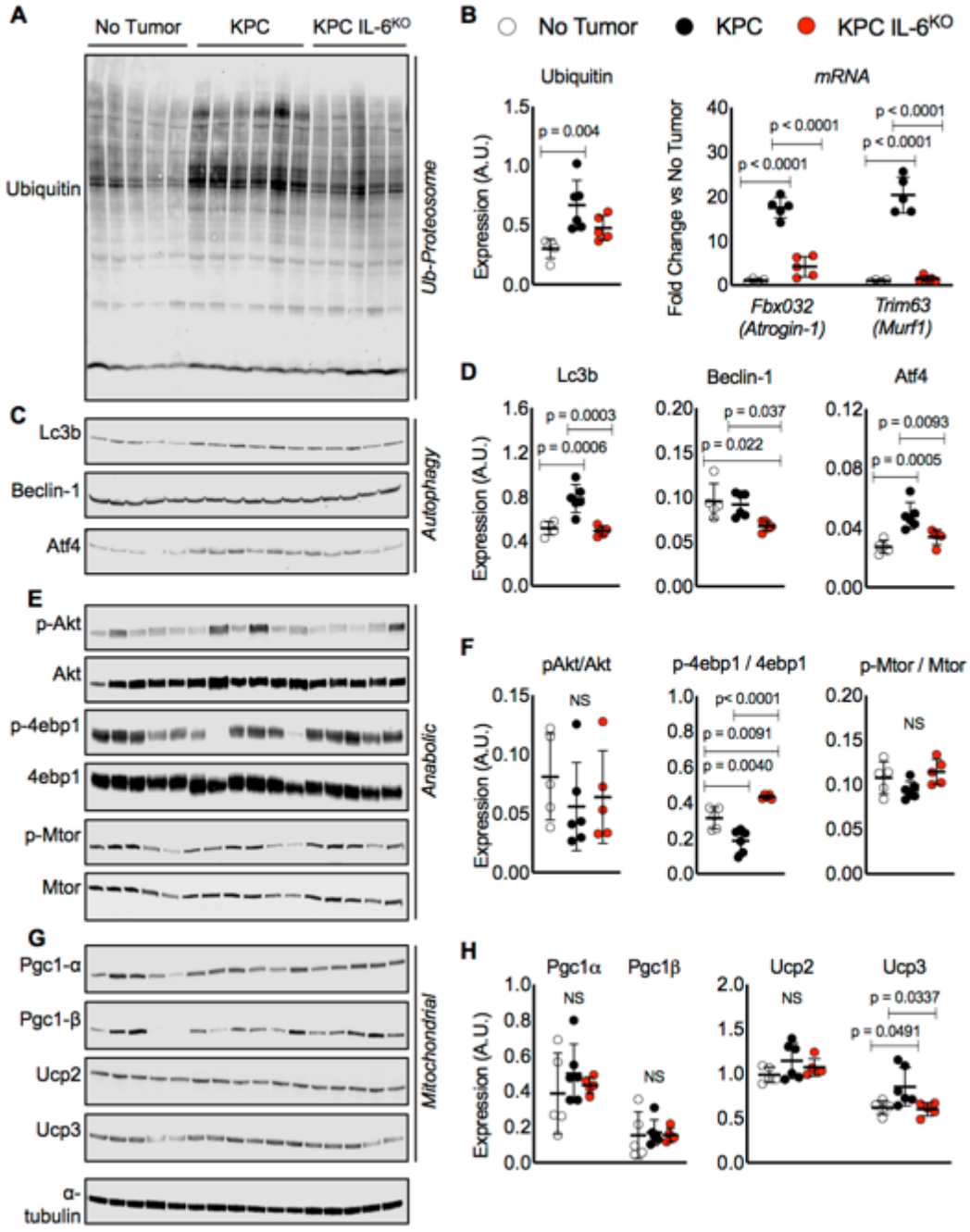
A
No Tumor
KPC
KPC IL-6KO
Ubiquitin
Ub-Profeosome
B
No Tumor
KPC
KPC IL-6KO
Ubiquitin
Expression (A.U.)
p = 0.004
mRNA
Fold Change vs No Tumor
p < 0.0001
p < 0.0001
p < 0.0001
p < 0.0001
Fbx032 (Atrogin-1)
Trim63 (Murf1)
C
Lc3b
Beclin-1
Atf4
Autophagy
D
Lc3b
Beclin-1
Atf4
p = 0.0003
p = 0.0006
p = 0.037
p = 0.022
p = 0.0093
p = 0.0005
E
p-Akt
Akt
p-4ebp1
4ebp1
p-Mtor
Mtor
Anabolic
F
pAkt/Akt
p-4ebp1 / 4ebp1
p-Mtor / Mtor
NS
p< 0.0001
p = 0.0091
p = 0.0040
NS
G
Pgc1-α
Pgc1-β
Ucp2
Ucp3
Mitochondrial
α-tubulin
H
Pgc1α
Pgc1β
Ucp2
Ucp3
NS
NS
NS
p = 0.0337
p = 0.0491

Figure 2.7. Measurement of protein expression for common molecular pathways associated with muscle wasting. Western blotting results evaluating muscle proteins involved in ubiquitination (**A and B**), autophagy (**C and D**), anabolism (**E and F**) and mitochondria biogenesis and metabolism (**G and H**) from protein lysates made from quadriceps harvested at euthanasia. Analysis of qPCR results for mRNA expression of E3 ubiquitin ligases *Atrogin-1* and *Murf1* in quadriceps was also performed (**B, right**). Error bars are standard deviation and significant differences between group means measured using ANOVA.

2.3.5 KPC but not KPC IL-6^{KO} Tumors Induced Inflammation, Lipid Accumulation and Oxidative Stress in Skeletal Muscle

RNA sequencing revealed 3480 up-regulated and 3793 down-regulated genes [fold change $\geq |1.5|$; false discovery rate (FDR) of 0.05] in the muscle of KPC tumor mice, while only 24 up-regulated and 69 down-regulated genes were found in the muscle of mice with KPC-IL-6^{KO} tumors (Figure 2.8 A). Pathway analysis implicated a number of affected pathways in muscle including adipogenesis, oxidative stress, inflammation, fatty acid oxidation (all generally increased) and glycolysis, which was decreased (Figure 2.8 B-F). These were largely unchanged in mice with KPC-IL-6^{KO} tumors, save fatty acid oxidation, which was decreased relative to controls (Figure 2.8 E). Consistent with the pathway analysis, Oil Red O staining demonstrated intramyocellular lipid accumulation (myosteatosis) in quadriceps of KPC tumor-bearing mice, but not in KPC-IL-6^{KO} tumor-bearing or control mice (Figure 2.8 G, top and 2.8 H, left). Succinate dehydrogenase (SDH) histochemistry, an indicator of mitochondrial respiration and localization, revealed aberrant localization and decreased respiratory capacity in the muscle of KPC tumor mice and to some degree in muscle from KPC IL-6^{KO} tumor mice (Figure 2.8 G, bottom and 2.8 H, right).

Figure 2.8

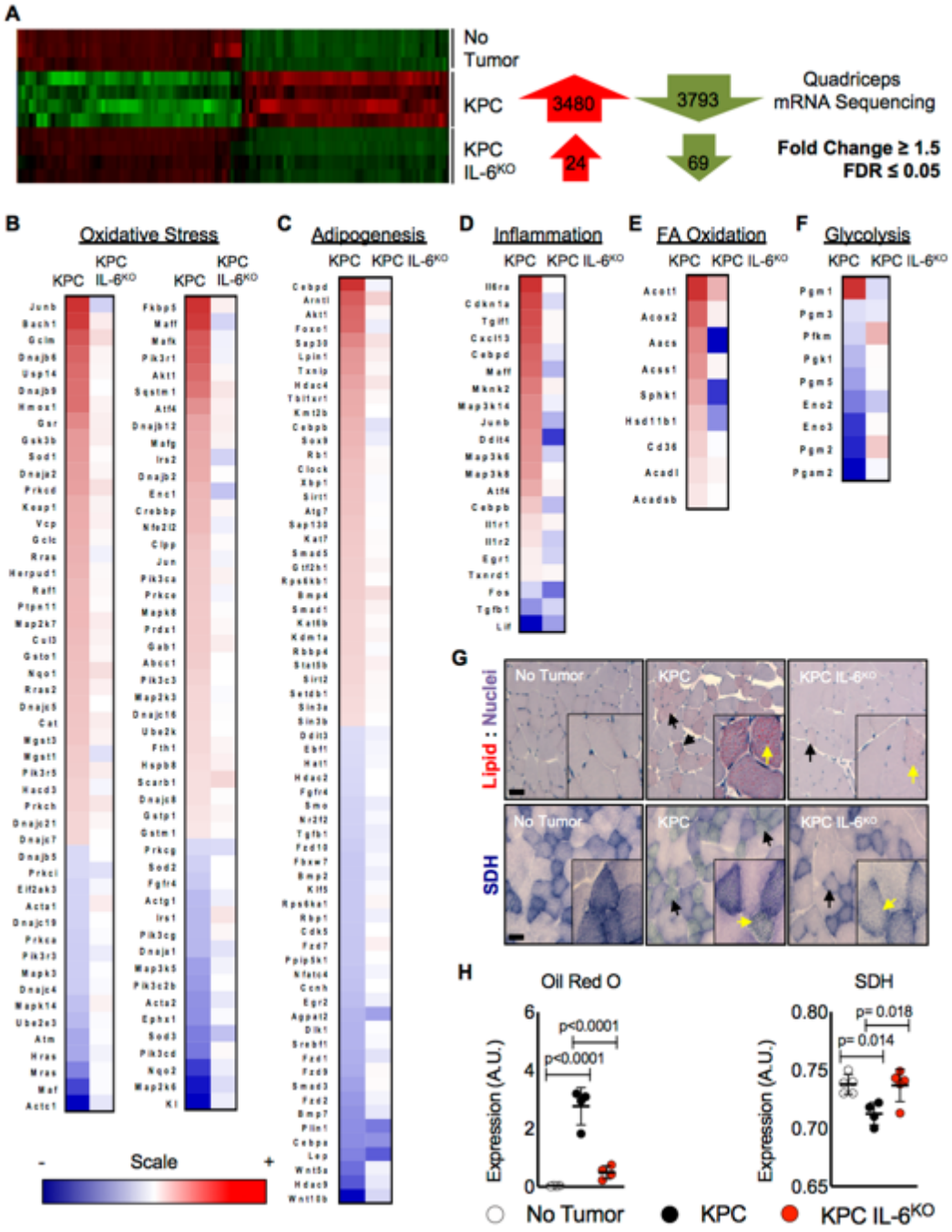
A
No Tumor
KPC
KPC IL-6KO
3480
3793
24
69
Quadriceps mRNA Sequencing
Fold Change ≥ 1.5
FDR ≤ 0.05
B
Oxidative Stress
C
Adipogenesis
D
Inflammation
E
FA Oxidation
F
Glycolysis
KPC
KPC IL-6KO
Scale
G
Lipid : Nuclei
SDH
No Tumor
KPC
KPC IL-6KO
H
Oil Red O
SDH
Expression (A.U.)
p<0.0001
p<0.0001
p= 0.018
p= 0.014
No Tumor
KPC
KPC IL-6KO

Figure 2.8. Deletion of IL-6 from KPC cells reduces activation of key cachexia pathways in muscle. Isolated RNA from the quadriceps of no tumor, KPC tumor and KPC IL-6^{KO} tumor mice was sequenced and differentially regulated genes (fold-change ≥ 1.5 and FDR ≤ 0.05) were compared across groups (**A**). Ingenuity Pathway Analysis (IPA) using quadriceps RNA sequencing data identified various altered pathways and their associated genes (shown in heat map format) that have roles in muscle wasting including adipogenesis (**B**), Oxidative Stress (**C**), Inflammation (**D**), Fatty Acid (FA) Oxidation (**E**) and Glycolysis (**F**); the scale bar illustrates increased (Red) and decreased (Blue) gene expression for the heat maps. Measurements of muscle lipids using Oil Red O staining (**G and H**) and succinate dehydrogenase activity as a marker for mitochondria oxidative capacity (**G and I**) were performed on quadriceps muscle cross-sections; scale bar = 50 μm, arrows indicate fibers with increased lipid accumulation and aberrant SDH reactivity. Error bars are standard deviation and significant differences shown in charts.

2.3.6 Adipose Tissue is Not Preserved by Tumor-cell Deletion of IL-6

Because IL-6 has been shown to promote lipolysis, we evaluated tumor effects on adipose tissue wasting. Both KPC and KPC-IL-6^{KO} tumor mice had wasting of the epididymal fat pad versus no tumor mice, although fat wasting in KPC-IL-6^{KO} tumor mice was significantly attenuated (Figure 2.9 A). Consistent with this lesser fat wasting, plasma fatty acids and glycerol were increased only in the KPC tumor mice (Figure 2.9 B and 2.9 C). RNAseq of adipose tissue demonstrated a similar intermediate phenotype, with 268 up-regulated and 145 down-regulated genes in fat pads of mice with KPC tumors, and 209 up-regulated and 0 down-regulated genes in the KPC-IL-6^{KO} group (fold change $\geq |1.5|$; FDR 0.05) (Figure 2.9 D). Granulocyte adhesion/diapedesis, LXR/RXR activation, acute phase signaling, and IL-6 signaling were among the top altered pathways associated with cachexia in adipose tissue (Figure 2.9 E-H), with activated genes similar across both tumor conditions. These results suggest that adipose tissue is more sensitive to tumor-produced factors as well as lower plasma IL-6 levels than muscle.

Figure 2.9

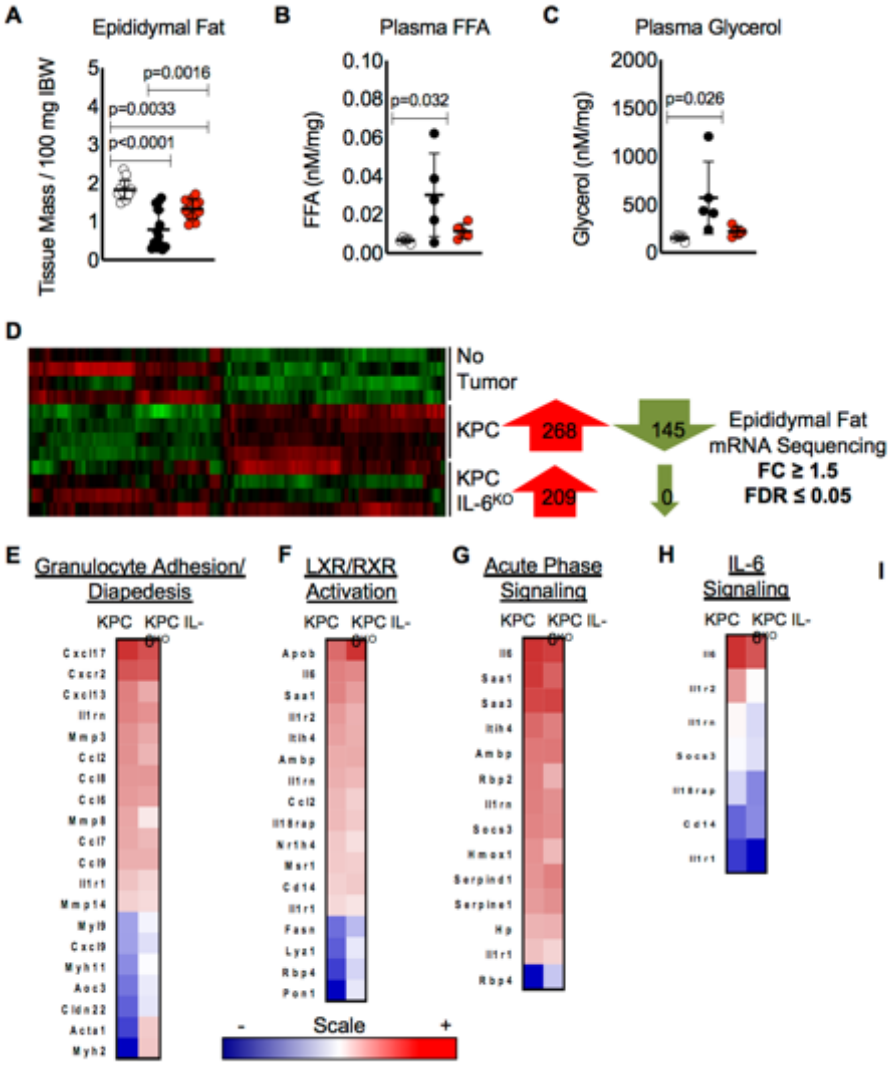
A
Epididymal Fat
Tissue Mass / 100 mg IBW
p=0.0016
p=0.0033
p<0.0001
B
Plasma FFA
FFA (nM/mg)
p=0.032
C
Plasma Glycerol
Glycerol (nM/mg)
p=0.026
D
No Tumor
KPC
KPC IL-6KO
268
145
209
0
Epididymal Fat mRNA Sequencing
FC ≥ 1.5
FDR ≤ 0.05
E
Granulocyte Adhesion/ Diapedesis
F
LXR/RXR Activation
G
Acute Phase Signaling
H
IL-6 Signaling
I
KPC
KPC IL-6KO
Scale
-
+

Figure 2.9. Deletion of IL-6 from KPC cells reduces fat wasting but did not hinder change in gene expression versus KPC tumor mice. Epididymal fat pad mass was measured at euthanasia and normalized to initial body weight (IBW) (**A**). Characterization of lipolysis using measurements of plasma glycerol (**B**) and fatty acids (**C**) normalized to epididymal fat pad mass from mice. Isolated RNA from the epididymal fat pads was sequenced and differentially regulated genes (compared to no tumor group, fold-change ≥ 1.5 and FDR ≤ 0.05) were compared across groups (**D**). Ingenuity Pathway Analysis (IPA) using epididymal fat pad RNA sequencing data identified various altered pathways and their associated genes (shown in heat map format) that have roles in inflammation and lipolysis including Granulocyte Adhesion/Diapedesis (**E**), LXR/RXR Activation (**F**), Acute Phase Signaling (**G**) and IL-6 Signaling (**H**); the scale bar illustrates increased (Red) and decreased (Blue) gene expression for the heat maps.

2.3.7 IL-6 Pathway Proteins are Differentially Expressed in Fat Versus Muscle of Mice with PDAC, Implicating IL6R Trans-signaling from Muscle to Fat.

Given the differential sensitivity of muscle and fat to tumor-derived IL-6, we sought to investigate tissue crosstalk in PDAC cachexia. As expected, implanted KPC tumor cells and host stromal cells expressed IL-6, while KPC-IL6^{KO} tumors showed expression only in stroma (Figure 2.3 I). Plasma levels of IL-6 were correspondingly increased, with a significant increase (~150-fold) in KPC tumor mice over baseline levels, while mice with KPC-IL6^{KO} tumors showed roughly half that increase, and the difference were not significantly different from normal controls (Figure 2.10 A). Plasma soluble IL-6 receptor (sIL6R), which is largely produced by shedding of a 55 kDa fragment from the membrane-bound IL6R into the circulation, was also significantly increased in KPC tumor mice (~25-fold) over controls; plasma sIL6R levels in KPC-IL6^{KO} mice were not different from controls (Figure 2.10 B).

To identify the sources of IL-6 and sIL6R, I measured mRNA in muscle, fat, liver and tumor and protein in the quadriceps muscle and the epididymal fat pads via western blotting. The results indicate that both muscle and fat express IL-6 in PDAC cachexia, and further that muscle is a source of circulating sIL6R, enabling trans-signaling of IL-6 in adipose tissue. Specifically, *Il6* mRNA was significantly increased 37-fold in epididymal fat from mice with KPC tumors (Figure 2.10 C) and although not significant likely from increased variation and smaller sample size, a trend in increased *Il6* was observed in muscle (6.4-fold, p=0.06) and liver (8.5-fold, p=0.1) from KPC tumor-bearing mice (Figure 2.10 C).

In contrast, *Il6r* mRNA was significantly increased in the quadriceps (8.9-fold) and liver (2.6-fold) but unchanged in the adipose tissue from KPC tumor mice (Figure 2.10 D). Interestingly, compared to KPC tumors, *Il6* mRNA was increased in the KPC IL-6^{KO} tumors (Figure 2.10 E), yet tumor *Il6r* mRNA was actually decreased in KPC IL-6^{KO} tumors (Figure 2.10 F). Since changes in *Il6* and *Il6r* mRNA expression were only observed in muscle and fat of KPC tumor-bearing mice, I investigated in more detail the source of these altered gene expressions by dissociating the tissue and analyzing the mononuclear cell fractions (MNC) in no tumor and KPC tumor-bearing mice. Compared to no tumor mice, *Il6* mRNA expression was unchanged in the muscle MNC fraction from KPC tumor-bearing mice while unexpectedly; it was reduced in the fat MNC fraction from KPC tumor-bearing mice (Figure 2.10 G). *Il6r* mRNA expression was increased, although modestly, in the muscle MNC fraction from KPC tumor-bearing mice and unchanged in fat compared to no tumor mice (Figure 2.10 H). These results indicate that the MNC fractions from muscle and fat are not significantly contributing to *Il6* mRNA expression, but the muscle MNC fraction likely contributes in part to whole tissue *Il6r* mRNA expression in skeletal muscle.

In contrast to the mRNA expression, there was no change in IL-6R protein expression in quadriceps and a significant increase of IL-6R protein in adipose tissue of KPC tumor mice (Figure 2.10 I and 2.10 J). Interestingly, only KPC mice had significantly increased STAT3 phosphorylation (pSTAT3) in quadriceps, while both tumor-bearing groups had increased pSTAT3 in fat (Figure 2.10 I and 2.10 K). Immunofluorescence demonstrated IL6R protein in myofibers in all

groups (Figure 2.10 L, top) as well as robust staining in muscle blood vessels only in the KPC tumor mice (Figure 2.10 L, bottom). Strong IL-6 expression was observed in the fat from KPC tumor-bearing mice (Figure 2.10 M, top). In adipose tissue, visualization of the IL6R showed accumulation near cells positioned between adipocytes in all groups (Figure 2.10 M, bottom). Taken together, these results suggest tumor cell and adipose tissue IL-6 production contribute to systemic IL-6 levels and intricate crosstalk between stromal and tumor cells may be occurring in the KPC IL-6^{KO} tumors requiring further investigation. Furthermore, these findings also implicate muscle as a primary source for circulating sIL6R, which likely promotes its accumulation in fat.

Figure 2.10

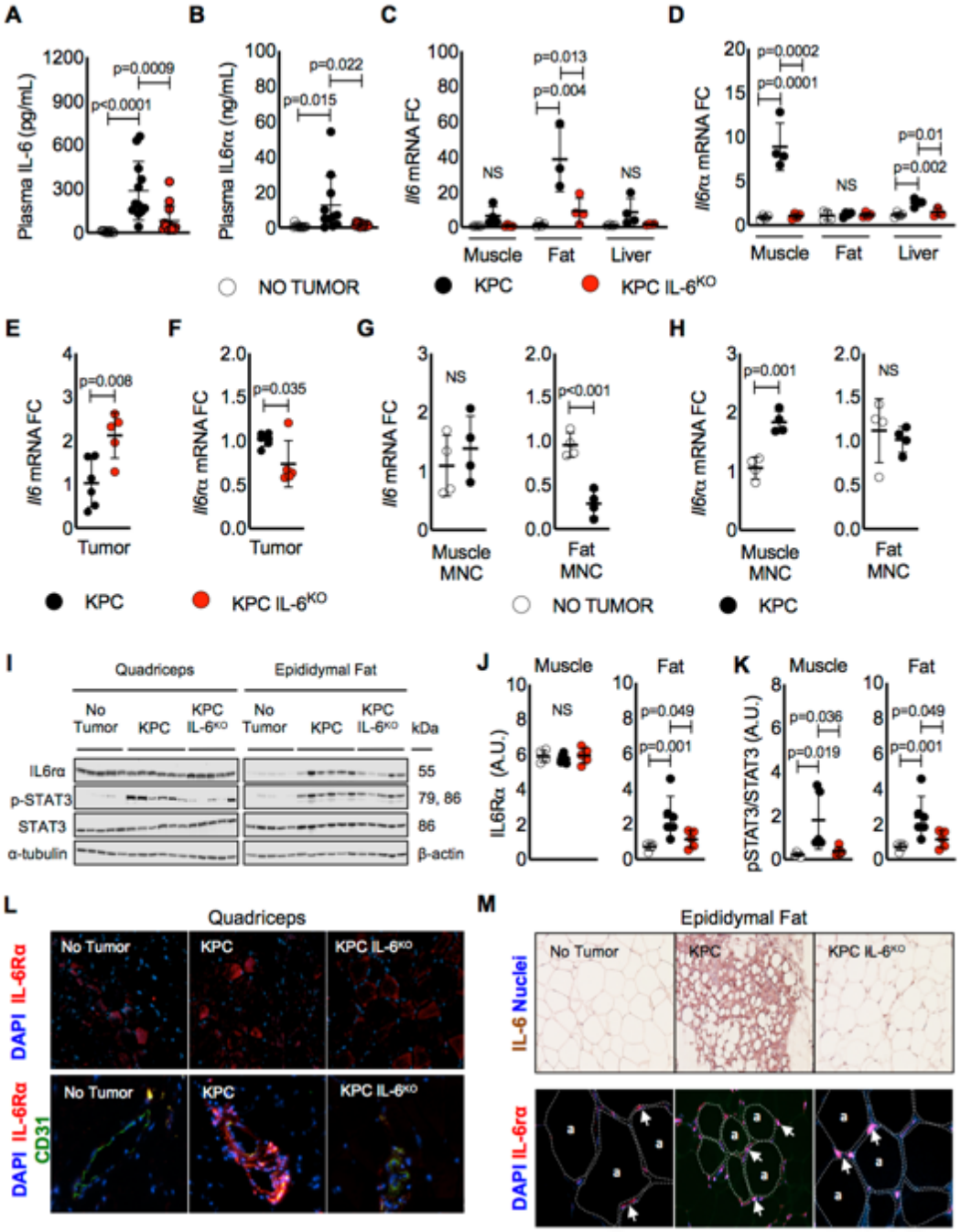
A
B
C
D
Plasma IL-6 (pg/mL)
Plasma IL6rα (ng/mL)
Il6 mRNA FC
Il6rα mRNA FC
p=0.0009
p<0.0001
p=0.022
p=0.015
p=0.013
p=0.004
p=0.0002
p=0.0001
p=0.01
p=0.002
NS
Muscle
Fat
Liver
NO TUMOR
KPC
KPC IL-6KO
E
F
G
H
p=0.008
p=0.035
p<0.001
p=0.001
Tumor
Muscle MNC
Fat MNC
I
J
K
Quadriceps
Epididymal Fat
No Tumor
KPC
KPC IL-6KO
kDa
IL6rα
p-STAT3
STAT3
α-tubulin
55
79, 86
86
β-actin
IL6Rα (A.U.)
pSTAT3/STAT3 (A.U.)
p=0.049
p=0.036
p=0.019
L
M
DAPI IL-6Rα
DAPI IL-6Rα CD31
IL-6 Nuclei
DAPI IL-6rα

Figure 2.10. Evidence for an IL-6, IL6R circuit among tumor, adipose tissue and skeletal muscle in PDAC cachexia. Plasma from no tumor, KPC tumor and KPC IL-6^{KO} tumor mice was harvested immediately prior to euthanasia and measured for IL-6 (**A**) and IL6R (**B**) protein expression using an ELISA. Isolated RNA from quadriceps, epididymal fat, and liver of mice was used to measure mRNA expression of *Il6* (**C**) and *Il6r* (**D**) in tissues and presented as fold change versus no tumor mice. Isolated RNA from KPC and KPC IL-6^{KO} tumors was used to measure mRNA expression of *Il6* (**E**) and *Il6r* (**F**) in tumors and presented as fold change versus KPC tumors. To determine with increased detail the source of *Il6* mRNA in fat and *Il6r* in muscle, tissues were dissociated and isolated RNA from the mononuclear cell fractions (MNC) was used to measure mRNA expression of *Il6* (**G**) and *Il6r* (**H**). Protein expression for IL6R and STAT3 phosphorylation was quantified in the quadriceps and epididymal fat pads of mice using western blotting (**I, J, K**). Immunofluorescence showing the expression of IL6R protein (red) and nuclei (blue, DAPI) in the quadriceps muscle fibers of mice (**L, top**) and IL6R protein (red), the endothelial protein marker CD31 (green) and nuclei (blue, DAPI) to visualize IL6R expression in and around blood vessels in the quadriceps muscle of mice (**L, bottom**). IHC for IL-6 protein expression in the epididymal fat pads of mice (**M, top**) and immunofluorescence showing the expression of IL6R protein (red) and nuclei (blue, DAPI) in epidiymal fat (**M, bottom**); arrows indicate positive IL6R staining and dotted lines outline adipocytes denoted with the letter “a”. Error bars are standard deviation and significant differences between group means are shown in the charts.

2.3.8 Similar Changes to Tissue Wasting and Il6 and Il6r mRNA Expression are Observed with In Vitro Studies of the Tumor-Adipose-Muscle Crosstalk

My results indicate that KPC tumors increase lipid accumulation, *Il6r* expression, and atrophy in skeletal muscle, and also activate lipolysis and *Il6* expression in fat (Figures 2.8-2.10). These effects on distant tissues could be mediated directly by tumor-derived products or indirectly through other cellular or molecular mediators. I tested whether products of KPC cells could affect muscle and fat directly. Indeed, KPC conditioned media (CM) was associated with myotube atrophy (Figure 2.11 A) and similar to in vivo results, increased *Il6* and *Il6ra* mRNA expression was observed in myotubes after KPC CM treatment (Figure 2.11 B). KPC CM also increased 3T3L1 adipocyte lipolysis as measured by media glycerol concentration (Figure 2.11 C) and again, in parallel with my in vivo results, *Il6* but not *Il6ra* mRNA expression was increased in 3T3L1 adipocytes after treatment with KPC CM (Figure 2.11 D).

KPC tumor-induced fat wasting produced increased circulating fatty acids and glycerol in vivo (Figure 2.9 B and 2.9 C). Moreover, increased *Il6r* mRNA expression was increased in muscle but IL6R protein was increased in fat. Extracellular lipids have been implicated in muscle dysfunction in diabetes and metabolic syndrome, and muscle IL6R expression, but the effects in PDAC cachexia are not described. I modeled the effect of the tumor-fat-muscle crosstalk axis in vitro using a series of CM swapping experiments. 3T3L1 adipocytes were treated using KPC CM to induce lipolysis and the resulting 3T3L1 CM was then used to treat myotubes and measure the effects on myotube

diameter. Myotubes treated with CM from 3T3L1 adipocytes after KPC CM treatment showed significant decrease in myotube diameter (Figure 2.11 E). To investigate the tumor-muscle-fat crosstalk axis, I treated C2C12 myotubes with KPC CM to induce atrophy and used the resulting C2C12 CM to treat 3T3L1 adipocytes. Treatment of 3T3L1 adipocytes with C2C12 myotube CM after KPC CM treatment significantly induced lipolysis, which was determined by glycerol release into the media (Figure 2.11 F). Finally, I investigated whether physiological concentrations of IL-6, IL-6R or the combination could induce wasting in both myotubes and adipocytes. Myotube diameter was decreased in the presence of IL-6 (300 pg/mL) or IL6R (25 ng/mL) versus controls, however, the combination of IL-6 and IL6R produced the most severe myotube atrophy (Figure 2.11 G). Interestingly, IL-6 treatment of 3T3L1 adipocytes using physiological levels did not induce lipolysis, yet presence of the IL6R was sufficient to induce lipolysis with or without exogenous IL-6 (Figure 2.11 H). These results suggest that adipocytes are likely more sensitive to lipolysis in the presence of the IL6R and not IL-6 alone. These findings also support that IL-6 and lipids can both mediate muscle loss, and further, that activation of adipose lipolysis likely contributes to muscle wasting in PDAC.

Figure 2.11

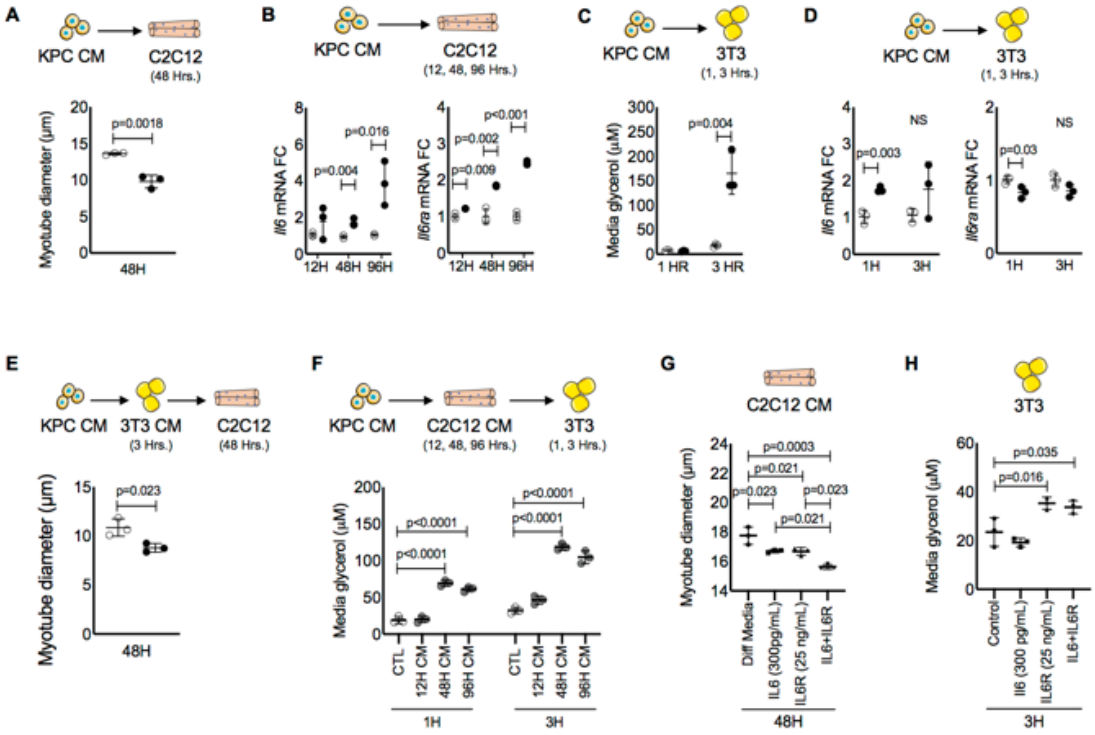
A
KPC CM
C2C12
(48 Hrs.)
Myotube diameter (μm)
p=0.0018
48H
B
KPC CM
C2C12
(12, 48, 96 Hrs.)
Il6 mRNA FC
p=0.004
p=0.016
12H 48H 96H
Il6ra mRNA FC
p=0.009
p=0.002
p<0.001
12H 48H 96H
C
KPC CM
3T3
(1, 3 Hrs.)
Media glycerol (μM)
p=0.004
1 HR 3 HR
D
KPC CM
3T3
(1, 3 Hrs.)
Il6 mRNA FC
p=0.003
NS
1H 3H
Il6ra mRNA FC
p=0.03
NS
1H 3H
E
KPC CM 3T3 CM C2C12
(3 Hrs.) (48 Hrs.)
Myotube diameter (μm)
p=0.023
48H
F
KPC CM C2C12 CM 3T3
(12, 48, 96 Hrs.) (1, 3 Hrs.)
Media glycerol (μM)
p<0.0001
p<0.0001
p<0.0001
p<0.0001
CTL 12H CM 48H CM 96H CM
1H
CTL 12H CM 48H CM 96H CM
3H
G
C2C12 CM
Myotube diameter (μm)
p=0.0003
p=0.021
p=0.023
p=0.023
p=0.021
Diff Media
Il6 (300pg/mL)
Il6R (25 ng/mL)
Il6+Il6R
48H
H
3T3
Media glycerol (μM)
p=0.035
p=0.016
Control
Il6 (300 pg/mL)
Il6R (25 ng/mL)
Il6+Il6R
3H

Figure 2.11. Modeling of IL-6, IL6R tumor-tissue crosstalk in vitro. C2C12 myotubes were incubated with conditioned media (CM) from KPC tumor cells for 48 hours and atrophy measured (**A**) and for 12, 24 and 96 hours and isolated RNA was used to measure mRNA expression of *Il6* and Il6r at each time point (**B**). 3T3 adipocytes were incubated with KPC CM for one and three hours and glycerol was measured as a marker for lipolysis (**C**); 3T3 adipocyte RNA was harvested at each time point and used to measure mRNA expression of *Il6* and *Il6r* (**D**). The tumor-fat-muscle crosstalk was investigated by incubating 3T3 adipocytes with KPC CM and then using the 3T3 CM to treat myotubes for 48 hours and measure atrophy (**E**). The tumor-muscle-fat crosstalk was investigated by treating myotubes for 12, 24 and 96 hours with KPC CM and then using the myotube CM to treat 3T3 adipocytes for 1 and 3 hours to measure lipolysis via media glycerol content (**F**). To decipher the effects of IL-6 and IL-6R in muscle and fat, myotubes and adipocytes were treated in vitro. Myotubes were incubated with differentiation media (DM), physiological levels of recombinant murine IL-6, physiological levels of recombinant murine IL6R, or the combination of IL-6 and IL6R for 48 hours and atrophy measured (**G**). 3T3 adipocytes were incubated with growth media (Control), physiological levels of recombinant murine IL-6, physiological levels of recombinant murine IL6R, or the combination of IL-6 and IL6R for 3 hours and media glycerol measured (**H**). Significant differences are shown in each chart.

2.4 Summary

Here I demonstrate novel tumor-tissue crosstalk in the macroenvironment of PDAC cachexia and further provide evidence of central roles for tumor cell-derived IL-6 and IL-6 trans-signaling. In KPC tumor mice, both tumor cells and stromal cells in the tumor microenvironment produced IL-6; this signal was amplified distantly by production of IL-6 from adipose tissue and likely also in part from skeletal muscle in the “tumor macroenvironment” of the whole host body. Adipose tissue loss was proportionate to circulating IL-6 and halved by elimination of IL-6 from tumor cells, while muscle loss was abolished by tumor-cell depletion of IL-6.

These results indicate that adipose tissue was proportionately more sensitive to the effects of PDAC as measured by the induction of adipose wasting, lipolysis, and release of fatty acids and glycerol into the blood. Under these conditions, skeletal muscle exhibited steatosis, mitochondrial dysfunction, metabolic impairment, and wasting. As well, *Il6r* mRNA expression was increased by PDAC only in muscle and not fat, yet sIL6R protein accumulated in fat, and STAT3 phosphorylation indicated signaling in both peripheral tissue compartments. In vitro experiments showed similar Il6 and *Il6r* mRNA expression in muscle and fat cells after treatment with KPC CM. I also demonstrate that products of lipolysis (modeled with 3T3 CM after exposure to KPC CM) exacerbate muscle wasting and that products of muscle atrophy (modeled with C2C12 CM after exposure to KPC CM) can promote lipolysis. These results suggest that sIL6R is produced outside adipose tissue but accumulates in fat to

mediate IL-6 signaling and lipolysis in adipocytes and further, that skeletal muscle is a major source of this sIL6R in cachexia. Thus, providing an explanation of how adipose and muscle crosstalk in the presence of a tumor can augment wasting in each tissue (Figure 2.12)

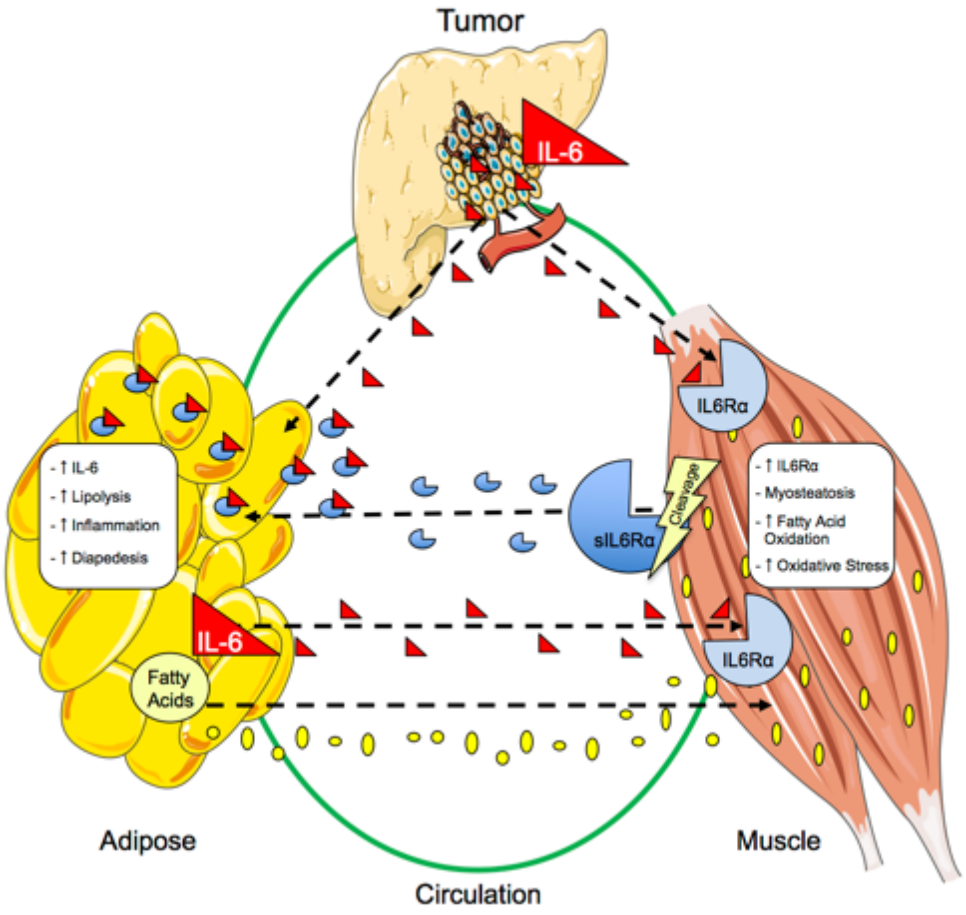

Figure 2.12. Illustration of tumor-fat-muscle crosstalk in PDAC. Using my results this illustration summarizes my findings with respect to tumor, fat and muscle crosstalk in PDAC. Tumor cell-derived IL-6 affects both muscle and fat, leading to increases in fat and muscle wasting concomitantly with elevated circulating fatty acids. Increased circulating fatty acids promote myosteatosis, which is associated with increased oxidative stress in muscle. Increased IL6R production from muscle contributes to circulating levels of sIL6R to augment fat wasting. Therefore, in the presence of a tumor, muscle and fat act in a feed forward mechanism to augment cachexia.

CHAPTER 3: THE EFFECTS OF TUMOR-DERIVED IL-6 ON MUSCLE METABOLISM

3.1 Overview

Cachexia is associated with significantly altered muscle metabolism adding another stressor to the milieu of factors contributing to muscle wasting. Changes to metabolism modify energy demands in the tissue. Resting energy demand in approximately 50% of patients with cancer cachexia was increased by more than 100% of predicted values (Bosaeus, Daneryd, Svanberg, & Lundholm, 2001). With increased resting energy expenditure, it is conceivable that diet alone may be inadequate for sufficient energy and must be supplemented through the breakdown of host tissues, the direct phenotype defined by cachexia. Skeletal muscle and adipose tissues are both nutrient dense, where fat is a prime source for lipids and muscle a main source of amino acids. Among the amino acids, branch chain amino acids (BCAAs) are essential for anabolic processes. BCAAs are usually obtained from the diet however, during times of nutrient deprivation or disease, BCAAs can come from the catabolism of skeletal muscle (Cahill & Aoki, 1971). Changes in BCAA levels in muscle and plasma have been reported during cachexia (Eley, Russell, & Tisdale, 2007; O'Connell, 2013).

Lipid metabolism is a crucial process for skeletal muscle metabolic homeostasis. Robust changes in gene expression of lipolytic and lipogenic pathways are concomitant with myosteatosis observed in muscle from KPC tumor-bearing mice (Figure 2.5), suggesting severe dysfunction of lipid

metabolism in muscle during PDAC. Alterations in both glucose and lipid metabolism in muscle can influence downstream processes including the TCA cycle and the ETC in mitochondria. For instance, during normal carbohydrate metabolism PDH enables glucose-derived pyruvate, to enter the TCA cycle for complete oxidation. However, if Akt activation is reduced, Pdk4 expression can increase as a result of increased activation of FOXO transcription factors, leading to inhibition of PDH and a shift toward FAO to generate ATP. Indeed, excessive FAs can overwhelm and exhaust the mitochondria in muscle, leading to myosteatosis, mitophagy and reduced efficiency of mitochondrial metabolism. Evidence for these exists in Figure 2.8 where aberrant SDH reaction patterning was observed, indicating dysfunctional mitochondria localization and reduced oxidative potential. Mitochondrial exhaustion is associated with incomplete FAO. This occurs when oxidation of FA begins in mitochondria but due to insufficient levels of CoA and FAD, mitochondria cannot complete this process. This situation of “mitochondrial overload” can be characterized by elevated levels of medium and short chain acyl-carnitines (Muoio & Koves, 2007; Muoio & Neufer, 2012). Thus, illustrating the delicate balance between glucose and fatty acid metabolic pathways, mitochondria dysfunction and atrophy in skeletal muscle.

Deletion of tumor cell-derived IL-6 resulted in reduced inflammation, attenuated fat wasting and decreased myosteatosis (Chapter 2). This suggests the influence of tumor IL-6 on inflammation and adipose lipolysis may play a major role in muscle dysmetabolism, especially regarding the accumulation of lipids, in PDAC cachexia. Therefore, I aim to investigate the alterations and

interplay of BCAA metabolism, FAO, and glycolysis in skeletal muscle during PDAC associated cachexia. Furthermore, I report the effects of deleting tumor cell-derived IL-6 on these metabolic pathways.

3.2 Materials and Methods

3.2.1 Animal Models

Tissue for metabolic analyses was obtained from mice used in experiments described in Chapter 2. For animal use, euthanasia and skeletal muscle excision please refer to the relevant methods reported in Chapter 2.

3.2.2 Sample Preparation for NMR

Plasma samples for NMR analysis were prepared diluting 100 ml of plasma with 500 ml of deuterated phosphate buffer solution (pH = 7.4) containing 2,2,-dimethyl-2-silapentane-5-sulfonate sodium salt (DSS) with a final concentration of 0.5 mM to be used as a chemical shift and quantitation reference. The solution was then filtered through a 10 KDa, molecular weight cutoff filter to remove the proteins. Samples were placed in 5 mm NMR tube for analysis. Gastrocnemius muscle tissues for NMR analysis were prepared according to the methanol/chloroform water procedure described by Beckonert *et. al*. (Beckonert et al., 2007). Tissue samples of approximately 100 mgs were used for all samples, but actual weights were recorded to normalize the data.

3.2.3 Sample Preparation for Mass Spectrometry

Samples for targeted mass spectrometry analysis were conducted using the Biocrates Absolute IDQ kit (Biocrates, Innsbruck, Austria). Each plate contains 16 wells reserved for selected internal standards to optimize the metabolite quantification. For serum analysis, 10 ml aliquots were loaded directly into the 96 well plate followed by derivatization and extraction per vendor protocols. Muscle tissue was prepared according to vendor protocols (Biocrates, *Preparation of Tissue and Feces Samples for Metabolic Phenotyping*, version 1.0).

3.2.4 NMR Data Collection

NMR data were acquired on a Bruker Advance III 700MHz NMR spectrometer with a TXI triple resonance probe operating at 25C. Spectra were collected with a 1D NOESY pulse sequence covering 12 ppm. The spectra were digitized with 32768 points during a 3.9 second acquisition time. The mixing time was set to 100 ms and the relaxation delay between scans was set to 2.0 seconds.

3.2.5 NMR Data Processing

The data were processed using Advanced Chemistry Development Spectrus Processor (version 2016.1, Toronto, Canada). The spectra were zero filled to 65536 points, apodized using a 0.3Hz decaying exponential function and fast Fourier transformed. Automated phase correction and 3rd order polynomial

baseline correction was applied to all samples. Metabolite concentrations were quantified using the Chenomx NMR Suite (version 8.2, Edmonton, Canada). The DSS-d_6 was used as a chemical shift and quantification reference for all spectra and was set to a chemical shift of 0.00 and a concentration of 500 μM. Quantitative fitting of each spectrum was carried out in batch mode, followed by manual adjustment for some spectra to correct for errors arising from spectral overlap. For tissue samples, the final concentrations were normalized based on the weight of the tissue used to prepare each sample. The quantification of glycogen in muscle and liver tissue was carried out using spectral integration rather than spectral fitting with the Chenomx software. As glycogen is a heterogeneous polysaccharide of different chain lengths, the NMR signals are composed of overlapping peaks in specific windows of the spectrum. The integration range from 5.37 to 5.43 ppm was used and the concentrations are given in spectral intensity units.

3.2.6 Mass Spectrometry Data Collection

This Biocrates AbsoluteIDQ p180 assay quantifies 188 metabolites from five chemical classes: acylcarnitines, amino acids, biogenic amines, hexoses (sum of hexoses), PCs, and sphingomyelins (SMs). Data were collected on an AB Sciex 4000 QTRAP coupled to an Acquity UPLC system with the selective mass-spectrometric detection using multiple reaction monitoring (MRM) pairs. The amino acids and biogenic amines were detected using and LC-MS/MS

method and the lipid species were detected using a flow injection analysis (FIA) MS/MS method per vendor-defined settings.

3.2.7 Mass Spectrometry Data Analysis

Data analysis including normalization (tissue weight) for quantification of metabolite concentrations and quality assessment were performed with the MetIDQ software package, which is an integral part of the AbsoluteIDQ kit. The metabolite concentration of each metabolite in each experimental condition was compared with the measurement detection limit specifications as reported by the manufacturer of the AbsoluteIDQ p180 kit (Biocrates). A metabolite was excluded from further analyses if its concentration measurement data did not meet all of the following criteria: (1) minor of 20% of missing values (non-detectable peak) for each quantified metabolite in each experimental group (2) 50% of all measured sample concentrations for the metabolite had to be above the limit of detection (LOD).

3.2.8 Western Blotting

Tissue protein lysates were made by homogenizing snap frozen tissue in ice cold RIPA buffer (Harlow & Lane, 2006) using a Polytron PT 10/35 homogenizer with PCU 11 controller (Kinematica; Luzern, Switzerland). Protein lysate concentration was measured using the Pierce™ BCA Protein Assay Kit (PI23228, Thermo Scientific; Waltham, MA USA). Protein lysate was then added 1:1 to 2X sample buffer (125 mM Tris; pH 6.8, 4% (w/v) SDS, 20% glycerol, 100

mM DTT, 0.02% (w/v) bromophenol blue) and heated at 95˚C for five minutes. Proteins were then separated via SDS-PAGE by loading 30 μg of protein from each sample into wells on a 4-15% Criterion™ TGX™ gel (5671084, Bio-Rad; Hercules, CA, USA) in running buffer (25 mM Tris, 192 mM glycine, 0.1% SDS) at 140 volts for one hour using a Power Pac HC (Bio-Rad; Hercules, CA, USA). The proteins were transferred to 0.2μm nitrocellulose membranes (1620233, Bio-Rad; Hercules, CA, USA) in ice-cold transfer buffer (25 mM Tris, 192 mM glycine, 20% (v/v) methanol, pH 8.3) at 100 volts for thirty minutes. Membranes were blocked using Sea Block (37527, Thermo Scientific; Waltham, MA USA) for one hour at room temperature on a shaker table. Proteins were detected using antigen specific primary antibodies, anti-Pdk4 (ab214938, Abcam; Cambridge, MA, USA) diluted 1:1000 in Sea block with 0.1% Tween 20 (BP337-500, Fisher Scientific; Waltham, MA USA) and incubated with the membranes overnight at 4°C. Membranes were then washed twice with PBS and primary antibodies were visualized using florescent DyLight™ secondary antibodies (Cell Signaling; Danvers, MA, USA) with specificity against the primary antibodies and imaged on an Odyssey CLx (LiCor; Lincoln, NE, USA). The quantification of target proteins was done by normalizing target protein expression to the loading control protein expression (α-tubulin) specific to each membrane using Image Studio version 4.0 (LiCor; Lincoln, NE, USA). Normalized protein expression was then presented as fold-change versus no tumor bearing mice.

3.2.9 Gene Expression Analyses

Evaluation of gene expression was performed using fold-change as measured in the RNA sequencing analyses described in Chapter 2.2.10. For mRNA extraction refer to the relevant methods in Chapter 2.2.10. Differentially expressed genes were selected as having a fold-change of ≥1.5 and an FDR of ≤ 0.05. Differentially expressed genes were then analyzed using Ingenuity Pathway Analysis (IPA) to determine specific changes in known metabolic pathways. Gene expression was referenced against established metabolic signaling networks contained within the IPA software.

3.2.10 Statistical Analysis

Statistical comparison of metabolites for each of the groups was carried out in GraphPad Prism (GraphPad, La Jolla, CA) using a one-way ANOVA with Tukey's multiple comparison test. Protein expression as measured by western blotting was compared between groups using a one-way ANOVA with Tukey's multiple comparison test. Please refer to the statistical analysis in the methods section of Chapter 2.2.10 for detailed analysis of RNA-sequencing. Briefly, differential expression analysis was performed using edgeR and the false discovery rate (FDR) was computed from p-values using the Benjamini-Hochberg procedure. Differentially expressed genes were determined as having a fold change of ≥1.5 and an FDR of ≤ 0.05.

3.3 Results

3.3.1 Deletion of Tumor Cell-derived IL-6 Mitigates Changes to Global Metabolic Expression Profiles in Plasma

A representation of the overall changes to the metabolic expression profiles in plasma from KPC and KPC IL-6^{KO} tumor-bearing mice versus no tumor mice are depicted in the heatmap in Figure 3.1. The serum metabolite data presented in Figure 3.1 quantifies 187 metabolites from the targeted MS panel and 31 metabolites included in the NMR platform. Data are presented as Z-scores with K-nearest neighbor clustering. These results show significant changes in metabolite levels in mice bearing KPC tumors, while metabolite levels in KPC IL-6^{KO} tumor-bearing mice more closely resemble those of mice without tumors (Figure 3.1). In the following analyses, I present metabolomic and gene expression data representing the most severely affected metabolic pathways in KPC tumor-bearing mice.

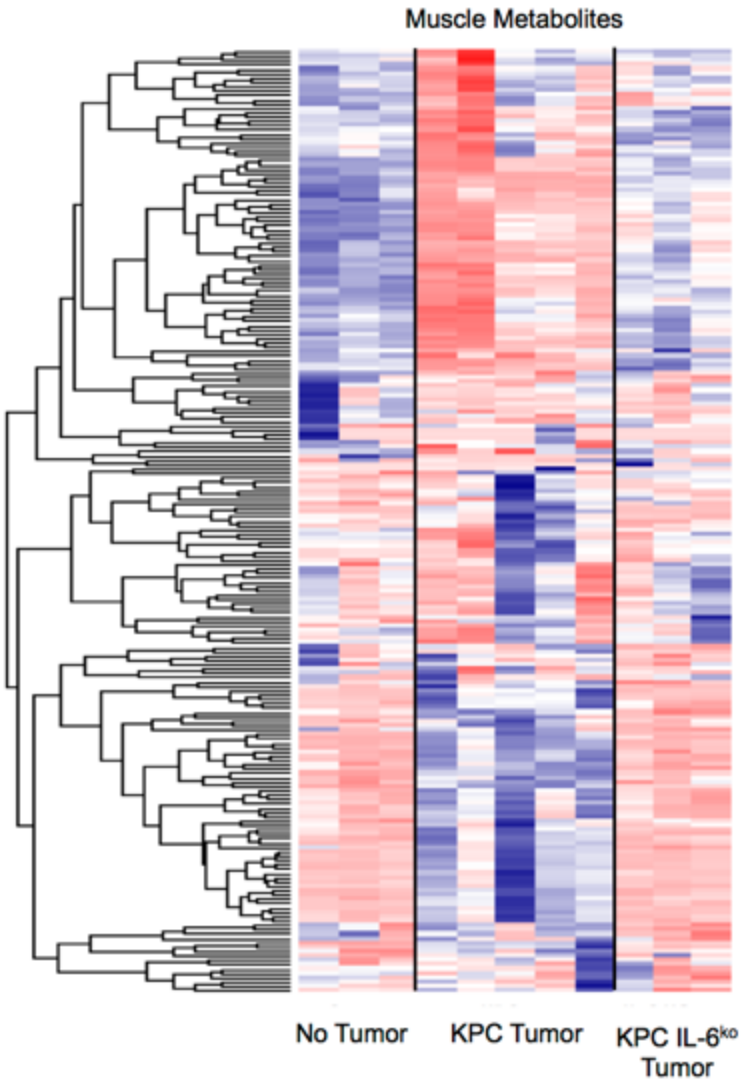

Figure 3.1. Deletion of tumor cell-derived IL-6 mitigates changes to plasma metabolites. Overall assessment of plasma metabolites in No Tumor, KPC Tumor and KPC IL-6^{KO} Tumor bearing mice. Increased metabolite expression (red) and decreased metabolite expression (blue) are presented as a comparison against the No Tumor group. The heat map illustrates 187 metabolites.

3.3.2 Tumor Cell-derived IL-6 is Associated with Increased BCAA Oxidation in Skeletal Muscle

In cachexia, changes to BCAA oxidation in muscle have been reported in the presence of tumors. Therefore, I investigated the BCAA oxidation pathway in skeletal muscle of mice with PDAC. BCAA oxidation requires the coordination of multiple signaling pathways including activation of the ubiquitin/proteasome pathway for the degradation of large peptides and the activation of the branched-chain alpha-keto acid dehydrogenase complex (BCKDH) for oxidation of BCAAs into acetyl-CoA and succinyl-CoA for use in the TCA cycle (Figure 3.2 A). The E3 ligase muscle RING-finger protein-1(Murf1) encoded by the Trim63 gene plays a crucial role in the poly-ubiquitination of peptides targeting them for degradation in the proteasome (Figure 3.2 A). The subunits Bckdha and Bckdhb are components of the BCKDH and activation of the branched chain keto acid dehydrogenase kinase (Bckdk) inhibits function of the BCKDH (Figure 3.2 A). BCAA quantification in plasma (Figure 3.2 B) and muscle (Figure 3.2 C) showed increases in all three (leucine, isoleucine and valine) BCAA in both plasma and muscle of KPC tumor bearing mice versus no tumor mice. No significant increase in BCAAs was observed in plasma or muscle of KPC IL-6^{KO} tumor bearing mice (Figure 3.2 B and 3.2 C).

Ingenuity Pathway Analysis (IPA) in combination with previously obtained RNA-sequencing data (Chapter 2) from this tumor model revealed significant alterations to pathways involved in BCAA metabolism and amino acid transport in muscle of KPC tumor mice. Differential expression of genes involved in BCAA

metabolism was observed including down-regulation of *Bckdk* and up-regulation of *Trim63*, *Bckdha*, and *Bckdhb* (Figure 3.2 D). Additionally, two of three genes identified in the BCAA transport pathway were up regulated (Figure 3.2 E). Multiple down-regulated (Figure 3.2 F, top) and up-regulated (Figure 3.2 F, bottom) genes important in amino acid transport were identified. Transportation of amino acids involves additional chaperone and membrane transporter proteins. Genes encoding these proteins were also differentially expressed in muscle from KPC tumor mice (Figure 3.2 G).

Figure 3.2

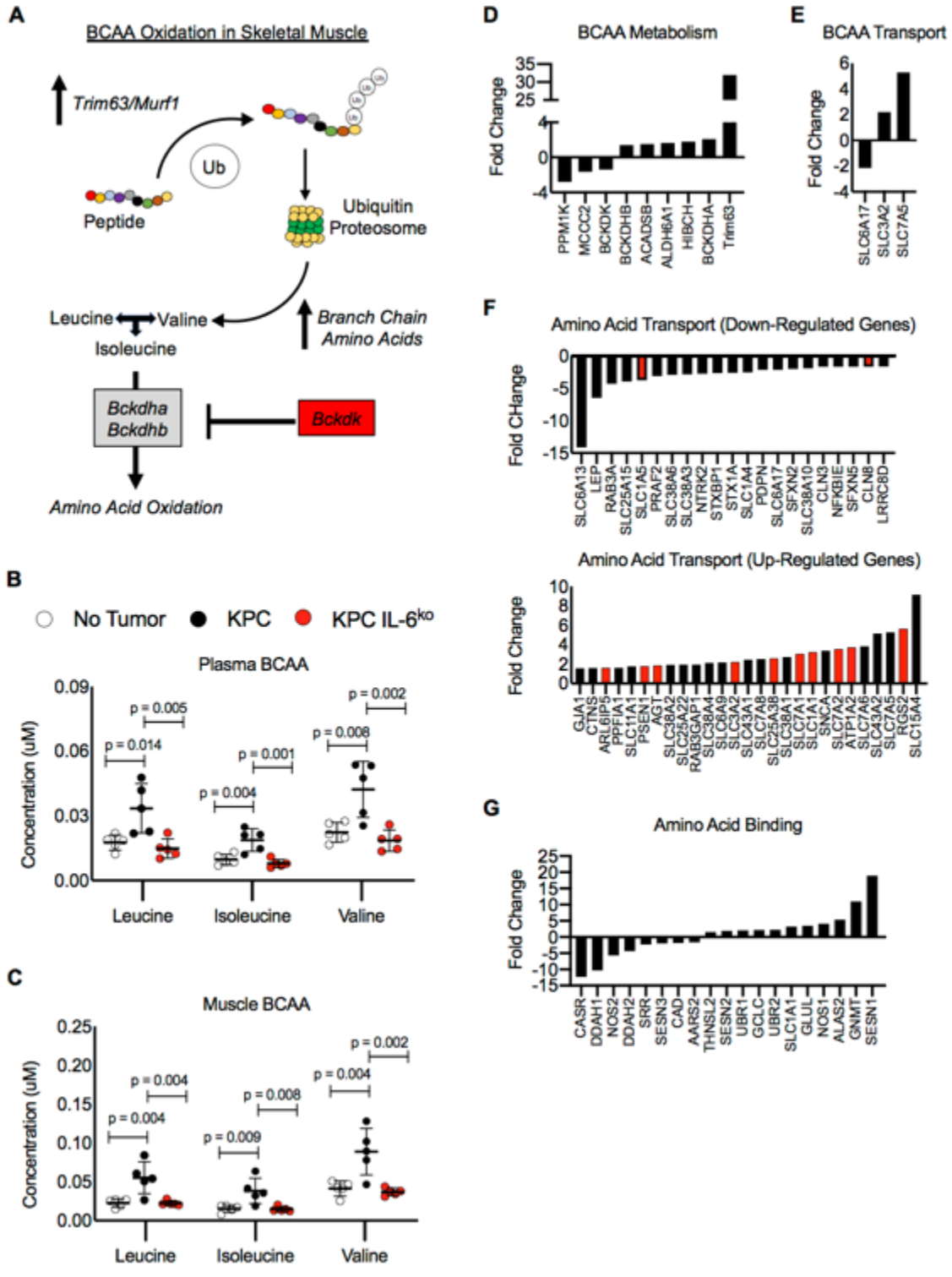
A
BCAA Oxidation in Skeletal Muscle
Trim63/Murf1
Ub
Peptide
Ubiquitin
Proteosome
Leucine
Valine
Isoleucine
Branch Chain
Amino Acids
Bckdha
Bckdhb
Bckdk
Amino Acid Oxidation
B
No Tumor
KPC
KPC IL-6ko
Plasma BCAA
Concentration (uM)
Leucine
Isoleucine
Valine
C
Muscle BCAA
Concentration (uM)
Leucine
Isoleucine
Valine
D
BCAA Metabolism
Fold Change
PPM1K
MCCC2
BCKDK
BCKDHB
ACADSB
ALDH6A1
HIBCH
BCKDHA
Trim63
E
BCAA Transport
Fold Change
SLC6A17
SLC3A2
SLC7A5
F
Amino Acid Transport (Down-Regulated Genes)
Fold Change
Amino Acid Transport (Up-Regulated Genes)
Fold Change
G
Amino Acid Binding
Fold Change

Figure 3.2 BCAA oxidation is increased in the muscle of KPC tumor mice. Key molecules in the ubiquitin proteasome mediated catabolism of proteins and the oxidation of BCAAs (leucine, isoleucine and valine) are depicted (**A**). Plasma and muscle BCAAs were measured (**B and C**). Using previously obtained RNAseq data from these mice, differentially expressed genes(DEG) (fold-change ≥ 1.5 and FDR ≤ 0.05) were referenced against curated pathway gene sets from the Gene Set Enrichment Analysis (GSEA) database and DEG genes involved in BCAA metabolism (**D**), BCAA transport (**E**), amino acid transport (**F**) and amino acid binding (**G**) are shown. Bars shaded red indicate genes coding for transmembrane proteins (**F**). Statistical differences are depicted in the charts.

3.3.3 Glucose Oxidation and TCA Cycle Activity are Decreased in KPC Tumor Mice

Pyruvate sits at a metabolic nexus where it can be reduced to lactate with the formation of NAD+ or it can enter the TCA cycle to complete the oxidative process. Increased lactate formation can occur during conditions of impaired glucose regulation, which is associated with myosteatosis. Therefore, I investigated changes in the concentrations of glucose, pyruvate, and lactate in plasma and skeletal muscle concomitant with determination of changes to relevant gene expressions in the glycolysis pathway. Using the IPA established glycolysis pathway, a number of key enzymes in glycolysis had altered activity in the muscle of KPC tumor-bearing mice. Specifically, in the muscle of KPC tumor-bearing mice, increases in glucose-6-phosphate and fructose-bisphosphate aldolase activity were identified (Figure 3.3 A), while decreased activity of triose-phosphate isomerase, phosphoglycerate mutase, and phophospyruvate hydratase were predicted (Figure 3.3 A). Multiple genes were also identified as directly or indirectly interacting with these intermediates (Figure 3.3 A) These changes were almost eliminated when IL-6 was deleted from the tumor however, expression of the thyroid hormone responsive (*Thrsp)* gene was significantly decreased in both KPC and KPC IL-6^{KO} (Figure 3.3 A and 3.3 B). Interestingly, this gene is involved in regulating lipogenesis and the synthesis of triacylglycerol from medium length fatty acids. Plasma glucose was decreased in both KPC and KPC IL-6^{KO} tumor mice (Figure 3.3 C) and decreased plasma pyruvate was only observed in KPC versus KPC IL-6^{KO} tumor mice (Figure 3.3 C), while plasma

lactate was only decreased in the KPC IL-6^{KO} group (Figure 3.3 C). Muscle lactate was only increased in KPC tumor mice (Figure 3.3 D).

The interactions between carbohydrate and fatty acid metabolism in muscle are regulated by the pyruvate dehydrogenase (PDH) complex and the pyruvate dehydrogenase kinase (PDK). In muscle, Pdk4 is the predominant isoform and when increased, inhibits PDH activity, resulting in impaired mitochondrial oxidation of glucose and a shift toward increased reliance on FAO to fuel the TCA cycle. The subunit Pdha is a crucial component of the PDH complex and encoded by the *Pdha* gene. In muscle of KPC tumor mice, *Pdha* expression was significantly decreased (-1.28-fold) while expression of the *Pdk4* gene was increased (12.13-fold) versus no tumor mice. Furthermore, muscle Pdk4 protein expression was increased in KPC tumor mice alone (Figure 3.3 E and 3.3 F). These results suggest that glycolysis in muscle is significantly affected by the presence of a tumor and glucose oxidation is likely decreased with downstream effects on TCA cycle function.

Figure 3.3

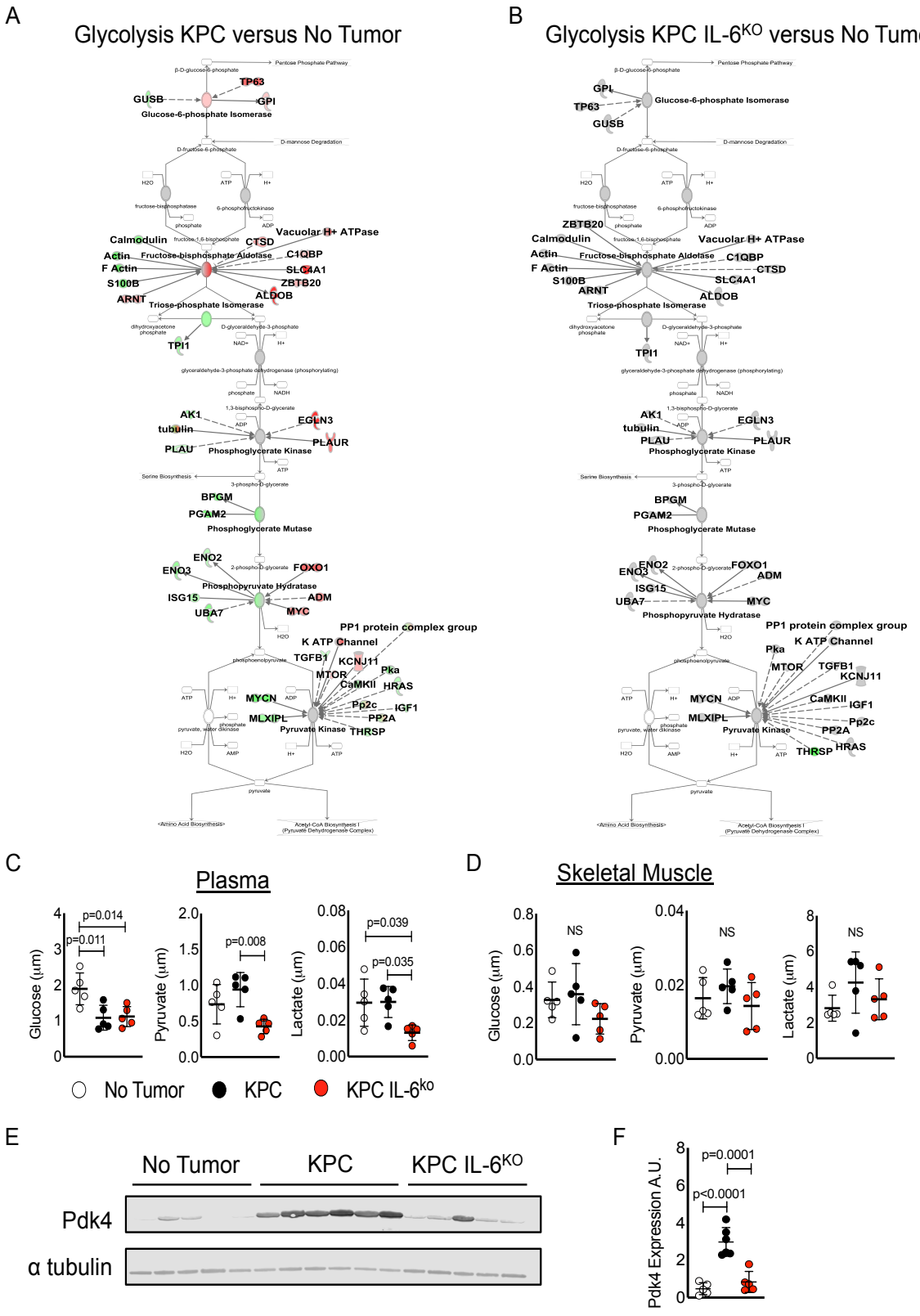
A
Glycolysis KPC versus No Tumor
B
Glycolysis KPC IL-6KO versus No Tumor
C
Plasma
Glucose (µm)
Pyruvate (µm)
Lactate (µm)
p=0.014
p=0.011
p=0.008
p=0.039
p=0.035
No Tumor
KPC
KPC IL-6ko
D
Skeletal Muscle
NS
E
No Tumor
KPC
KPC IL-6KO
Pdk4
α tubulin
F
Pdk4 Expression A.U.
p=0.0001
p<0.0001

Figure 3.3 Glycolysis is altered in the muscle of KPC tumor mice. Ingenuity Pathway Analysis (IPA) was used to analyze the glycolysis pathway using my previously obtained RNAseq data in muscle. Multiple molecules important in glycolysis were predicted to be differentially regulated in the muscle of KPC tumor mice (**A**) and these molecules were unchanged in the muscle of KPC IL-6^{KO} tumor mice (**B**). The metabolites Glucose, pyruvate and lactate are involved in glycolysis and were measured in plasma (**C**) and muscle (**D**) in mice. Pyruvate dehydrogenase kinase 4 (Pdk4) is a key regulator of the pyruvate dehydrogenase complex (PDH), which activation or inhibition of PDH determines the fate of pyruvate oxidation and acetyl-CoA production. Pdk4 protein expression in the muscle of mice was measured using western blotting (**E and F**). Error bars are standard deviation and significant differences are shown in the charts.

3.3.4 KPC Tumor Mice have reduced TCA cycle activity and decreases in key metabolites important for TCA cycle function.

Metabolomic analysis of key TCA cycle intermediates revealed differences in citrate, succinate, fumurate and malate. In plasma, acetate, fumurate and malate were significantly decreased in both KPC and KPC IL-6^{KO} tumor groups (Figure 3.4 A, 3.4 D, and 3.4 E). Plasma citrate was increased in the KPC tumor group alone (Figure 3.4 B). There were no changes observed in succinate levels in either group (Figure 3.4 C). Interestingly, while changes in plasma metabolites were measured, skeletal muscle metabolite levels remained largely unchanged (Figure 3.4 A-E). To determine if key enzymes important for TCA cycle function were affected, RNA-sequencing data were cross-referenced with the established TCA cycle pathway genes in IPA. While aconitate hydratase (also known as aconitase) was unchanged, the majority of genes involved in its activity were down regulated in muscle from KPC tumor-bearing mice (Figure 3.4 F). In KPC tumor-bearing mice, decreased activity was predicted for isocitrate dehydrogenase and succinate dehydrogenase in muscle concomitantly with decreased expression of genes involved in the activity of these enzymes (Figure 3.4 F). Interestingly, an increase in 2-ketogluturate dehydrogenase complex was predicted to be increased in muscle from KPC tumor-bearing mice (Figure 3.4 F). These changes were ultimately absent in the KPC IL-6^{KO} tumor group (Figure 3.4 G).

Figure 3.4

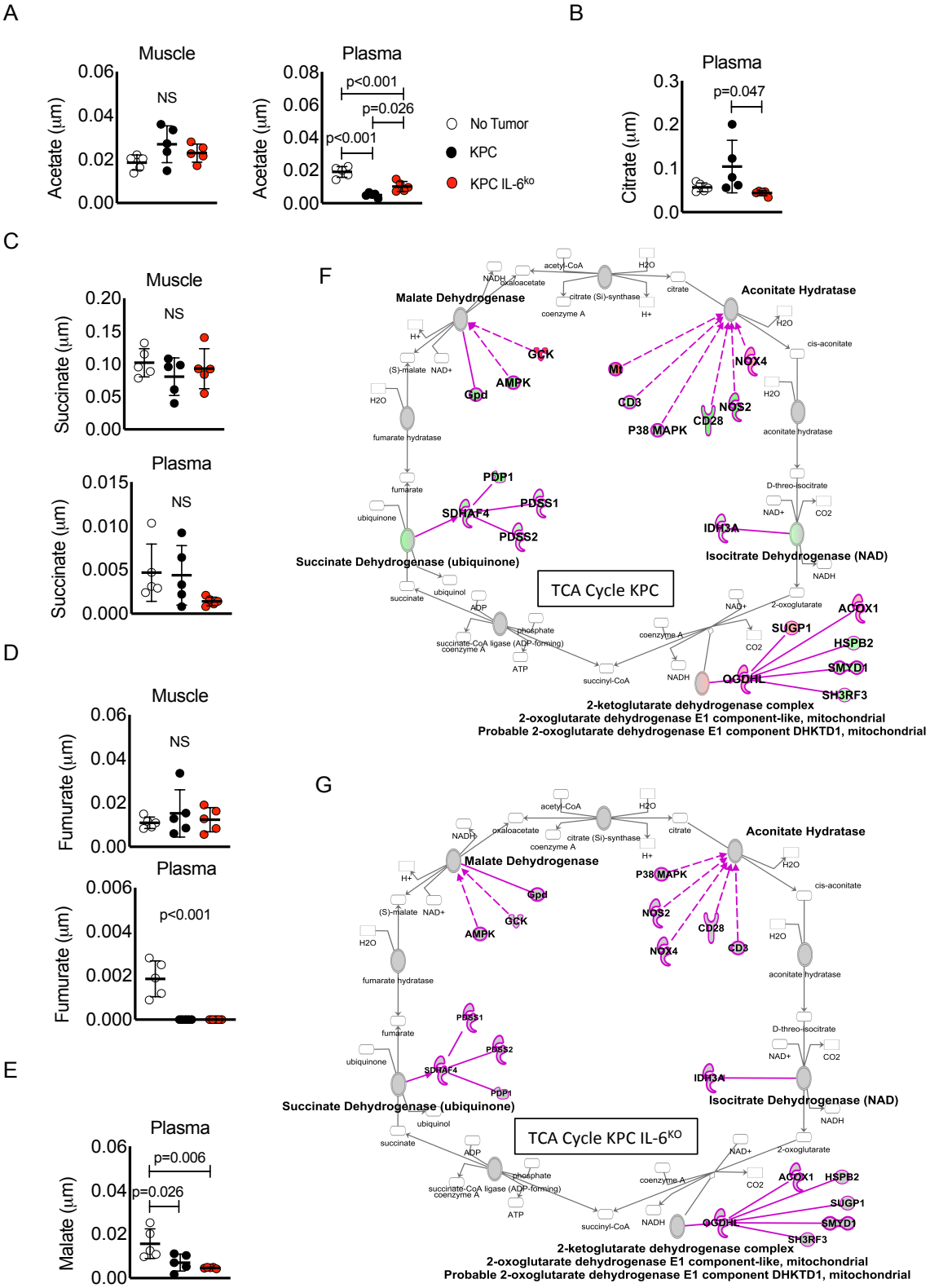
A
Muscle
Acetate (μm)
NS
Plasma
p<0.001
p=0.026
p<0.001
No Tumor
KPC
KPC IL-6ko
B
Plasma
Citrate (μm)
p=0.047
C
Muscle
Succinate (μm)
NS
Plasma
NS
D
Muscle
Fumarate (μm)
NS
Plasma
p<0.001
E
Plasma
Malate (μm)
p=0.006
p=0.026
F
Malate Dehydrogenase
Aconitate Hydratase
Succinate Dehydrogenase (ubiquinone)
Isocitrate Dehydrogenase (NAD)
TCA Cycle KPC
2-ketoglutarate dehydrogenase complex
2-oxoglutarate dehydrogenase E1 component-like, mitochondrial
Probable 2-oxoglutarate dehydrogenase E1 component DHKTD1, mitochondrial
G
Malate Dehydrogenase
Aconitate Hydratase
Succinate Dehydrogenase (ubiquinone)
Isocitrate Dehydrogenase (NAD)
TCA Cycle KPC IL-6KO
2-ketoglutarate dehydrogenase complex
2-oxoglutarate dehydrogenase E1 component-like, mitochondrial
Probable 2-oxoglutarate dehydrogenase E1 component DHKTD1, mitochondrial

Figure 3.4. Conventional function of the TCA Cycle is significantly changed in the muscle of KPC tumor mice. Intermediate metabolites involved in the TCA Cycle were measured in plasma and muscle (**A-E**). Ingenuity Pathway Analysis (IPA) was used to analyze key molecules in the TCA Cycle using my previously obtained RNAseq data in muscle. Multiple molecules important in TCA Cycle function were predicted to be differentially regulated in the muscle of KPC tumor mice (**F**) and these changes were largely absent in the muscle of KPC IL-6^{KO} tumor mice (**G**). Error bars are standard deviation and differences are depicted within each chart.

3.3.5 KPC Tumor-bearing Mice have Altered Muscle Lipid Metabolism in Association with Accumulation of Acylcarnitines.

The significant loss of adipose tissue and resulting myosteatosis associated with KPC tumors (Chapter 2) is likely contributing to changes in muscle metabolism. To investigate this, I compared gene expression data for known lipid metabolism pathways with measurements of plasma and muscle acylcarnitines. Beta-oxidation was significantly altered in the muscle of KPC tumor-bearing mice, specifically by changes in expression of genes involved in long-chain-fatty-acid-CoA ligase, dodecenoyl-CoA D-isomerase, enoyl-CoA hydratase, and acetyl-CoA C-acyltransferase (Figure 3.5 A). Muscle of KPC IL-6^{KO} did not show any significant changes in the expression of these genes (Figure 3.5 B).

Multiple genes involved in the activity of acyl-CoA synthetase long chain family member 5 (Ascl5) and acyl-CoA synthetase long chain family member 6 (Ascl6), important for triacylglycerol synthesis, were differentially regulated in the muscle of KPC tumor mice (Figure 3.5 C). Again, these changes in gene expression were undetected in muscle from KPC IL-6^{KO} tumor mice (Figure 3.5 D). Acyl-CoA hydrolysis is important for the metabolism of fatty acids and is subsequently affected by changes in lipid metabolism. In the muscle of KPC tumor mice, palmitoyl-CoA hydrolase was significantly altered and changes in gene expression, in particular decreases in *Ces1e*, *Acot11*, *Them4*, *Ppt1* and increases in *Acot2*, *Acot4* gene expression were measured (Figure 3.5 E). Acyl-

CoA hydrolysis was largely unaltered in muscle of KPC IL-6^{KO} tumor mice (Figure 3.5 F).

Finally, measurements of plasma and muscle acylcarnitines supported the changes in gene expression observed in the fatty acid activation and acyl-CoA hydrolysis pathway analyses. KPC tumor mice had elevated acylcarnitines, specifically C4 and C5 and C12-C18 compared to no tumor mice (Figure 3.5 G). In muscle, only the acylcarnitines C5 and C16 were elevated in KPC tumor mice and interestingly, C16 was also increased in KPC IL-6^{KO} tumor mouse muscle when compared against no tumor mice (Figure 3.5 H). The increase in C5 acylcarnitine is expected since BCAA oxidation was also increased and increased C5 acylcarnitine is a prominent marker of BCAA catabolism (Lerin et al., 2016; Newgard, 2017). Taken together, these results show significant alterations to muscle lipid metabolism especially with regards to beta-oxidation and acyl-CoA hydrolysis. These data also suggest that tumor IL-6 augments these changes in muscle metabolism.

Figure 3.5

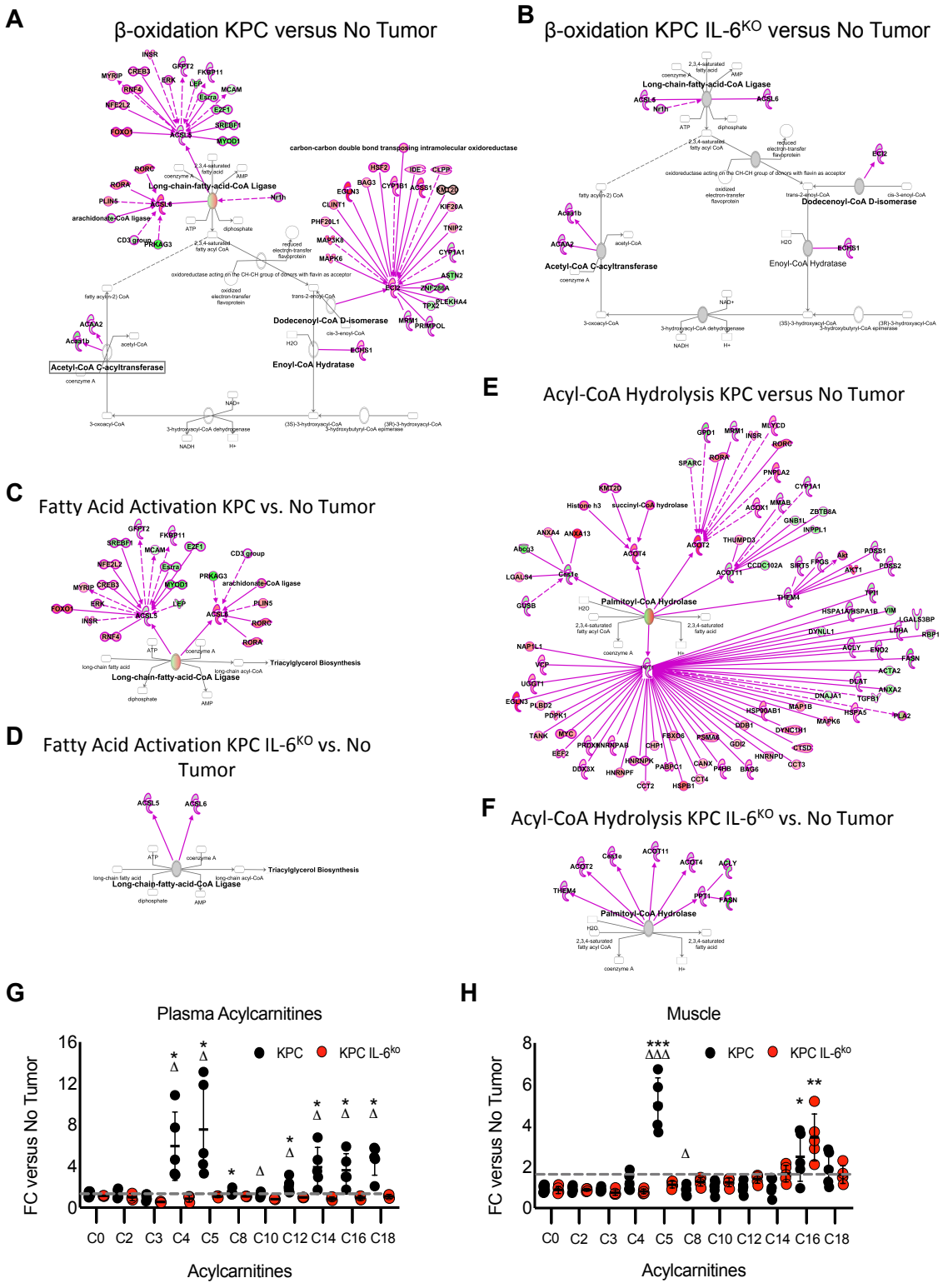
A
β-oxidation KPC versus No Tumor
Long-chain-fatty-acid-CoA Ligase
Acetyl-CoA C-acyltransferase
Dodecenoyl-CoA D-isomerase
Enoyl-CoA Hydratase
B
β-oxidation KPC IL-6KO versus No Tumor
C
Fatty Acid Activation KPC vs. No Tumor
Triacylglycerol Biosynthesis
D
Fatty Acid Activation KPC IL-6KO vs. No Tumor
E
Acyl-CoA Hydrolysis KPC versus No Tumor
Palmitoyl-CoA Hydrolase
F
Acyl-CoA Hydrolysis KPC IL-6KO vs. No Tumor
G
Plasma Acylcarnitines
KPC
KPC IL-6ko
FC versus No Tumor
Acylcarnitines
C0 C2 C3 C4 C5 C8 C10 C12 C14 C16 C18
H
Muscle

Figure 3.5. Lipid metabolism is significantly altered in the muscle of KPC tumor mice. Ingenuity Pathway Analysis (IPA) was used to analyze beta-oxidation (A and B), triacylglycerol synthesis (C and D), and Acyl-CoA hydrolysis (E and F) pathways in the muscle of KPC and KPC IL-6^{KO} tumor mice using my previously obtained RNAseq data. Acylcarnitine levels were measured in plasma (**G**) and muscle (**H**) from KPC and KPC IL-6^{KO} tumor mice and shown as fold change versus no tumor mice (dotted line). Significant differences from no tumor mice are indicated by * and differences from KPC IL-6^{KO} tumor mice are indicated by Δ, where * or Δ is $p<0.05$, ** is $p<0.001$ and *** or $\Delta\Delta\Delta$ is $p<0.0001$. Error bars are standard deviation.

3.4 Summary

Deletion of tumor cell-derived IL-6 mitigated the changes to metabolism observed in KPC tumor mice. Mice bearing KPC tumors had increased protein catabolism as evident from the robust increase in the E3 ubiquitin ligase *Trim63* and elevated BCAAs in both plasma and muscle. Increased BCAAs were also accompanied by changes in expression of genes important for BCAA oxidation and transport. Expression was also altered in genes responsible for the chaperoning and transport of amino acids. These results indicate significant alterations to protein catabolism and BCAA metabolism in skeletal muscle associated with PDAC.

Glycolysis was significantly altered in KPC tumor mice specifically with predicted increases in glucose-6-phosphate isomerase and fructose-bisphosphate aldolase function and decreased function of trios-phosphate isomerase, phosphoglycerate mutase, and phosphopyruvate hydrolase. Changes in gene expression affecting these enzymes were not observed in KPC IL-6^{KO} tumor mice. Furthermore, changes in metabolites associated with glycolysis including glucose, pyruvate and lactate were primarily observed in the plasma of tumor bearing mice. Skeletal muscle lacked any significant changes in these metabolites and remained largely homeostatic across groups. The expression of Pdk4, a primary inhibitor of the PDH complex, was increased in the muscle of KPC tumor mice. This result, along with changes in glycolysis activity suggests that oxidative metabolism is limited with glucose going to lactate rather than entering TCA cycle.

Indeed, differentially expressed genes alluded to changes in key enzymes in the TCA cycle in the muscle of KPC tumor mice. Specifically, decreases in isocitrate dehydrogenase and succinate dehydrogenase were predicted. Again, plasma analyses showed the most robust changes to TCA cycle metabolites including citrate, fumurate and malate, with muscle remaining homeostatic.

Lipid metabolism was the most severely altered amongst the pathways analyzed. Changes to beta-oxidation, triacylglycerol synthesis and acyl-CoA hydrolysis were distinct in the muscle of KPC tumor mice. Additionally, KPC tumor mice had significant increases in acylcarnitines in both plasma and muscle. These changes were absent in the plasma and muscle of KPC IL-6^{KO} tumor mice with the exception of the increase in the acylcarnitine C16 in muscle. Taken together, these results suggest that significant changes occur to muscle metabolism in the presence of PDAC, with perhaps the lipid metabolism being the most severely affected.

CHAPTER 4: DELETION OF PKC THETA ATTENUATES MUSCLE WASTING IN PDAC-ASSOCIATED CACHEXIA

4.1 Overview

PKCθ belongs to the nPKC subfamily and is the predominant PKC isozyme in skeletal muscle (Osada et al., 1992). PKC has been linked to a variety of pathologies including cancer (Gu et al., 2019; Isakov, 2018; Motegi et al., 2005; J. Wu et al., 2016; Yao et al., 2019), neuropathies (Kurumatani et al., 1998; Shukla, Banerjee, & Tripathi, 2018; Tsubaki et al., 2015), muscular dystrophy (Dobrowolny et al., 2018; Kumar, Shanmugasundaram, Sundaram, & Anandaraj, 2002; Lozanoska-Ochser et al., 2018), and metabolic diseases such as type-2 diabetes and obesity (Y. Chen et al., 2019; Egan Benova et al., 2019; Itani, Pories, Macdonald, & Dohm, 2001; C. H. Liu et al., 2018; Serra et al., 2003). More specifically, the association of PKC-theta (PKCθ) ablation with decreased pathogenicity in muscle from models of type-2 diabetes (T2D) and Duchenne's muscular dystrophy (DMD) is perhaps the most relevant to cancer cachexia. Both T2D and DMD are characterized in part by chronic inflammation, myosteatosis and muscle atrophy (Dahlqvist et al., 2019; Janssens et al., 2015; Jonkers, van Loon, Nicolay, & Prompers, 2013; Srivastava, Yadav, Mukherjee, Pal, & Sinha, 2017). In the *mdx* model of muscular dystrophy, ablation of PKCθ reduced muscle degeneration and inflammation while increasing muscle regeneration (Madaro et al., 2012; Marrocco et al., 2017). Deletion of PKCθ in skeletal muscle also reduced myosteatosis and muscle insulin resistance in mice

fed a high fat diet (Peck et al., 2018), while supplementation of excess fatty acids in rats was associated with elevated muscle lipid accumulation, activation of PKCθ and increased insulin resistance (Griffin et al., 1999). Taken together, these results present a clear relationship between inflammation, lipid accumulation and PKCθ in diseases associated with muscle wasting.

Studies investigating lipid accumulation in muscle have also identified the association between elevated plasma fatty acids and increased muscle DAG content, an important secondary messenger for complete activation of PKCθ (Boden, 2008; Itani, Ruderman, Schmieder, & Boden, 2002). As already shown, KPC tumor-bearing mice have significant lipolysis with increases in plasma fatty acids and myosteatosis. Therefore, I aim to investigate the effects of PDAC - induced myosteatosis on PKCθ activation in skeletal muscle, which has not been previously reported. I also investigate the effects of PKCθ deletion on muscle and fat wasting in PDAC.

4.2 Materials and Methods

4.2.1 Animal Models

Experiments that included mice were approved by and performed in accordance with the Indiana University School of Medicine Institutional Animal Care and Use Committee. The gene encoding the PKCθ protein is *Prkcq*. *Prkcq*$^{-/-}$ mice were purchased from Jackson laboratories (004658, Bar Harbor, Maine, USA) and bred in the animal facility at IUSM. Pups were weaned at 21-days, separated by sex, and group-housed in a barrier facility with ad libitum access to

autoclaved food (Envigo: Huntingdon, Cambridgeshire, United Kingdom), sterile water, maintained on a 12hr light/dark cycle and allowed to acclimate to the facility for four weeks. Wild type mice C57BL/6J mice (000664, Jackson Laboratory; Bar Harbor, Maine, USA) were also purchased and bred alongside the *Prkcq*$^{-/-}$ mice to control for environmental and breeding factors.

4.2.2 Orthotopic Implantation of KPC tumor cells

Detailed methods on this procedure have been explained previously in section 2.2.8.

4.2.3 Euthanasia of Mice and Excision of Tissues

Detailed methods regarding euthanasia and tissue excision are reported in section 2.2.9.

4.2.4 Western Blotting

Homogenization and preparation of quadriceps tissue protein lysates have been described in detail in section 2.2.11. Additionally, the western blotting protocol used in this chapter is also reported in section 2.2.11. Primary antibodies were purchased from Cell Signaling (Cell Signaling; Danvers, MA, USA) and used at a dilution of 1:1000 for phosphorylated PKCθ (#9377P), PKCθ (#13643S), PKCθ substrates (#9615S) and ubiquitin (3933S).

4.2.5 Myotube Staining and Diameter Measurement and Muscle CSA

The proliferation and differentiation of myoblasts into myotubes is described in section 2.2.3. Fixation, sectioning and fiber CSA quantification is reported in section 2.2.15. Plasma was isolated from KPC tumor-bearing mice and used to treat mature myotubes at a concentration of 2% of final volume in combination with vehicle (PBS) or the PKCθ inhibitor Sotrastaurin (S2791, Selleck Chemicals; Houston, TX, USA) at a concentration of 500 nM for 48 hours. Myotubes were then fixed, visualized and diameter quantified using established protocols in section 2.2.15.

4.2.6 Measurement of Muscle Force Production In Vivo

Muscle force production in vivo was measured using a 1300A dual-mode force transducer with footplate and data analyzed using the 605A dynamic muscle data acquisition and analysis system from Aurora Scientific (Aurora, ON, Canada). Briefly, mice were anesthetized using 2-4% isoflurane and place in a supine position and the right hind limb was attached to the footplate of the force transducer. The foot and knee were secured in such a way that formed an approximate 90° angle between the foot, knee and hip of the mouse. Stimulation of the lower limb and plantar flexion of the foot was achieved by the placement of electrodes into the medial-posterior thigh near the sciatic nerve. Electrical stimulation was supplied in volts to the electrodes via a 701C electrical stimulator from Aurora Scientific. Stimulation was gradually increased until a maximum force production was reached, where further increases in stimulation did not

increase force production. Then, the voltage was increased by 20% to produce a supramaximal stimulation ensuring complete stimulation of the hind limb muscles. The muscles were then stimulated for durations of 0.2 milliseconds (ms) at frequencies of 10, 25, 40, 60, 80, 100, 125, and 150 Hz. Force was measured as millinewtons (mN) per meter (m) and normalized to initial body weight (IBW).

4.3 Results

4.3.1 PKCθ Activation is Increased in Muscle from KPC Tumor Mice and Inhibition of PKCθ Maintains Myotube Diameter in the Presence of Atrophic Stimuli

PKCθ activation has been implicated in a number of pathologies and conditions associated with myosteatosis. Thus, given the accumulation of lipids observed in muscle of KPC tumor mice, PKCθ activation was measured in muscle. This was accomplished through quantification of PKCθ phosphorylation at threonine 538 (Thr538), which is located in the activation loop of PKCθ and phosphorylation of Thr538 is specific to this isozyme for activation (X. Wang, Chuang, Li, & Tan, 2012). To further verify activation of PKCθ, measurement of the phosphorylation of downstream PKCθ substrates was done using western blotting. Phosphorylation of PKCθ was increased in muscle from KPC but not KPC IL-6^{KO} tumor mice (Figure 4.1 A and 4.1 B). Moreover, measurement of the phosphorylation of PKCθ substrates showed increases in PKCθ substrate phosphorylation in KPC but not KPC IL-6^{KO} muscle (Figure 4.1 C and 4.1 D).

Given that KPC tumor mice had significant myosteatosis and atrophy when compared with KPC IL-6^{KO} mice (Chapter 2), these results suggests that the degree of myosteatosis is associated with PKCθ activation and muscle atrophy.

Thus, I investigated the effects of inhibiting PKCθ in myotubes in vitro on myotube atrophy when presented with an atrophic stimulus. Myoblasts were differentiated into myotubes and treated with 2% KPC tumor mouse plasma in combination with a vehicle or the PKCθ inhibitor sotrastaurin for 48 hours (Figure 4.1 E). Myotubes were then visualized using immunofluorescence for MHC (Figure 4.1 F) and myotube diameter measured. Myotubes treated with KPC tumor mouse plasma and vehicle had a significant decrease in myotube diameter compared to those treated with KPC mouse plasma and sotrastaurin (Figure 4.1 F and 4.1 G). These results suggest that PKCθ is activated in muscle in the presence of PDAC tumors and the inhibition of PKCθ attenuates myotube wasting in vitro.

Figure 4.1

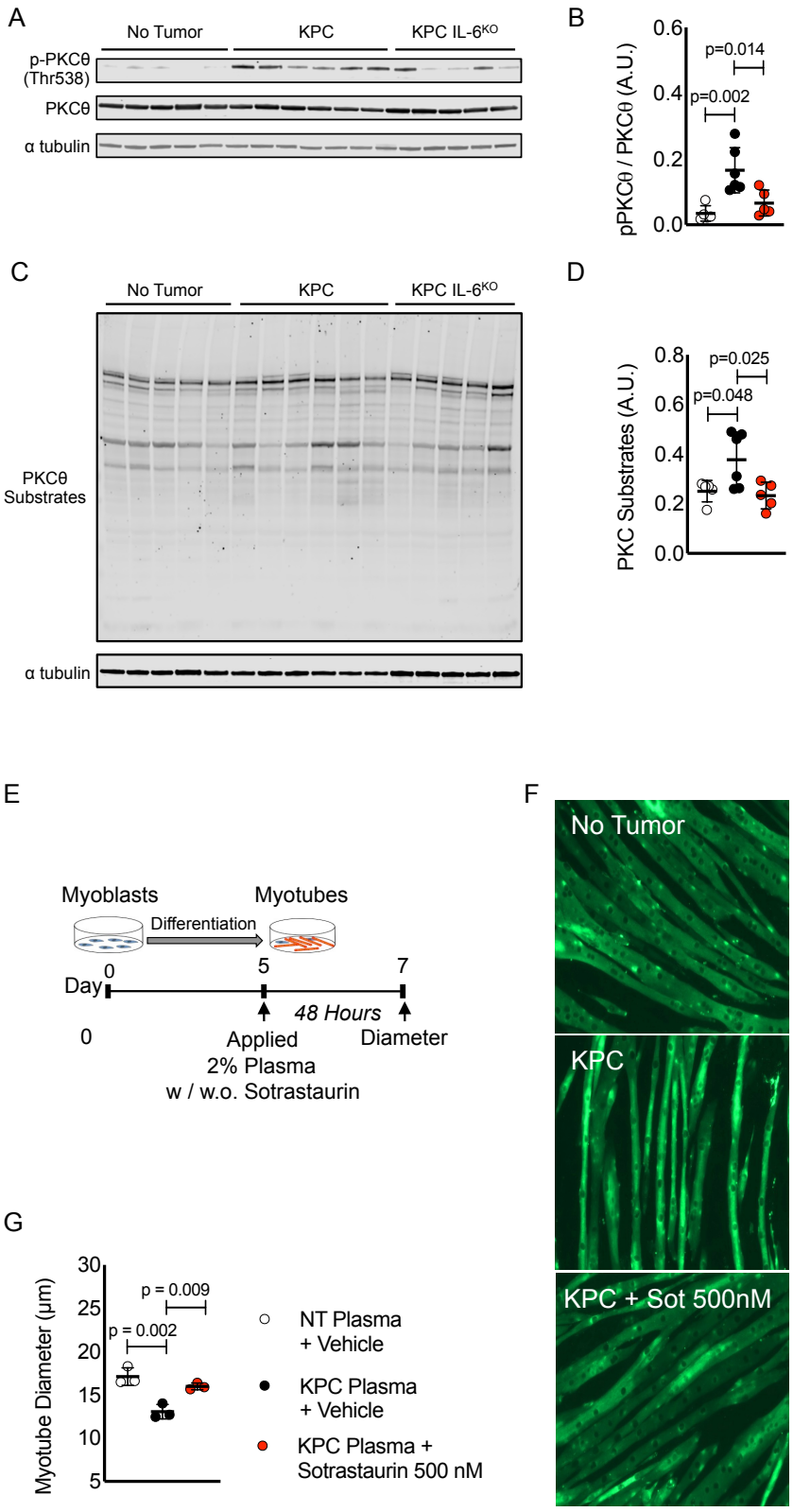
A
No Tumor
KPC
KPC IL-6KO
p-PKCθ (Thr538)
PKCθ
α tubulin
B
pPKCθ / PKCθ (A.U.)
p=0.014
p=0.002
C
PKCθ Substrates
α tubulin
D
PKC Substrates (A.U.)
p=0.025
p=0.048
E
Myoblasts
Myotubes
Differentiation
Day
0
5
7
48 Hours
Applied
2% Plasma
w / w.o. Sotrastaurin
Diameter
F
No Tumor
KPC
KPC + Sot 500nM
G
Myotube Diameter (μm)
p = 0.009
p = 0.002
NT Plasma
+ Vehicle
KPC Plasma
+ Vehicle
KPC Plasma +
Sotrastaurin 500 nM

Figure 4.1. PKCθ phosphorylation is increased in muscle of KPC tumor mice and inhibiting PKCθ protects against myotube atrophy in vitro. Activation of PKCθ in part requires its phosphorylation. Phosphorylation of PKCθ was measured by western blotting in the quadriceps of mice (**A and B**). To further investigate if PKCθ was activated, phosphorylation of PKCθ substrates were measured in the quadriceps muscle of mice by western blotting (**C and D**). To investigate the effects of inhibiting PKCθ on muscle wasting, C2C12 myotubes were treated with 2% plasma from KPC tumor mice with or without the PKCθ inhibitor Sotrastaurin (**E**). Myotubes were visualized using immunofluorescence for MHC and atrophy measured (**F and G**). Error bars are standard deviation and significant differences are shown in the charts.

4.3.2 Prkcq$^{-/-}$ Tumor Bearing Mice Have Increased Survival and Higher Muscle Force Production versus Prkcq$^{+/+}$ Mice.

Prkcq is the gene encoding the PKCθ protein. Therefore, I used *Prkcq*$^{-/-}$ mice to investigate the effects of deleting PKCθ on survival, and muscle force production in vivo. *Prkcq*$^{-/-}$ KPC tumor mice although modest, had a significant increase in survival compared to *Prkcq*$^{+/+}$ KPC tumor mice (Figure 4.2 A). *Prkcq*$^{-/-}$ KPC tumor mice showed no significant difference in tumor size versus wild type mice (Figure 4.2 B).

In vivo muscle force production was measured for tumor-bearing mice at 8 days and 15 days after tumor cell implantation. There was no difference in normalized muscle force production between *Prkcq*$^{+/+}$ and *Prkcq*$^{-/-}$ tumor-bearing mice at day 8 (Figure 4.2 C). *Prkcq*$^{-/-}$ tumor-bearing mice had significantly higher muscle force production compared to *Prkcq*$^{+/+}$ KPC tumor mice at day 15 (Figure 4.2 D). To assess changes to muscle force production within the specific groups, force production for day 8 and day 15 were compared directly for *Prkcq*$^{+/+}$ and *Prkcq*$^{-/-}$ KPC tumor mice. *Prkcq*$^{+/+}$ KPC tumor mice had a significant decline in muscle force production between day 8 and day 15 at stimulation frequencies of 60-125 Hz (Figure 4.2 E). There was no difference in force production between day 8 and day 15 for *Prkcq*$^{-/-}$ KPC tumor mice (Figure 4.2 F). To verify that PKCθ expression was indeed ablated, mice were euthanized and PKCθ protein expression in the quadriceps muscle was measured. *Prkcq*$^{+/+}$ no tumor and KPC tumor mice had PKCθ expression in muscle, which was undetectable in *Prkcq*$^{-/-}$ no tumor and KPC tumor mice (Figure 4.2 G).

Figure 4.2

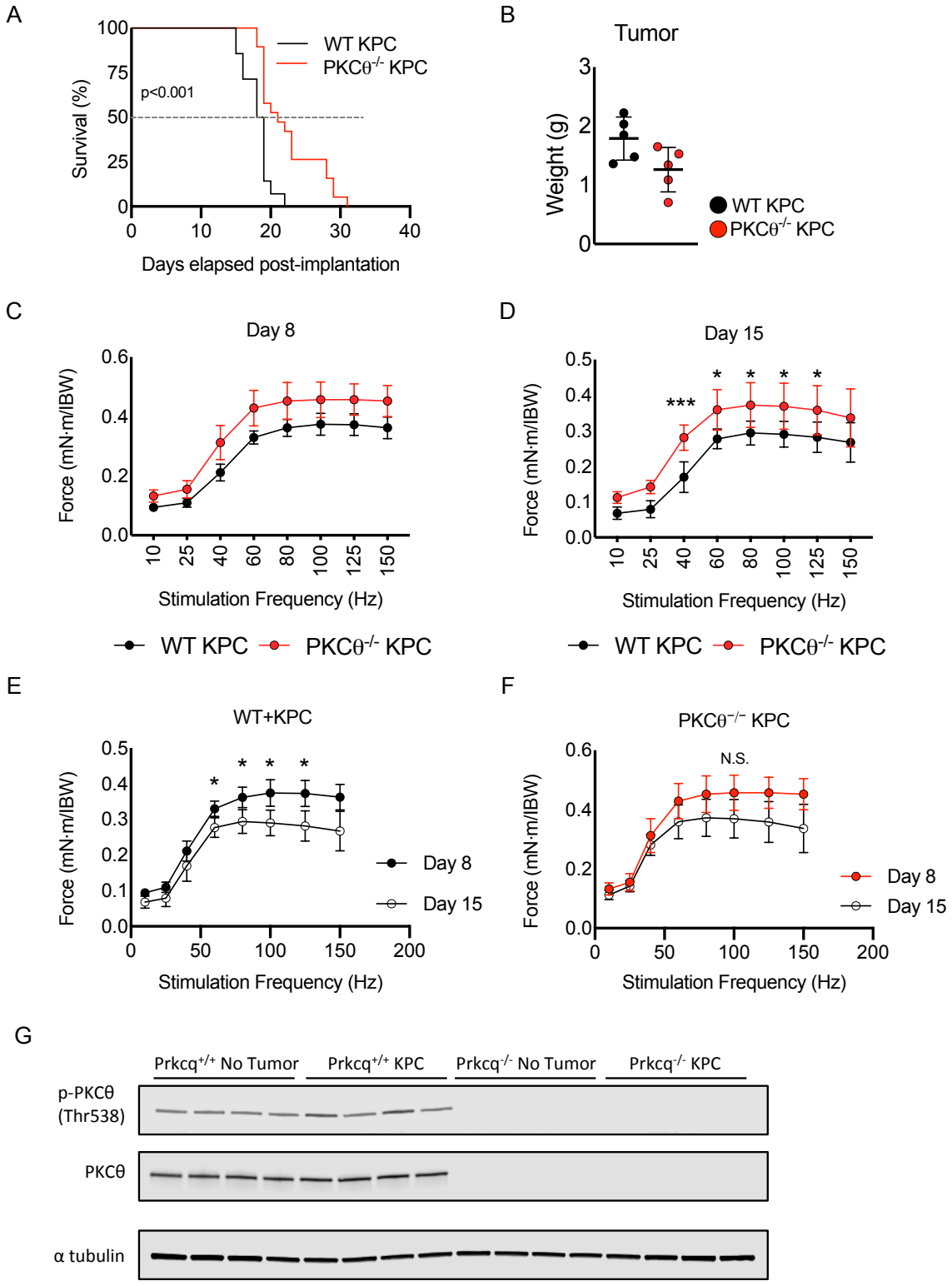
A
Survival (%)
100
75
50
25
0
p<0.001
WT KPC
PKCθ-/- KPC
0
10
20
30
40
Days elapsed post-implantation
B
Tumor
Weight (g)
3
2
1
0
WT KPC
PKCθ-/- KPC
C
Day 8
Force (mN·m/lBW)
0.6
0.4
0.2
0.0
10
25
40
60
80
100
125
150
Stimulation Frequency (Hz)
WT KPC
PKCθ-/- KPC
D
Day 15
Force (mN·m/lBW)
0.5
0.4
0.3
0.2
0.1
0.0
***
*
*
*
*
10
25
40
60
80
100
125
150
Stimulation Frequency (Hz)
WT KPC
PKCθ-/- KPC
E
WT+KPC
Force (mN·m/lBW)
0.5
0.4
0.3
0.2
0.1
0.0
*
*
*
*
0
50
100
150
200
Stimulation Frequency (Hz)
Day 8
Day 15
F
PKCθ-/- KPC
N.S.
Force (mN·m/lBW)
0.6
0.4
0.2
0.0
0
50
100
150
200
Stimulation Frequency (Hz)
Day 8
Day 15
G
Prkcq+/+ No Tumor
Prkcq+/+ KPC
Prkcq-/- No Tumor
Prkcq-/- KPC
p-PKCθ (Thr538)
PKCθ
α tubulin

Figure 4.2. Deletion of PKCθ increases survival and is associated with increased muscle force production in vivo in KPC tumor bearing mice. KPC tumor-bearing mice ablated for the gene *Prkcq*$^{-/-}$, which codes for the protein PKCθ, had increased survival compared to *Prkcq*$^{+/+}$ mice with tumors (**A**). Tumor size was not significantly different between *Prkcq*$^{-/-}$ and *Prkcq*$^{+/+}$ mice (**B**). In vivo muscle force production was unchanged between wild type (*Prkcq*$^{+/+}$*)* and *Prkcq*$^{-/-}$ tumor-bearing mice at 8 days after KPC tumor implantation (**C**),but was significantly changed at 15 days after KPC tumor implantation (**D**). Wild type KPC tumor bearing mice had a significant difference in muscle force production between day 8 and day 15 after tumor implantation (**E**), where the was no statistical difference in muscle force production between day 8 and day 15 in the *Prkcq*$^{-/-}$ tumor mice (**F**). To verify PKCθ expression was abolished in mice, PKCθ protein was measured in the quadriceps of *Prkcq*$^{+/+}$ and *Prkcq*$^{-/-}$ mice by western blotting (**G**).

4.3.3 Prkcq$^{-/-}$ KPC tumor mice have attenuated muscle wasting and decreased protein ubiquitination versus Prkcq$^{+/+}$ KPC tumor mice.

Muscles were excised and weighed from mice to determine the severity of muscle wasting. *Prkcq*$^{+/+}$ KPC tumor had significant loss of muscle mass for the quadriceps, gastrocnemius, tibialis and heart muscles compared to *Prkcq*$^{-/-}$ KPC tumor mice (Figure 4.3 A). Moreover, muscle fiber CSA and total protein ubiquitination were measured to verify the presence of muscle wasting. Cross sections from the quadriceps muscle were visualized using immunofluorescence for dystrophin (Figure 4.3 D). *Prkcq*$^{+/+}$ KPC tumor mice had a significantly smaller average muscle fiber CSA when compared to *Prkcq*$^{+/+}$ no tumor and *Prkcq*$^{-/-}$ KPC tumor mice (Figure 4.3 B). *Prkcq*$^{+/+}$ KPC tumor mice also had a larger percentage of smaller CSA fibers, illustrated by a leftward shift in the frequency distribution curve, when compared against the other groups (Figure 4.3 D). Finally, protein ubiquitination was increased in *Prkcq*$^{+/+}$ KPC tumor mice compared with *Prkcq*$^{+/+}$ no tumor and *Prkcq*$^{-/-}$ KPC tumor mice (Figure 4.3 E and 4.3 F). Interestingly, *Prkcq*$^{-/-}$ no tumor mice had increased protein ubiquitination versus *Prkcq*$^{+/+}$ no tumor mice (Figure 4.3 E and 4.3 F) and may indicate an underlying phenotype specific to the *Prkcq*$^{-/-}$ background.

Figure 4.3

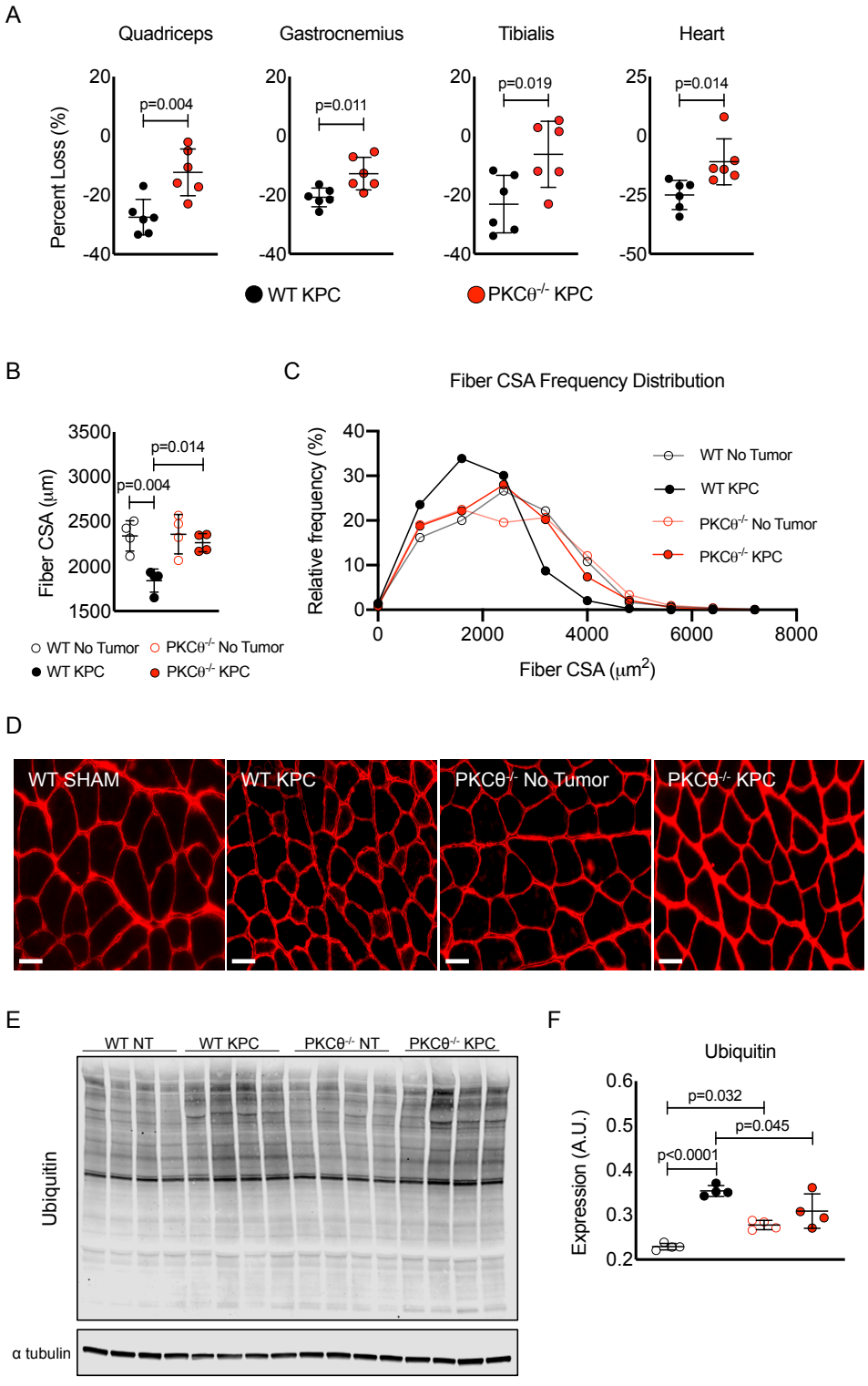
A
Quadriceps
Gastrocnemius
Tibialis
Heart
Percent Loss (%)
p=0.004
p=0.011
p=0.019
p=0.014
WT KPC
PKCθ-/- KPC
B
Fiber CSA (μm)
p=0.014
p=0.004
WT No Tumor
PKCθ-/- No Tumor
WT KPC
PKCθ-/- KPC
C
Fiber CSA Frequency Distribution
Relative frequency (%)
WT No Tumor
WT KPC
PKCθ-/- No Tumor
PKCθ-/- KPC
Fiber CSA (μm2)
D
WT SHAM
WT KPC
PKCθ-/- No Tumor
PKCθ-/- KPC
E
WT NT
WT KPC
PKCθ-/- NT
PKCθ-/- KPC
Ubiquitin
α tubulin
F
Ubiquitin
Expression (A.U.)
p=0.032
p=0.045
p<0.0001

Figure 4.3. Deletion of PKCθ attenuates atrophy and protein ubiquitination in muscle of tumor bearing mice. Muscle wasting was measured in tumor bearing mice using tissue weight and fiber CSA analysis in the quadriceps muscle. At euthanasia, the quadriceps, gastrocnemius, tibialis and heart muscles were excised and weighed (**A**). Changes in muscle weights were verified using muscle fiber CSA analysis on quadriceps sections. Sections from the quadriceps muscle were reacted for dystrophin to visualize myofibers (**D**) and myofiber CSA was measured (**B**). Cumulative myofiber CSA measurements were pooled to visualize the frequency distribution, observing the classic leftward shift in the *Prkcq*$^{+/+}$ tumor bearing group, indicative of a higher percentage of smaller fibers (**C**). total protein ubiquitination was measured in the quadriceps using western blotting (**E and F**). Error bars are standard deviation and statistical differences are shown in the charts.

4.4 Summary

PKCθ is activated in diseases associated with myosteatosis and contributes to altered tissue metabolism and muscle atrophy. In the muscle of KPC tumor mice, phosphorylation of PKCθ and PKCθ substrates was increased compared to no tumor mice. Deletion of tumor cell IL-6 attenuated phosphorylation of PKCθ and its downstream substrates. In vitro, the administration of the PKCθ inhibitor Sotrastaurin rescued myotube atrophy during treatment with plasma from KPC tumor mice.

In vivo, deletion of *Prkcq*, the gene encoding PKCθ, was associated with increased survival and higher muscle force production in tumor-bearing mice. Moreover, *Prkcq*$^{-/-}$ tumor mice had reduced loss of skeletal and cardiac muscle mass concomitantly with increased muscle fiber CSA when compared to *Prkcq*$^{-/-}$ tumor mice. Protein ubiquitination, a classic indication of increased protein catabolism via the ubiquitin proteasome, was decreased in the muscle of *Prkcq*-/- tumor mice comparatively. These results suggest that PKCθ inhibition is an encouraging target in muscle for the improvement of muscle atrophy and force production in the treatment of PDAC-induced cachexia.

CHAPTER 5: DISCUSSION

5.1 Tumor, Adipose, Skeletal Muscle Crosstalk in PDAC Cachexia

IL-6 production by tumor epithelial cells is largely unstudied in PDAC. My data indicate that a substantial number of human PDAC tumors exhibit expression of IL-6 in the epithelial compartment and further, that IL-6 is produced by a majority of established PDAC tumor cell lines. This has clear implications for PDAC tumor biology. Here, I demonstrate novel tumor-tissue crosstalk in the macro environment of PDAC cachexia and further provide evidence of central roles for tumor cell-derived IL-6 and IL-6 trans-signaling. In my studies, autocrine IL-6 production was not required for KPC tumor cell proliferation in vitro, although IL-6 null tumors in vivo were smaller. Blood levels of IL-6 are generally correlated with increased cachexia and mortality in patients with late stage PDAC, and IL-6 production by fibroblasts and myeloid cells in the tumor microenvironment has been implicated in PDAC development and tumor growth, progression, metastasis and drug resistance (Holmer et al., 2014; Mace et al., 2018; Ohlund et al., 2017). I found that both the tumor cells and stromal cells in the tumor microenvironment expressed IL-6 in KPC tumor mice. KPC IL-6^{KO} tumor cells were negative for IL-6 expression. Mice with IL-6^{KO} tumors also exhibited reduced circulating IL-6, which was halved by the elimination of IL-6 from tumor cells. Adipose tissue loss was proportionate to circulating IL-6 in the tumor groups, since KPC IL-6^{KO} tumor mice had approximately half as much plasma IL-

6 and fat wasting versus KPC tumor mice. Interestingly, muscle loss was essentially abolished by tumor-cell depletion of IL-6.

My investigation into tissue crosstalk showed that crosstalk between the tumor and adipose tissue acted to amplify IL-6 expression distantly, as adipose tissue had the highest *Il6* mRNA expression amongst the tissues analyzed. Additionally, 3T3 adipocytes treated with KPC CM had increased *Il6* mRNA expression, corroborating my in vivo tissue analyses. These results indicate that adipose tissue was proportionately more sensitive to the effects of PDAC as measured by the induction of adipose wasting, lipolysis, and release of fatty acids and glycerol into the blood. My findings are similar to those reported in human patients with cachexia. Adipose inflammation is noted in patients with cancer cachexia (Camargo et al., 2015), and furthermore, the magnitude of fat loss (~30%) exceeded that of muscle loss (7%) in patients on FOLFIRINOX for advanced disease (Kays et al., 2018), while only fat was lost in patients with PDAC on neoadjuvant therapy (Sandini et al., 2018).

In the KPC tumor mice, the skeletal muscle exhibited steatosis, mitochondrial dysfunction, metabolic impairment, and wasting. The expression of *Il6r* mRNA was increased only in the muscle but not fat of KPC tumor mice, yet these mice accumulated soluble IL6R protein in fat. Again, in vitro experiments concurred with my in vivo findings as C2C12 myotubes treated with KPC CM had increased expression of *Il6r* mRNA. *Il6r* mRNA expression was unchanged in 3T3 adipocytes treated with KPC CM. STAT3 phosphorylation was increased in both muscle and fat of KPC tumor mice, indicating signaling in both peripheral

tissue compartments. Deletion of tumor IL-6 mitigated most of these effects. These results suggest that skeletal muscle is a major source of the sIL6R in cachexia and its accumulation in fat likely mediates the effects of IL-6 signaling on adipocytes and furthers lipolysis.

My observation of myosteatosis in the KPC tumor group proposes a role for lipid accumulation in muscle atrophy. I verify this using an in vitro approach with products of lipolysis (modeled with CM from KPC CM treated 3T3 adipocytes) used to treat C2C12 myotubes. Myotubes treated with KPC stimulated 3T3 adipocyte CM had exacerbated wasting. Thus, increased lipolysis and IL-6 production from adipocytes as a result of PDAC offers an explanation of how adipose loss can lead to muscle wasting. Suggesting that PDAC cachexia is promoted in a feed forward mechanism, where tumor IL-6 promotes wasting of both fat and muscle, which stimulates crosstalk between fat and muscle via sIL6R and myosteatosis, which augments cachexia (Figure 2.9). Low skeletal muscle mass is predictive of mortality across diseases (Martin et al., 2013), which could be attributable to functional decline and respiratory or cardiac failure; however, the significance of fat loss is less clear. Indeed, the authors of a recent study discount adipose loss as participating in PDAC mortality, based upon feeding pancreatic enzymes to mice with pancreatic cancer and upon cross sectional body composition data in patients (Danai et al., 2018). Against that singular interpretation, however, are both clinical-correlative and mechanistic studies. Fat loss in the absence of muscle loss has been observed in cohorts of patients with PDAC (Sandini et al., 2018), (Kays et al., 2018), consistent with

these being separable phenomena, and higher rates of adipose loss are associated with mortality in PDAC (Di Sebastiano et al., 2013). As well, obese patients with PDAC exhibit higher losses in weight, skeletal muscle, and adipose tissue along with poorer survival (Dalal et al., 2012). Even absent muscle wasting, low fat mass or "adipopenia" is associated with mortality in patients with diffuse large B-cell lymphoma treated with immunotherapy (Camus et al., 2014) and in patients with heart failure (Melenovsky et al., 2013), among other conditions. Furthermore, our longitudinal analysis of patients with advanced PDAC on FOLFIRINOX demonstrates equivalent mortality for patients with fat-only loss versus patients with both fat and muscle loss, with overall 10 months reduced survival than patients without loss of either depot (Kays et al., 2018). Thus, the preponderance of clinical data point to an important role for adipose in PDAC cachexia and mortality. Moreover, preserving adipose tissue via pharmacological or genetic manipulation of lipolysis and lipogenesis protects muscle in other cachexia models (Das et al., 2011; Rohm et al., 2016) (Tsoli, Swarbrick, & Robertson, 2016), although in all of these studies multiple tissues in addition to adipose were affected by the intervention.

Whether changes in tumor growth were due to reduced IL-6 or due to reduced substrate availability from the relative preservation of fat and muscle require further investigation. Conversely, whether reduced cachexia was due to decreased circulating IL-6 or due to other IL-6-dependent tumor properties including altered tumor phenotype and secretome are complex questions, which I am actively investigating. Indeed, tumor size did not correlate with muscle or fat

wasting in my investigations, suggesting that the tumor secretome may be more telling for the severity of cachexia rather than simply assuming that larger tumors are associated with increased cachexia. Notably, IL-6 has been shown to have importance in tumor proliferation and differentiation in vivo (ref). Regardless, clearly IL-6 production from tumor cells can orchestrate cachexia and this tumor characteristic could have diagnostic and therapeutic implications for PDAC.

5.2 Metabolic Alterations in Skeletal Muscle with PDAC

Cachexia imposes significant modifications to the normal energy demands in tissues, which ultimately affects metabolic homeostasis. I posit that adipose wasting promotes muscle dysmetabolism and atrophy and thus, strongly contributes to mortality. KPC tumor mice had significant changes in muscle metabolism and these changes were largely absent when IL-6 was deleted from the tumor. Lipolysis of adipose tissue resulted in elevated circulating fatty acids and subsequent lipid accumulation and myosteatosis in muscle of KPC tumor mice (Figures 2.8 and 2.9). Myosteatosis, sarcopenia and the combination are associated with reduced survival in one study of resectable patients with pancreatic and periampullary adenocarcinomas (Stretch et al., 2018), while only myosteatosis was associated with inflammation and reduced survival in another study of patients with unresectable pancreatic cancer or cholangiocarcinoma (Rollins et al., 2016). After a period of muscle metabolic adaptation this ultimately results in lipotoxicity, including metabolic derangement, cellular stress, and muscle wasting. My histological and RNAseq data support this interpretation.

In KPC tumor mice, RNA sequencing analysis revealed differential expression of genes associated with IL-6 signaling, lipid metabolism, and glycolysis in muscle. In the epididymal fat pads, pathways related to diapedesis, LXR/RXR activation—important regulators of cholesterol, lipid and glucose homeostasis, acute phase signaling, and IL-6 signaling pathways were also affected. Importantly, gene expression correlated with wasting in both tissues. While muscle from mice with IL-6^{KO} tumors was unaffected for mass and nearly normal in terms of gene expression, moderate adipose wasting and altered gene expression changes were clearly well established in KPC IL-6^{KO} tumor mice. Thus, investigation of muscle metabolism was clearly warranted in these models.

My investigations into muscle metabolism identified significant changes to branch chain amino acid (BCAA) oxidation, glycolysis and TCA Cycle function, and alterations in lipid metabolism especially regarding beta-oxidation and triacylglycerol synthesis. BCAA metabolism was increased in the muscle of KPC tumor mice determined by increases in expression of genes crucial for BCAA oxidation and transport, with concomitant increases in both plasma and muscle BCAA levels. BCAA metabolism is important for organismal survival during conditions of reduced nutrient availability and increased BCAA catabolism for use as an energy source has been reported with cachexia. Changes in glycolysis and TCA cycle function were also observed in the muscle of KPC tumor mice, although changes in plasma metabolites and muscle gene expression were more sensitive and a better indicator of cachexia than muscle metabolite measurements alone. Decreased plasma glucose was observed in both KPC and

KPC IL-6^{KO} tumor mice. This result is similar to other studies that also report low blood glucose in cancer. Compared to KPC IL-6^{KO} tumor mice, pyruvate was increased in the muscle of KPC tumor mice. This was accompanied by significant increases in PDK4 expression in KPC tumor mouse muscle, suggesting inhibition of the PDH complex activity and reduced entry of pyruvate into the TCA cycle. Typically, this would result in accumulation of lactate but interestingly muscle and plasma lactate levels were unchanged in KPC tumor mice and actually decreased in KPC IL-6^{KO} tumor mice. Increased consumption of lactate by the liver for gluconeogenesis may explain the maintenance of homeostatic lactate levels, via the Cori Cycle (Streja, Steiner, Marliss, & Vranic, 1977). This theory is confounded however by the decrease in blood glucose, which may be occurring due to increased utilization of blood glucose by the tumor. Further investigation is needed especially regarding liver and tumor metabolism to increase our understanding of these results.

A reduction in TCA cycle function was predicted for a number of key enzymes using my RNAseq data. Interestingly, plasma metabolite levels again were a better predictor of cachexia. While unchanged in muscle, increased acetate with decreases in fumurate and malate were measured in plasma. The increases in acyl-CoA synthetase short chain family member 2 (*Acss2)* and acetate, along with decreases in fumurate and malate suggests that acetyl-CoA generated from acetate metabolism may be primarily used for lipogenesis of accumulating fatty acids and thus, leave insufficient acetyl-CoA levels to fuel proper TCA Cycle function. Acetyl-CoA can also be generated from oxidation of

fatty acids during beta-oxidation, providing additional mechanisms for activation of the TCA Cycle. Therefore, impaired TCA Cycle function in muscle may also be indicative of aberrant muscle lipid metabolism. Indeed, I observed significant changes to muscle lipid metabolism. RNAseq data and IPA analysis indicated a decrease in multiple genes important in beta-oxidation, triacylglycerol synthesis, and acyl-CoA hydrolysis. These findings were further supported by increases in both plasma and muscle acylcarnitine levels in KPC tumor mice. Suggesting aberrant lipid metabolism and incomplete beta-oxidation in muscle. Moreover, impaired beta-oxidation was found to be central to muscle wasting in experimental renal cell carcinoma models, and inhibition of fatty acid oxidation improved body weight and muscle mass in mice (Fukawa et al., 2016). These results support clinical relevance of my observations here.

5.3 Deletion of PKC theta Attenuates Muscle Wasting

My results clearly implicate the importance of IL-6 signaling between fat and muscle, especially through sIL6R trans signaling, and the capability of subsequent myosteatosis to augment atrophy and dysmetabolism in muscle. Therefore, I postulated the existence of a common molecule in muscle that is affected by changes in metabolism and also has an effect on systemic inflammation. Soluble IL6R is associated with increased inflammation in disease and sIL6R is largely produced by proteolytic cleavage of membrane GP80, which in mice and humans is mediated by ADAM10 and ADAM17 proteases (Schumacher et al., 2015). PKCθ activation is a known rate-limiting step for

shedding of IL-6R largely through activation of ADAM10 and ADAM17 (Mullberg et al., 1992). Since PKCθ belongs to the nPKC family its activation is dependent on the presence of diacylglycerol (DAG). Muscle steatosis is correlated with increases in diacylglycerol (DAG), insulin resistance and increased activation of PKC theta (Szendroedi et al., 2014). Thus, these previous findings suggest a connection between adipose wasting and induction of trans-signaling via muscle-derived sIL6R.

Indeed, PKCθ phosphorylation was increased in muscle of KPC but not KPC IL-6^{KO} tumor mice, coinciding with increased myosteatosis in the KPC tumor mouse muscle. Deletion of PKCθ was associated with increased survival and maintenance of skeletal and cardiac muscle masses in the presence of PDAC. Moreover, muscle force production was higher in $PKC\theta^{-/-}$ tumor mice versus $PKC\theta^{+/+}$ tumor mice, suggesting preservation of both mass and function. PKCθ has been implicated in a number of other cachexia-associated diseases including diabetes and muscular dystrophy, where deletion of PKCθ improved muscle wasting in these conditions. While its relationship with protein ubiquitination is unknown in muscle, PKCθ has been shown to affect the ubiquitination and subsequent degradation via the ubiquitin proteasome of proteins in T cells (Gruber et al., 2009) and neurons (Upadhya, Ding, Smith, & Hegde, 2006). It is therefore possible that PKCθ may be affecting the ubiquitination of critical proteins in muscle and contributing to muscle catabolism in cachexia. These studies along with my findings here suggest inhibition of PKCθ is beneficial in

PDAC cachexia and suggests PKCθ as a novel target for improving the effects of pancreatic cancer.

5.4 Future Directions and Limitations

Cancer cachexia is a systemic syndrome and understanding changes to tissue crosstalk in the presence of a tumor is critical for designing effective treatment. The data provided here strongly support the targeted inhibition of IL-6R to treat PDAC cachexia. Pre-clinical studies document improved response to chemotherapy in mice with pancreatic cancer treated with anti-IL6R antibodies (Long et al., 2017); whether those mice also demonstrated reduced cachexia was not reported. An ongoing trial of the IL6R inhibitor Tocilizumab with gemcitabine and nab-paclitaxel in patients with advanced and metastatic disease might provide important insights on this approach in PDAC (I. Chen et al., 2017).

My results add to the literature by implicating fat loss as a potential driver of cachexia mortality and immunomodulation in cancer (Tsoli et al., 2016), since fat loss was more profound and occurred earlier than muscle loss in the presence of a tumor. I have also identified adipose tissue as a significant source of IL-6 production in PDAC, greatly increasing circulating levels of IL-6 and systemic inflammation. These results will impact future patient therapies by supporting the need to monitor adipose tissue in patients with cachexia-associated cancers. Moreover, my studies also suggest that diverse strategies aimed at returning metabolic homeostasis may improve the outcomes of patients with PDAC. For instance, the reduction or inhibition of adipose tissue lipolysis

would decrease circulating fatty acids and may lead to decreased myosteatosis, which may restore metabolic homeostasis in muscle. There already exist inhibitors of the enzyme adipose triglyceride lipase (A*tgl*) as well as *Atgl* ablated mice. Studies in have shown that inhibition or ablation of *Atgl* is associated with less cachexia in the presence of a tumor(Das et al., 2011) and decreased tumor growth(Zagani, El-Assaad, Gamache, & Teodoro, 2015)

Thus, in future studies I aim to target both plasma sIL6R and muscle metabolism. Given the ability of PKCθ to affect both inflammation and dysmetabolism in muscle, I plan to utilize PKCθ$^{-/-}$ mice implanted with KPC tumors and administer anti-sIL6R agents to neutralize plasma sIL6R. Using this approach, I predict that a significant reduction in systemic inflammation will be observed coinciding with a return to metabolic homeostasis in skeletal muscle. If this occurs, a reduction in cachexia and an increase in survival will likely also be obtained. I recognize my use of a global PKCθ knockout murine model is an inferior approach to using a conditional muscle PKCθ knockout, however the current unavailability of the conditional knockout limits my studies to one genetic model. This approach will also provide an opportunity to investigate in detail, the changes to muscle metabolism occurring with PDAC in the absence of PKCθ. I aim to use proteomic analyses in addition with RNAseq to provide an improved understanding of functional results for key metabolic enzymes and pathways. I will focus on identifying changes in metabolites, proteins and gene expressions in early onset disease with or without the expression of PKCθ. This will allow me to

identify possible novel biomarkers to diagnose PDAC earlier, which could increase treatment efficacy and increase patient survival.

Furthermore, the ability to track the IL6R from muscle to adipose tissue would strengthen my hypotheses. The genetic model R26-MetRS (028071, Jackson Laboratories) is a genetic model with a mutated methionyl-tRNA synthetase (MetRS), which when crossed with a tissue specific Cre-recombinase mouse strain, will label all the proteins synthesized in the tissue of interest with the mutated methionyl residue. Downstream utilization of click chemistry in various tissues allows for the isolation of proteins that originated within the tissue of interest (Takayama, Kusamori, & Nishikawa, 2019). Thus, I aim to cross the R26-MetRS with the HSA-Cre strains to specifically label peptides in the muscle proteome. These mice will then be implanted with KPC tumors and adipose tissue harvested and analyzed for the presence of muscle labeled IL6R. This approach is beneficial in two ways, the first showing that muscle IL6R trans locates to fat in PDAC and second, plasma from these mice can be used to characterize the muscle secretome in PDAC. Results from these future studies will greatly improve our understanding of the crosstalk between fat and muscle in PDAC and provide insight for novel targets for the treatment of PDAC cachexia.

REFERENCES

Acharyya, S., Butchbach, M. E., Sahenk, Z., Wang, H., Saji, M., Carathers, M., . . . Guttridge, D. C. (2005). Dystrophin glycoprotein complex dysfunction: a regulatory link between muscular dystrophy and cancer cachexia. *Cancer Cell, 8*(5), 421-432. doi:10.1016/j.ccr.2005.10.004

Al-Shanti, N., & Stewart, C. E. (2012). Inhibitory effects of IL-6 on IGF-1 activity in skeletal myoblasts could be mediated by the activation of SOCS-3. *J Cell Biochem, 113*(3), 923-933. doi:10.1002/jcb.23420

Almuraikhy, S., Kafienah, W., Bashah, M., Diboun, I., Jaganjac, M., Al-Khelaifi, F., . . . Elrayess, M. A. (2016). Interleukin-6 induces impairment in human subcutaneous adipogenesis in obesity-associated insulin resistance. *Diabetologia, 59*(11), 2406-2416. doi:10.1007/s00125-016-4031-3

Argiles, J. M., Busquets, S., Stemmler, B., & Lopez-Soriano, F. J. (2015). Cachexia and sarcopenia: mechanisms and potential targets for intervention. *Curr Opin Pharmacol, 22*, 100-106. doi:10.1016/j.coph.2015.04.003

Argiles, J. M., Stemmler, B., Lopez-Soriano, F. J., & Busquets, S. (2018). Inter-tissue communication in cancer cachexia. *Nat Rev Endocrinol, 15*(1), 9-20. doi:10.1038/s41574-018-0123-0

Ayo, S. H., Radnik, R., Garoni, J. A., Troyer, D. A., & Kreisberg, J. I. (1991). High glucose increases diacylglycerol mass and activates protein kinase C in mesangial cell cultures. *Am J Physiol, 261*(4 Pt 2), F571-577. doi:10.1152/ajprenal.1991.261.4.F571

Babic, A., Schnure, N., Neupane, N. P., Zaman, M. M., Rifai, N., Welch, M. W., . . . Ng, K. (2018). Plasma inflammatory cytokines and survival of pancreatic cancer patients. *Clin Transl Gastroenterol, 9*(4), 145. doi:10.1038/s41424-018-0008-5

Baltgalvis, K. A., Berger, F. G., Pena, M. M., Davis, J. M., Muga, S. J., & Carson, J. A. (2008). Interleukin-6 and cachexia in ApcMin/+ mice. *Am J Physiol Regul Integr Comp Physiol, 294*(2), R393-401. doi:10.1152/ajpregu.00716.2007

Baltgalvis, K. A., Berger, F. G., Pena, M. M., Davis, J. M., White, J. P., & Carson, J. A. (2009). Muscle wasting and interleukin-6-induced atrogin-I expression in the cachectic Apc (Min/+) mouse. *Pflugers Arch, 457*(5), 989-1001. doi:10.1007/s00424-008-0574-6

Baracos, V. E., Martin, L., Korc, M., Guttridge, D. C., & Fearon, K. C. H. (2018). Cancer-associated cachexia. *Nat Rev Dis Primers, 4*, 17105. doi:10.1038/nrdp.2017.105

Beckonert, O., Keun, H. C., Ebbels, T. M., Bundy, J., Holmes, E., Lindon, J. C., & Nicholson, J. K. (2007). Metabolic profiling, metabolomic and metabonomic procedures for NMR spectroscopy of urine, plasma, serum and tissue extracts. *Nat Protoc, 2*(11), 2692-2703. doi:10.1038/nprot.2007.376

Bell, R. M., & Burns, D. J. (1991). Lipid activation of protein kinase C. *J Biol Chem, 266*(8), 4661-4664. Retrieved from https://www.ncbi.nlm.nih.gov/pubmed/2002013

Bian, A. L., Hu, H. Y., Rong, Y. D., Wang, J., Wang, J. X., & Zhou, X. Z. (2017). A study on relationship between elderly sarcopenia and inflammatory factors IL-6 and TNF-alpha. *Eur J Med Res, 22*(1), 25. doi:10.1186/s40001-017-0266-9

Black, B. L., & Olson, E. N. (1998). Transcriptional control of muscle development by myocyte enhancer factor-2 (MEF2) proteins. *Annu Rev Cell Dev Biol, 14*, 167-196. doi:10.1146/annurev.cellbio.14.1.167

Boden, G. (2008). Obesity and free fatty acids. *Endocrinol Metab Clin North Am, 37*(3), 635-646, viii-ix. doi:10.1016/j.ecl.2008.06.007

Bohnert, K. R., Gallot, Y. S., Sato, S., Xiong, G., Hindi, S. M., & Kumar, A. (2016). Inhibition of ER stress and unfolding protein response pathways causes skeletal muscle wasting during cancer cachexia. *FASEB J, 30*(9), 3053-3068. doi:10.1096/fj.201600250RR

Bonetto, A., Aydogdu, T., Jin, X., Zhang, Z., Zhan, R., Puzis, L., . . . Zimmers, T. A. (2012). JAK/STAT3 pathway inhibition blocks skeletal muscle wasting downstream of IL-6 and in experimental cancer cachexia. *Am J Physiol Endocrinol Metab, 303*(3), E410-421. doi:10.1152/ajpendo.00039.2012

Bonetto, A., Aydogdu, T., Kunzevitzky, N., Guttridge, D. C., Khuri, S., Koniaris, L. G., & Zimmers, T. A. (2011). STAT3 activation in skeletal muscle links muscle wasting and the acute phase response in cancer cachexia. *PLoS One, 6*(7), e22538. doi:10.1371/journal.pone.0022538

Bosaeus, I., Daneryd, P., Svanberg, E., & Lundholm, K. (2001). Dietary intake and resting energy expenditure in relation to weight loss in unselected cancer patients. *Int J Cancer, 93*(3), 380-383. doi:10.1002/ijc.1332

Bowker-Kinley, M. M., Davis, W. I., Wu, P., Harris, R. A., & Popov, K. M. (1998). Evidence for existence of tissue-specific regulation of the mammalian pyruvate dehydrogenase complex. *Biochem J, 329 (Pt 1)*, 191-196. doi:10.1042/bj3290191

Brack, A. S., & Rando, T. A. (2012). Tissue-specific stem cells: lessons from the skeletal muscle satellite cell. *Cell Stem Cell, 10*(5), 504-514. doi:10.1016/j.stem.2012.04.001

Burfeind, K. G., Zhu, X., Levasseur, P. R., Michaelis, K. A., Norgard, M. A., & Marks, D. L. (2018). TRIF is a key inflammatory mediator of acute sickness behavior and cancer cachexia. *Brain Behav Immun, 73*, 364-374. doi:10.1016/j.bbi.2018.05.021

Byun, M. K., Cho, E. N., Chang, J., Ahn, C. M., & Kim, H. J. (2017). Sarcopenia correlates with systemic inflammation in COPD. *Int J Chron Obstruct Pulmon Dis, 12*, 669-675. doi:10.2147/COPD.S130790

Cahill, G. F., Jr., & Aoki, T. T. (1971). Starvation and body nitrogen. *Trans Am Clin Climatol Assoc, 82*, 43-51. Retrieved from https://www.ncbi.nlm.nih.gov/pubmed/4934018

Camargo, R. G., Riccardi, D. M., Ribeiro, H. Q., Carnevali, L. C., Jr., de Matos-Neto, E. M., Enjiu, L., . . . Seelaender, M. (2015). NF-kappaBp65 and

Expression of Its Pro-Inflammatory Target Genes Are Upregulated in the Subcutaneous Adipose Tissue of Cachectic Cancer Patients. *Nutrients, 7*(6), 4465-4479. doi:10.3390/nu7064465

Camus, V., Lanic, H., Kraut, J., Modzelewski, R., Clatot, F., Picquenot, J. M., . . . Jardin, F. (2014). Prognostic impact of fat tissue loss and cachexia assessed by computed tomography scan in elderly patients with diffuse large B-cell lymphoma treated with immunochemotherapy. *Eur J Haematol, 93*(1), 9-18. doi:10.1111/ejh.12285

Cantini, M., Massimino, M. L., Rapizzi, E., Rossini, K., Catani, C., Dalla Libera, L., & Carraro, U. (1995). Human satellite cell proliferation in vitro is regulated by autocrine secretion of IL-6 stimulated by a soluble factor(s) released by activated monocytes. *Biochem Biophys Res Commun, 216*(1), 49-53. doi:10.1006/bbrc.1995.2590

Carow, B., & Rottenberg, M. E. (2014). SOCS3, a Major Regulator of Infection and Inflammation. *Front Immunol, 5*, 58. doi:10.3389/fimmu.2014.00058

Chang, N. C., & Rudnicki, M. A. (2014). Satellite cells: the architects of skeletal muscle. *Curr Top Dev Biol, 107*, 161-181. doi:10.1016/B978-0-12-416022-4.00006-8

Chen, I., Johansen, J. S., Zimmers, T. A., Dehlendorff, C., Kirk Parner, V., Vittrup Jensen, B., & Nielsen, D. (2017). PACTO: A single center, randomized, phase II study of the combination of nab-paclitaxel and gemcitabine with or without tocilizumab, an IL-6R inhibitor, as first-line treatment in patients with locally advanced or metastatic pancreatic cancer *Ann Oncol, 28*, mdx369.158. doi:https://doi.org/10.1093/annonc/mdx369.158

Chen, J. L., Walton, K. L., Qian, H., Colgan, T. D., Hagg, A., Watt, M. J., . . . Gregorevic, P. (2016). Differential Effects of IL6 and Activin A in the Development of Cancer-Associated Cachexia. *Cancer Res, 76*(18), 5372-5382. doi:10.1158/0008-5472.CAN-15-3152

Chen, Y., Chen, J., Zhang, C., Yang, S., Zhang, X., Liu, Y., & Su, Z. (2019). Deficiency in the short-chain acyl-CoA dehydrogenase protects mice against diet-induced obesity and insulin resistance. *FASEB J, 33*(12), 13722-13733. doi:10.1096/fj.201901474RR

Ciciliot, S., & Schiaffino, S. (2010). Regeneration of mammalian skeletal muscle. Basic mechanisms and clinical implications. *Curr Pharm Des, 16*(8), 906-914. doi:10.2174/138161210790883453

Cohen, S., Nathan, J. A., & Goldberg, A. L. (2015). Muscle wasting in disease: molecular mechanisms and promising therapies. *Nat Rev Drug Discov, 14*(1), 58-74. doi:10.1038/nrd4467

Cortez, M., Carmo, L. S., Rogero, M. M., Borelli, P., & Fock, R. A. (2013). A high-fat diet increases IL-1, IL-6, and TNF-alpha production by increasing NF-kappaB and attenuating PPAR-gamma expression in bone marrow mesenchymal stem cells. *Inflammation, 36*(2), 379-386. doi:10.1007/s10753-012-9557-z

Cramer, Z., Sadek, J., Vazquez, G. G., Di Marco, S., Pause, A., Pelletier, J., & Gallouzi, I. E. (2018). eIF4A inhibition prevents the onset of cytokine-

induced muscle wasting by blocking the STAT3 and iNOS pathways. *Sci Rep, 8*(1), 8414. doi:10.1038/s41598-018-26625-9

Daemen, S., van Polanen, N., & Hesselink, M. K. C. (2018). The effect of diet and exercise on lipid droplet dynamics in human muscle tissue. *J Exp Biol, 221*(Pt Suppl 1). doi:10.1242/jeb.167015

Dahlqvist, J. R., Andersen, G., Khawajazada, T., Vissing, C., Thomsen, C., & Vissing, J. (2019). Relationship between muscle inflammation and fat replacement assessed by MRI in facioscapulohumeral muscular dystrophy. *J Neurol, 266*(5), 1127-1135. doi:10.1007/s00415-019-09242-y

Dalal, S., Hui, D., Bidaut, L., Lem, K., Del Fabbro, E., Crane, C., . . . Bruera, E. (2012). Relationships among body mass index, longitudinal body composition alterations, and survival in patients with locally advanced pancreatic cancer receiving chemoradiation: a pilot study. *J Pain Symptom Manage, 44*(2), 181-191. doi:10.1016/j.jpainsymman.2011.09.010

Danai, L. V., Babic, A., Rosenthal, M. H., Dennstedt, E. A., Muir, A., Lien, E. C., . . . Vander Heiden, M. G. (2018). Altered exocrine function can drive adipose wasting in early pancreatic cancer. *Nature, 558*(7711), 600-604. doi:10.1038/s41586-018-0235-7

Das, S. K., Eder, S., Schauer, S., Diwoky, C., Temmel, H., Guertl, B., . . . Hoefler, G. (2011). Adipose triglyceride lipase contributes to cancer-associated cachexia. *Science, 333*(6039), 233-238. doi:10.1126/science.1198973

de Sire, R., Rizzatti, G., Ingravalle, F., Pizzoferrato, M., Petito, V., Lopetuso, L., . . . Scaldaferri, F. (2018). Skeletal muscle-gut axis: emerging mechanisms of sarcopenia for intestinal and extra intestinal diseases. *Minerva Gastroenterol Dietol, 64*(4), 351-362. doi:10.23736/S1121-421X.18.02511-4

Di Sebastiano, K. M., Yang, L., Zbuk, K., Wong, R. K., Chow, T., Koff, D., . . . Mourtzakis, M. (2013). Accelerated muscle and adipose tissue loss may predict survival in pancreatic cancer patients: the relationship with diabetes and anaemia. *Br J Nutr, 109*(2), 302-312. doi:10.1017/S0007114512001067

Dobin, A., Davis, C. A., Schlesinger, F., Drenkow, J., Zaleski, C., Jha, S., . . . Gingeras, T. R. (2013). STAR: ultrafast universal RNA-seq aligner. *Bioinformatics, 29*(1), 15-21. doi:10.1093/bioinformatics/bts635

Dobrowolny, G., Martini, M., Scicchitano, B. M., Romanello, V., Boncompagni, S., Nicoletti, C., . . . Musaro, A. (2018). Muscle Expression of SOD1(G93A) Triggers the Dismantlement of Neuromuscular Junction via PKC-Theta. *Antioxid Redox Signal, 28*(12), 1105-1119. doi:10.1089/ars.2017.7054

Dotzert, M. S., McDonald, M. W., Murray, M. R., Nickels, J. Z., Noble, E. G., & Melling, C. W. J. (2018). Effect of Combined Exercise Versus Aerobic-Only Training on Skeletal Muscle Lipid Metabolism in a Rodent Model of Type 1 Diabetes. *Can J Diabetes, 42*(4), 404-411. doi:10.1016/j.jcjd.2017.09.013

Dueweke, J. J., Awan, T. M., & Mendias, C. L. (2017). Regeneration of Skeletal Muscle After Eccentric Injury. *J Sport Rehabil, 26*(2), 171-179. doi:10.1123/jsr.2016-0107

Dutil, E. M., Toker, A., & Newton, A. C. (1998). Regulation of conventional protein kinase C isozymes by phosphoinositide-dependent kinase 1 (PDK-1). *Curr Biol, 8*(25), 1366-1375. doi:10.1016/s0960-9822(98)00017-7

Ebrahimi, B., Tucker, S. L., Li, D., Abbruzzese, J. L., & Kurzrock, R. (2004). Cytokines in pancreatic carcinoma: correlation with phenotypic characteristics and prognosis. *Cancer, 101*(12), 2727-2736. doi:10.1002/cncr.20672

Eckstein, S. S., Weigert, C., & Lehmann, R. (2017). Divergent Roles of IRS (Insulin Receptor Substrate) 1 and 2 in Liver and Skeletal Muscle. *Curr Med Chem, 24*(17), 1827-1852. doi:10.2174/0929867324666170426142826

Egan Benova, T., Viczenczova, C., Szeiffova Bacova, B., Knezl, V., Dosenko, V., Rauchova, H., . . . Tribulova, N. (2019). Obesity-associated alterations in cardiac connexin-43 and PKC signaling are attenuated by melatonin and omega-3 fatty acids in female rats. *Mol Cell Biochem, 454*(1-2), 191-202. doi:10.1007/s11010-018-3463-0

Egerman, M. A., & Glass, D. J. (2014). Signaling pathways controlling skeletal muscle mass. *Crit Rev Biochem Mol Biol, 49*(1), 59-68. doi:10.3109/10409238.2013.857291

Eley, H. L., Russell, S. T., & Tisdale, M. J. (2007). Effect of branched-chain amino acids on muscle atrophy in cancer cachexia. *Biochem J, 407*(1), 113-120. doi:10.1042/BJ20070651

Evans, J. H., Murray, D., Leslie, C. C., & Falke, J. J. (2006). Specific translocation of protein kinase Calpha to the plasma membrane requires both Ca2+ and PIP2 recognition by its C2 domain. *Mol Biol Cell, 17*(1), 56-66. doi:10.1091/mbc.e05-06-0499

Farah, C. A., & Sossin, W. S. (2012). The role of C2 domains in PKC signaling. *Adv Exp Med Biol, 740*, 663-683. doi:10.1007/978-94-007-2888-2_29

Farese, R. V., Sajan, M. P., & Standaert, M. L. (2005). Insulin-sensitive protein kinases (atypical protein kinase C and protein kinase B/Akt): actions and defects in obesity and type II diabetes. *Exp Biol Med (Maywood), 230*(9), 593-605. doi:10.1177/153537020523000901

Fearon, K., Strasser, F., Anker, S. D., Bosaeus, I., Bruera, E., Fainsinger, R. L., . . . Baracos, V. E. (2011). Definition and classification of cancer cachexia: an international consensus. *Lancet Oncol, 12*(5), 489-495. doi:10.1016/S1470-2045(10)70218-7

Flint, T. R., Janowitz, T., Connell, C. M., Roberts, E. W., Denton, A. E., Coll, A. P., . . . Fearon, D. T. (2016). Tumor-Induced IL-6 Reprograms Host Metabolism to Suppress Anti-tumor Immunity. *Cell Metab, 24*(5), 672-684. doi:10.1016/j.cmet.2016.10.010

Fukawa, T., Yan-Jiang, B. C., Min-Wen, J. C., Jun-Hao, E. T., Huang, D., Qian, C. N., . . . Shyh-Chang, N. (2016). Excessive fatty acid oxidation induces

muscle atrophy in cancer cachexia. *Nat Med, 22*(6), 666-671. doi:10.1038/nm.4093
Furuyama, T., Kitayama, K., Yamashita, H., & Mori, N. (2003). Forkhead transcription factor FOXO1 (FKHR)-dependent induction of PDK4 gene expression in skeletal muscle during energy deprivation. *Biochem J, 375*(Pt 2), 365-371. doi:10.1042/BJ20030022
Griffin, M. E., Marcucci, M. J., Cline, G. W., Bell, K., Barucci, N., Lee, D., . . . Shulman, G. I. (1999). Free fatty acid-induced insulin resistance is associated with activation of protein kinase C theta and alterations in the insulin signaling cascade. *Diabetes, 48*(6), 1270-1274. doi:10.2337/diabetes.48.6.1270
Gruber, T., Hermann-Kleiter, N., Hinterleitner, R., Fresser, F., Schneider, R., Gastl, G., . . . Baier, G. (2009). PKC-theta modulates the strength of T cell responses by targeting Cbl-b for ubiquitination and degradation. *Sci Signal, 2*(76), ra30. doi:10.1126/scisignal.2000046
Gu, Z., Lin, C., Hu, J., Xia, J., Wei, S., & Gao, D. (2019). USP34 Regulated Human Pancreatic Cancer Cell Survival via AKT and PKC Pathways. *Biol Pharm Bull, 42*(4), 573-579. doi:10.1248/bpb.b18-00646
Guo, X., Sun, W., Luo, G., Wu, L., Xu, G., Hou, D., . . . Liu, T. (2019). Panax notoginseng saponins alleviate skeletal muscle insulin resistance by regulating the IRS1-PI3K-AKT signaling pathway and GLUT4 expression. *FEBS Open Bio, 9*(5), 1008-1019. doi:10.1002/2211-5463.12635
Haddad, F., Zaldivar, F., Cooper, D. M., & Adams, G. R. (2005). IL-6-induced skeletal muscle atrophy. *J Appl Physiol (1985), 98*(3), 911-917. doi:10.1152/japplphysiol.01026.2004
Han, J., & Kaufman, R. J. (2016). The role of ER stress in lipid metabolism and lipotoxicity. *J Lipid Res, 57*(8), 1329-1338. doi:10.1194/jlr.R067595
Han, M. S., White, A., Perry, R. J., Camporez, J. P., Hidalgo, J., Shulman, G. I., & Davis, R. J. (2020). Regulation of adipose tissue inflammation by interleukin 6. *Proc Natl Acad Sci U S A, 117*(6), 2751-2760. doi:10.1073/pnas.1920004117
Hardy, D., Besnard, A., Latil, M., Jouvion, G., Briand, D., Thepenier, C., . . . Chretien, F. (2016). Comparative Study of Injury Models for Studying Muscle Regeneration in Mice. *PLoS One, 11*(1), e0147198. doi:10.1371/journal.pone.0147198
Harlow, E., & Lane, D. (2006). Lysing tissue-culture cells for immunoprecipitation. *CSH Protoc, 2006*(4). doi:10.1101/pdb.prot4531
Harris, R. A., Bowker-Kinley, M. M., Huang, B., & Wu, P. (2002). Regulation of the activity of the pyruvate dehydrogenase complex. *Adv Enzyme Regul, 42*, 249-259. doi:10.1016/s0065-2571(01)00061-9
Hendifar, A. E., Petzel, M. Q. B., Zimmers, T. A., Denlinger, C. S., Matrisian, L. M., Picozzi, V. J., . . . Precision Promise, C. (2018). Pancreas Cancer-Associated Weight Loss. *Oncologist*. doi:10.1634/theoncologist.2018-0266
Hingorani, S. R., Wang, L., Multani, A. S., Combs, C., Deramaudt, T. B., Hruban, R. H., . . . Tuveson, D. A. (2005). Trp53R172H and KrasG12D cooperate to promote chromosomal instability and widely metastatic pancreatic

ductal adenocarcinoma in mice. *Cancer Cell, 7*(5), 469-483. doi:10.1016/j.ccr.2005.04.023
Holmer, R., Goumas, F. A., Waetzig, G. H., Rose-John, S., & Kalthoff, H. (2014). Interleukin-6: a villain in the drama of pancreatic cancer development and progression. *Hepatobiliary Pancreat Dis Int, 13*(4), 371-380. Retrieved from https://www.ncbi.nlm.nih.gov/pubmed/25100121
Hu, W., Ru, Z., Zhou, Y., Xiao, W., Sun, R., Zhang, S., . . . Yang, H. (2019). Lung cancer-derived extracellular vesicles induced myotube atrophy and adipocyte lipolysis via the extracellular IL-6-mediated STAT3 pathway. *Biochim Biophys Acta Mol Cell Biol Lipids, 1864*(8), 1091-1102. doi:10.1016/j.bbalip.2019.04.006
Huang, K. P. (1989). The mechanism of protein kinase C activation. *Trends Neurosci, 12*(11), 425-432. doi:10.1016/0166-2236(89)90091-x
Ikeda, S. I., Tamura, Y., Kakehi, S., Sanada, H., Kawamori, R., & Watada, H. (2016). Exercise-induced increase in IL-6 level enhances GLUT4 expression and insulin sensitivity in mouse skeletal muscle. *Biochem Biophys Res Commun, 473*(4), 947-952. doi:10.1016/j.bbrc.2016.03.159
Isakov, N. (2018). Protein kinase C (PKC) isoforms in cancer, tumor promotion and tumor suppression. *Semin Cancer Biol, 48*, 36-52. doi:10.1016/j.semcancer.2017.04.012
Itani, S. I., Pories, W. J., Macdonald, K. G., & Dohm, G. L. (2001). Increased protein kinase C theta in skeletal muscle of diabetic patients. *Metabolism, 50*(5), 553-557. doi:10.1053/meta.2001.22512
Itani, S. I., Ruderman, N. B., Schmieder, F., & Boden, G. (2002). Lipid-induced insulin resistance in human muscle is associated with changes in diacylglycerol, protein kinase C, and IkappaB-alpha. *Diabetes, 51*(7), 2005-2011. doi:10.2337/diabetes.51.7.2005
Janssens, S., Jonkers, R. A., Groen, A. K., Nicolay, K., van Loon, L. J., & Prompers, J. J. (2015). Effects of acute exercise on lipid content and dietary lipid uptake in liver and skeletal muscle of lean and diabetic rats. *Am J Physiol Endocrinol Metab, 309*(10), E874-883. doi:10.1152/ajpendo.00292.2015
Jonkers, R. A., van Loon, L. J., Nicolay, K., & Prompers, J. J. (2013). In vivo postprandial lipid partitioning in liver and skeletal muscle in prediabetic and diabetic rats. *Diabetologia, 56*(3), 618-626. doi:10.1007/s00125-012-2792-x
Jung, T. W., Lee, S. H., Kim, H. C., Bang, J. S., Abd El-Aty, A. M., Hacimuftuoglu, A., . . . Jeong, J. H. (2018). METRNL attenuates lipid-induced inflammation and insulin resistance via AMPK or PPARdelta-dependent pathways in skeletal muscle of mice. *Exp Mol Med, 50*(9), 122. doi:10.1038/s12276-018-0147-5
Kays, J. K., Shahda, S., Stanley, M., Bell, T. M., O'Neill, B. H., Kohli, M. D., . . . Zimmers, T. A. (2018). Three cachexia phenotypes and the impact of fat-only loss on survival in FOLFIRINOX therapy for pancreatic cancer. *J Cachexia Sarcopenia Muscle, 9*(4), 673-684. doi:10.1002/jcsm.12307

Kishimoto, A., Kajikawa, N., Shiota, M., & Nishizuka, Y. (1983). Proteolytic activation of calcium-activated, phospholipid-dependent protein kinase by calcium-dependent neutral protease. *J Biol Chem, 258*(2), 1156-1164. Retrieved from https://www.ncbi.nlm.nih.gov/pubmed/6296071

Knudsen, J. G., Gudiksen, A., Bertholdt, L., Overby, P., Villesen, I., Schwartz, C. L., & Pilegaard, H. (2017). Skeletal muscle IL-6 regulates muscle substrate utilization and adipose tissue metabolism during recovery from an acute bout of exercise. *PLoS One, 12*(12), e0189301. doi:10.1371/journal.pone.0189301

Konigsberg, I. R. (1963). Clonal analysis of myogenesis. *Science, 140*(3573), 1273-1284. doi:10.1126/science.140.3573.1273

Konno, Y., Ohno, S., Akita, Y., Kawasaki, H., & Suzuki, K. (1989). Enzymatic properties of a novel phorbol ester receptor/protein kinase, nPKC. *J Biochem, 106*(4), 673-678. doi:10.1093/oxfordjournals.jbchem.a122915

Kraakman, M. J., Kammoun, H. L., Allen, T. L., Deswaerte, V., Henstridge, D. C., Estevez, E., . . . Febbraio, M. A. (2015). Blocking IL-6 trans-signaling prevents high-fat diet-induced adipose tissue macrophage recruitment but does not improve insulin resistance. *Cell Metab, 21*(3), 403-416. doi:10.1016/j.cmet.2015.02.006

Kuang, S., & Rudnicki, M. A. (2008). The emerging biology of satellite cells and their therapeutic potential. *Trends Mol Med, 14*(2), 82-91. doi:10.1016/j.molmed.2007.12.004

Kumar, D. V., Shanmugasundaram, J., Sundaram, C., & Anandaraj, M. P. (2002). Activity of novel protein kinase C and distribution of protein kinase C theta in subcellular fractions of normal and Duchenne muscular dystrophic muscle. *Indian J Biochem Biophys, 39*(6), 377-381. Retrieved from https://www.ncbi.nlm.nih.gov/pubmed/22905394

Kurumatani, T., Fastbom, J., Bonkale, W. L., Bogdanovic, N., Winblad, B., Ohm, T. G., & Cowburn, R. F. (1998). Loss of inositol 1,4,5-trisphosphate receptor sites and decreased PKC levels correlate with staging of Alzheimer's disease neurofibrillary pathology. *Brain Res, 796*(1-2), 209-221. doi:10.1016/s0006-8993(98)00347-3

Laplante, M., & Sabatini, D. M. (2013). Regulation of mTORC1 and its impact on gene expression at a glance. *J Cell Sci, 126*(Pt 8), 1713-1719. doi:10.1242/jcs.125773

Lerin, C., Goldfine, A. B., Boes, T., Liu, M., Kasif, S., Dreyfuss, J. M., . . . Patti, M. E. (2016). Defects in muscle branched-chain amino acid oxidation contribute to impaired lipid metabolism. *Mol Metab, 5*(10), 926-936. doi:10.1016/j.molmet.2016.08.001

Lesina, M., Kurkowski, M. U., Ludes, K., Rose-John, S., Treiber, M., Kloppel, G., . . . Algul, H. (2011). Stat3/Socs3 activation by IL-6 transsignaling promotes progression of pancreatic intraepithelial neoplasia and development of pancreatic cancer. *Cancer Cell, 19*(4), 456-469. doi:10.1016/j.ccr.2011.03.009

Lipp, P., & Reither, G. (2011). Protein kinase C: the "masters" of calcium and lipid. *Cold Spring Harb Perspect Biol, 3*(7). doi:10.1101/cshperspect.a004556

Liu, C. H., Hua, N., Fu, X., Pan, Y. L., Li, B., & Li, X. D. (2018). Metformin regulates atrial SK2 and SK3 expression through inhibiting the PKC/ERK signaling pathway in type 2 diabetic rats. *BMC Cardiovasc Disord, 18*(1), 236. doi:10.1186/s12872-018-0950-x

Liu, Y., Graham, C., Li, A., Fisher, R. J., & Shaw, S. (2002). Phosphorylation of the protein kinase C-theta activation loop and hydrophobic motif regulates its kinase activity, but only activation loop phosphorylation is critical to in vivo nuclear-factor-kappaB induction. *Biochem J, 361*(Pt 2), 255-265. doi:10.1042/bj3610255

Long, K. B., Tooker, G., Tooker, E., Luque, S. L., Lee, J. W., Pan, X., & Beatty, G. L. (2017). IL6 Receptor Blockade Enhances Chemotherapy Efficacy in Pancreatic Ductal Adenocarcinoma. *Mol Cancer Ther, 16*(9), 1898-1908. doi:10.1158/1535-7163.MCT-16-0899

Lozanoska-Ochser, B., Benedetti, A., Rizzo, G., Marrocco, V., Di Maggio, R., Fiore, P., & Bouche, M. (2018). Targeting early PKCtheta-dependent T-cell infiltration of dystrophic muscle reduces disease severity in a mouse model of muscular dystrophy. *J Pathol, 244*(3), 323-333. doi:10.1002/path.5016

Mace, T. A., Shakya, R., Pitarresi, J. R., Swanson, B., McQuinn, C. W., Loftus, S., . . . Lesinski, G. B. (2018). IL-6 and PD-L1 antibody blockade combination therapy reduces tumour progression in murine models of pancreatic cancer. *Gut, 67*(2), 320-332. doi:10.1136/gutjnl-2016-311585

Madaro, L., Passafaro, M., Sala, D., Etxaniz, U., Lugarini, F., Proietti, D., . . . Puri, P. L. (2018). Denervation-activated STAT3-IL-6 signalling in fibro-adipogenic progenitors promotes myofibres atrophy and fibrosis. *Nat Cell Biol, 20*(8), 917-927. doi:10.1038/s41556-018-0151-y

Madaro, L., Pelle, A., Nicoletti, C., Crupi, A., Marrocco, V., Bossi, G., . . . Bouche, M. (2012). PKC theta ablation improves healing in a mouse model of muscular dystrophy. *PLoS One, 7*(2), e31515. doi:10.1371/journal.pone.0031515

Margolis, L. M., Wilson, M. A., Whitney, C. C., Carrigan, C. T., Murphy, N. E., Hatch, A. M., . . . Pasiakos, S. M. (2019). Exercising with low muscle glycogen content increases fat oxidation and decreases endogenous, but not exogenous carbohydrate oxidation. *Metabolism, 97*, 1-8. doi:10.1016/j.metabol.2019.05.003

Marrocco, V., Bogomolovas, J., Ehler, E., Dos Remedios, C. G., Yu, J., Gao, C., & Lange, S. (2019). PKC and PKN in heart disease. *J Mol Cell Cardiol, 128*, 212-226. doi:10.1016/j.yjmcc.2019.01.029

Marrocco, V., Fiore, P., Benedetti, A., Pisu, S., Rizzuto, E., Musaro, A., . . . Bouche, M. (2017). Pharmacological Inhibition of PKCtheta Counteracts Muscle Disease in a Mouse Model of Duchenne Muscular Dystrophy. *EBioMedicine, 16*, 150-161. doi:10.1016/j.ebiom.2017.01.001

Martignoni, M. E., Kunze, P., Hildebrandt, W., Kunzli, B., Berberat, P., Giese, T., . . . Friess, H. (2005). Role of mononuclear cells and inflammatory cytokines in pancreatic cancer-related cachexia. *Clin Cancer Res, 11*(16), 5802-5808. doi:10.1158/1078-0432.CCR-05-0185

Martin, L., Birdsell, L., Macdonald, N., Reiman, T., Clandinin, M. T., McCargar, L. J., . . . Baracos, V. E. (2013). Cancer cachexia in the age of obesity: skeletal muscle depletion is a powerful prognostic factor, independent of body mass index. *J Clin Oncol, 31*(12), 1539-1547. doi:10.1200/JCO.2012.45.2722

Massart, J., & Zierath, J. R. (2019). Role of Diacylglycerol Kinases in Glucose and Energy Homeostasis. *Trends Endocrinol Metab, 30*(9), 603-617. doi:10.1016/j.tem.2019.06.003

McCarthy, D. J., Chen, Y., & Smyth, G. K. (2012). Differential expression analysis of multifactor RNA-Seq experiments with respect to biological variation. *Nucleic Acids Res, 40*(10), 4288-4297. doi:10.1093/nar/gks042

McKinsey, T. A., Zhang, C. L., & Olson, E. N. (2002). MEF2: a calcium-dependent regulator of cell division, differentiation and death. *Trends Biochem Sci, 27*(1), 40-47. doi:10.1016/s0968-0004(01)02031-x

Mehlem, A., Hagberg, C. E., Muhl, L., Eriksson, U., & Falkevall, A. (2013). Imaging of neutral lipids by oil red O for analyzing the metabolic status in health and disease. *Nat Protoc, 8*(6), 1149-1154. doi:10.1038/nprot.2013.055

Melenovsky, V., Kotrc, M., Borlaug, B. A., Marek, T., Kovar, J., Malek, I., & Kautzner, J. (2013). Relationships between right ventricular function, body composition, and prognosis in advanced heart failure. *J Am Coll Cardiol, 62*(18), 1660-1670. doi:10.1016/j.jacc.2013.06.046

Mellor, H., & Parker, P. J. (1998). The extended protein kinase C superfamily. *Biochem J, 332 (Pt 2)*, 281-292. doi:10.1042/bj3320281

Milan, G., Romanello, V., Pescatore, F., Armani, A., Paik, J. H., Frasson, L., . . . Sandri, M. (2015). Regulation of autophagy and the ubiquitin-proteasome system by the FoxO transcriptional network during muscle atrophy. *Nat Commun, 6*, 6670. doi:10.1038/ncomms7670

Minamoto, V. B., Hulst, J. B., Lim, M., Peace, W. J., Bremner, S. N., Ward, S. R., & Lieber, R. L. (2007). Increased efficacy and decreased systemic-effects of botulinum toxin A injection after active or passive muscle manipulation. *Dev Med Child Neurol, 49*(12), 907-914. doi:10.1111/j.1469-8749.2007.00907.x

Mitchell, C. J., Churchward-Venne, T. A., Bellamy, L., Parise, G., Baker, S. K., & Phillips, S. M. (2013). Muscular and systemic correlates of resistance training-induced muscle hypertrophy. *PLoS One, 8*(10), e78636. doi:10.1371/journal.pone.0078636

Molkentin, J. D., & Olson, E. N. (1996). Defining the regulatory networks for muscle development. *Curr Opin Genet Dev, 6*(4), 445-453. doi:10.1016/s0959-437x(96)80066-9

Morales, P. E., Bucarey, J. L., & Espinosa, A. (2017). Muscle Lipid Metabolism: Role of Lipid Droplets and Perilipins. *J Diabetes Res, 2017*, 1789395. doi:10.1155/2017/1789395

Moses, A. G., Maingay, J., Sangster, K., Fearon, K. C., & Ross, J. A. (2009). Pro-inflammatory cytokine release by peripheral blood mononuclear cells from patients with advanced pancreatic cancer: relationship to acute phase response and survival. *Oncol Rep, 21*(4), 1091-1095. Retrieved from https://www.ncbi.nlm.nih.gov/pubmed/19288013

Motegi, A., Sakurai, S., Nakayama, H., Sano, T., Oyama, T., & Nakajima, T. (2005). PKC theta, a novel immunohistochemical marker for gastrointestinal stromal tumors (GIST), especially useful for identifying KIT-negative tumors. *Pathol Int, 55*(3), 106-112. doi:10.1111/j.1440-1827.2005.01806.x

Mullberg, J., Schooltink, H., Stoyan, T., Heinrich, P. C., & Rose-John, S. (1992). Protein kinase C activity is rate limiting for shedding of the interleukin-6 receptor. *Biochem Biophys Res Commun, 189*(2), 794-800. Retrieved from https://www.ncbi.nlm.nih.gov/pubmed/1335247

Munoz-Canoves, P., Scheele, C., Pedersen, B. K., & Serrano, A. L. (2013). Interleukin-6 myokine signaling in skeletal muscle: a double-edged sword? *FEBS J, 280*(17), 4131-4148. doi:10.1111/febs.12338

Muoio, D. M., & Koves, T. R. (2007). Lipid-induced metabolic dysfunction in skeletal muscle. *Novartis Found Symp, 286*, 24-38; discussion 38-46, 162-163, 196-203. doi:10.1002/9780470985571.ch4

Muoio, D. M., & Neufer, P. D. (2012). Lipid-induced mitochondrial stress and insulin action in muscle. *Cell Metab, 15*(5), 595-605. doi:10.1016/j.cmet.2012.04.010

Nalefski, E. A., & Falke, J. J. (1996). The C2 domain calcium-binding motif: structural and functional diversity. *Protein Sci, 5*(12), 2375-2390. doi:10.1002/pro.5560051201

Narsale, A. A., & Carson, J. A. (2014). Role of interleukin-6 in cachexia: therapeutic implications. *Curr Opin Support Palliat Care, 8*(4), 321-327. doi:10.1097/SPC.0000000000000091

Navale, A. M., & Paranjape, A. N. (2016). Glucose transporters: physiological and pathological roles. *Biophys Rev, 8*(1), 5-9. doi:10.1007/s12551-015-0186-2

Newgard, C. B. (2017). Metabolomics and Metabolic Diseases: Where Do We Stand? *Cell Metab, 25*(1), 43-56. doi:10.1016/j.cmet.2016.09.018

Newton, A. C. (1995). Protein kinase C: structure, function, and regulation. *J Biol Chem, 270*(48), 28495-28498. doi:10.1074/jbc.270.48.28495

Newton, A. C. (2001). Protein kinase C: structural and spatial regulation by phosphorylation, cofactors, and macromolecular interactions. *Chem Rev, 101*(8), 2353-2364. doi:10.1021/cr0002801

Nishizuka, Y. (1992). Intracellular signaling by hydrolysis of phospholipids and activation of protein kinase C. *Science, 258*(5082), 607-614. doi:10.1126/science.1411571

O'Connell, T. M. (2013). The complex role of branched chain amino acids in diabetes and cancer. *Metabolites, 3*(4), 931-945. doi:10.3390/metabo3040931

Ohlund, D., Handly-Santana, A., Biffi, G., Elyada, E., Almeida, A. S., Ponz-Sarvise, M., . . . Tuveson, D. A. (2017). Distinct populations of inflammatory fibroblasts and myofibroblasts in pancreatic cancer. *J Exp Med, 214*(3), 579-596. doi:10.1084/jem.20162024

Okada, S., Okusaka, T., Ishii, H., Kyogoku, A., Yoshimori, M., Kajimura, N., . . . Kakizoe, T. (1998). Elevated serum interleukin-6 levels in patients with pancreatic cancer. *Jpn J Clin Oncol, 28*(1), 12-15. Retrieved from https://www.ncbi.nlm.nih.gov/pubmed/9491135

Onesti, J. K., & Guttridge, D. C. (2014). Inflammation based regulation of cancer cachexia. *Biomed Res Int, 2014*, 168407. doi:10.1155/2014/168407

Osada, S., Mizuno, K., Saido, T. C., Suzuki, K., Kuroki, T., & Ohno, S. (1992). A new member of the protein kinase C family, nPKC theta, predominantly expressed in skeletal muscle. *Mol Cell Biol, 12*(9), 3930-3938. doi:10.1128/mcb.12.9.3930

Passey, S. L., Bozinovski, S., Vlahos, R., Anderson, G. P., & Hansen, M. J. (2016). Serum Amyloid A Induces Toll-Like Receptor 2-Dependent Inflammatory Cytokine Expression and Atrophy in C2C12 Skeletal Muscle Myotubes. *PLoS One, 11*(1), e0146882. doi:10.1371/journal.pone.0146882

Peake, J. M., Della Gatta, P., Suzuki, K., & Nieman, D. C. (2015). Cytokine expression and secretion by skeletal muscle cells: regulatory mechanisms and exercise effects. *Exerc Immunol Rev, 21*, 8-25. Retrieved from https://www.ncbi.nlm.nih.gov/pubmed/25826432

Peck, B., Huot, J., Renzi, T., Arthur, S., Turner, M. J., & Marino, J. S. (2018). Mice lacking PKC-theta in skeletal muscle have reduced intramyocellular lipid accumulation and increased insulin responsiveness in skeletal muscle. *Am J Physiol Regul Integr Comp Physiol, 314*(3), R468-R477. doi:10.1152/ajpregu.00521.2016

Pedersen, B. K., Steensberg, A., & Schjerling, P. (2001). Exercise and interleukin-6. *Curr Opin Hematol, 8*(3), 137-141. doi:10.1097/00062752-200105000-00002

Pellegrinelli, V., Rouault, C., Rodriguez-Cuenca, S., Albert, V., Edom-Vovard, F., Vidal-Puig, A., . . . Lacasa, D. (2015). Human Adipocytes Induce Inflammation and Atrophy in Muscle Cells During Obesity. *Diabetes, 64*(9), 3121-3134. doi:10.2337/db14-0796

Pendharkar, S. A., Singh, R. G., & Petrov, M. S. (2018). Pro-inflammatory cytokine-induced lipolysis after an episode of acute pancreatitis. *Arch Physiol Biochem, 124*(5), 401-409. doi:10.1080/13813455.2017.1415359

Pin, F., Barreto, R., Couch, M. E., Bonetto, A., & O'Connell, T. M. (2019). Cachexia induced by cancer and chemotherapy yield distinct perturbations to energy metabolism. *J Cachexia Sarcopenia Muscle, 10*(1), 140-154. doi:10.1002/jcsm.12360

Puppa, M. J., Gao, S., Narsale, A. A., & Carson, J. A. (2014). Skeletal muscle glycoprotein 130's role in Lewis lung carcinoma-induced cachexia. *FASEB J, 28*(2), 998-1009. doi:10.1096/fj.13-240580

Ramsey, M. L., Talbert, E., Ahn, D., Bekaii-Saab, T., Badi, N., Bloomston, P. M., . . . Hart, P. A. (2019). Circulating interleukin-6 is associated with disease progression, but not cachexia in pancreatic cancer. *Pancreatology, 19*(1), 80-87. doi:10.1016/j.pan.2018.11.002

Razidlo, G. L., Burton, K. M., & McNiven, M. A. (2018). Interleukin-6 promotes pancreatic cancer cell migration by rapidly activating the small GTPase CDC42. *J Biol Chem, 293*(28), 11143-11153. doi:10.1074/jbc.RA118.003276

Robinson, M. D., McCarthy, D. J., & Smyth, G. K. (2010). edgeR: a Bioconductor package for differential expression analysis of digital gene expression data. *Bioinformatics, 26*(1), 139-140. doi:10.1093/bioinformatics/btp616

Rohm, M., Schafer, M., Laurent, V., Ustunel, B. E., Niopek, K., Algire, C., . . . Herzig, S. (2016). An AMP-activated protein kinase-stabilizing peptide ameliorates adipose tissue wasting in cancer cachexia in mice. *Nat Med, 22*(10), 1120-1130. doi:10.1038/nm.4171

Rollins, K. E., Tewari, N., Ackner, A., Awwad, A., Madhusudan, S., Macdonald, I. A., . . . Lobo, D. N. (2016). The impact of sarcopenia and myosteatosis on outcomes of unresectable pancreatic cancer or distal cholangiocarcinoma. *Clin Nutr, 35*(5), 1103-1109. doi:10.1016/j.clnu.2015.08.005

Ron, D., & Kazanietz, M. G. (1999). New insights into the regulation of protein kinase C and novel phorbol ester receptors. *FASEB J, 13*(13), 1658-1676. Retrieved from https://www.ncbi.nlm.nih.gov/pubmed/10506570

Rong, Y. D., Bian, A. L., Hu, H. Y., Ma, Y., & Zhou, X. Z. (2018). Study on relationship between elderly sarcopenia and inflammatory cytokine IL-6, anti-inflammatory cytokine IL-10. *BMC Geriatr, 18*(1), 308. doi:10.1186/s12877-018-1007-9

Rosean, T. R., Tompkins, V. S., Tricot, G., Holman, C. J., Olivier, A. K., Zhan, F., & Janz, S. (2014). Preclinical validation of interleukin 6 as a therapeutic target in multiple myeloma. *Immunol Res, 59*(1-3), 188-202. doi:10.1007/s12026-014-8528-x

Sabourin, L. A., & Rudnicki, M. A. (2000). The molecular regulation of myogenesis. *Clin Genet, 57*(1), 16-25. doi:10.1034/j.1399-0004.2000.570103.x

Sanchez, P., De Carcer, G., Sandoval, I. V., Moscat, J., & Diaz-Meco, M. T. (1998). Localization of atypical protein kinase C isoforms into lysosome-targeted endosomes through interaction with p62. *Mol Cell Biol, 18*(5), 3069-3080. doi:10.1128/mcb.18.5.3069

Sandini, M., Patino, M., Ferrone, C. R., Alvarez-Perez, C. A., Honselmann, K. C., Paiella, S., . . . Fernandez-Del Castillo, C. (2018). Association Between Changes in Body Composition and Neoadjuvant Treatment for Pancreatic Cancer. *JAMA Surg, 153*(9), 809-815. doi:10.1001/jamasurg.2018.0979

Sandri, M. (2016). Protein breakdown in cancer cachexia. *Semin Cell Dev Biol, 54*, 11-19. doi:10.1016/j.semcdb.2015.11.002

Schaper, F., & Rose-John, S. (2015). Interleukin-6: Biology, signaling and strategies of blockade. *Cytokine Growth Factor Rev, 26*(5), 475-487. doi:10.1016/j.cytogfr.2015.07.004
Schiaffino, S., Dyar, K. A., Ciciliot, S., Blaauw, B., & Sandri, M. (2013). Mechanisms regulating skeletal muscle growth and atrophy. *FEBS J, 280*(17), 4294-4314. doi:10.1111/febs.12253
Schiaffino, S., & Reggiani, C. (2011). Fiber types in mammalian skeletal muscles. *Physiol Rev, 91*(4), 1447-1531. doi:10.1152/physrev.00031.2010
Schumacher, N., Meyer, D., Mauermann, A., von der Heyde, J., Wolf, J., Schwarz, J., . . . Rabe, B. (2015). Shedding of Endogenous Interleukin-6 Receptor (IL-6R) Is Governed by A Disintegrin and Metalloproteinase (ADAM) Proteases while a Full-length IL-6R Isoform Localizes to Circulating Microvesicles. *J Biol Chem, 290*(43), 26059-26071. doi:10.1074/jbc.M115.649509
Sciote, J. J., & Rowlerson, A. (1998). Skeletal fiber types and spindle distribution in limb and jaw muscles of the adult and neonatal opossum, Monodelphis domestica. *Anat Rec, 251*(4), 548-562. doi:10.1002/(SICI)1097-0185(199808)251:4<548::AID-AR10>3.0.CO;2-O
Serra, C., Federici, M., Buongiorno, A., Senni, M. I., Morelli, S., Segratella, E., . . . Bouche, M. (2003). Transgenic mice with dominant negative PKC-theta in skeletal muscle: a new model of insulin resistance and obesity. *J Cell Physiol, 196*(1), 89-97. doi:10.1002/jcp.10278
Serrano, A. L., Baeza-Raja, B., Perdiguero, E., Jardi, M., & Munoz-Canoves, P. (2008). Interleukin-6 is an essential regulator of satellite cell-mediated skeletal muscle hypertrophy. *Cell Metab, 7*(1), 33-44. doi:10.1016/j.cmet.2007.11.011
Shamim, B., Hawley, J. A., & Camera, D. M. (2018). Protein Availability and Satellite Cell Dynamics in Skeletal Muscle. *Sports Med, 48*(6), 1329-1343. doi:10.1007/s40279-018-0883-7
Shang, P., Zhang, B., Zhang, J., Duan, M., Wu, L., Gong, X., . . . Chamba, Y. (2019). Expression and single-nucleotide polymorphisms of the H-FABP gene in pigs. *Gene, 710*, 156-160. doi:10.1016/j.gene.2019.05.061
Shukla, R., Banerjee, S., & Tripathi, Y. B. (2018). Pueraria tuberosa extract inhibits iNOS and IL-6 through suppression of PKC-alpha and NF-kB pathway in diabetes-induced nephropathy. *J Pharm Pharmacol, 70*(8), 1102-1112. doi:10.1111/jphp.12931
Siegel, R. L., Miller, K. D., & Jemal, A. (2019). Cancer statistics, 2019. *CA Cancer J Clin, 69*(1), 7-34. doi:10.3322/caac.21551
Silva, K. A., Dong, J., Dong, Y., Dong, Y., Schor, N., Tweardy, D. J., . . . Mitch, W. E. (2015). Inhibition of Stat3 activation suppresses caspase-3 and the ubiquitin-proteasome system, leading to preservation of muscle mass in cancer cachexia. *J Biol Chem, 290*(17), 11177-11187. doi:10.1074/jbc.M115.641514
Sindhu, S., Thomas, R., Shihab, P., Sriraman, D., Behbehani, K., & Ahmad, R. (2015). Obesity Is a Positive Modulator of IL-6R and IL-6 Expression in the

Subcutaneous Adipose Tissue: Significance for Metabolic Inflammation. *PLoS One, 10*(7), e0133494. doi:10.1371/journal.pone.0133494

Snow, M. H. (1977). Myogenic cell formation in regenerating rat skeletal muscle injured by mincing. II. An autoradiographic study. *Anat Rec, 188*(2), 201-217. doi:10.1002/ar.1091880206

Srivastava, N. K., Yadav, R., Mukherjee, S., Pal, L., & Sinha, N. (2017). Abnormal lipid metabolism in skeletal muscle tissue of patients with muscular dystrophy: In vitro, high-resolution NMR spectroscopy based observation in early phase of the disease. *Magn Reson Imaging, 38*, 163-173. doi:10.1016/j.mri.2017.01.001

Stephens, N. A., Skipworth, R. J., Gallagher, I. J., Greig, C. A., Guttridge, D. C., Ross, J. A., & Fearon, K. C. (2015). Evaluating potential biomarkers of cachexia and survival in skeletal muscle of upper gastrointestinal cancer patients. *J Cachexia Sarcopenia Muscle, 6*(1), 53-61. doi:10.1002/jcsm.12005

Steyn, P. J., Dzobo, K., Smith, R. I., & Myburgh, K. H. (2019). Interleukin-6 Induces Myogenic Differentiation via JAK2-STAT3 Signaling in Mouse C2C12 Myoblast Cell Line and Primary Human Myoblasts. *Int J Mol Sci, 20*(21). doi:10.3390/ijms20215273

Strassmann, G., Fong, M., Kenney, J. S., & Jacob, C. O. (1992). Evidence for the involvement of interleukin 6 in experimental cancer cachexia. *J Clin Invest, 89*(5), 1681-1684. doi:10.1172/JCI115767

Streja, D. A., Steiner, G., Marliss, E. B., & Vranic, M. (1977). Turnover and recycling of glucose in man during prolonged fasting. *Metabolism, 26*(10), 1089-1098. doi:10.1016/0026-0495(77)90035-x

Stretch, C., Aubin, J. M., Mickiewicz, B., Leugner, D., Al-Manasra, T., Tobola, E., . . . Bathe, O. F. (2018). Sarcopenia and myosteatosis are accompanied by distinct biological profiles in patients with pancreatic and periampullary adenocarcinomas. *PLoS One, 13*(5), e0196235. doi:10.1371/journal.pone.0196235

Strohle, A., Zanker, K., & Hahn, A. (2010). Nutrition in oncology: the case of micronutrients (review). *Oncol Rep, 24*(4), 815-828. doi:10.3892/or.2010.815

Suh, S. Y., Choi, Y. S., Yeom, C. H., Kwak, S. M., Yoon, H. M., Kim, D. G., . . . Yim, E. (2013). Interleukin-6 but not tumour necrosis factor-alpha predicts survival in patients with advanced cancer. *Support Care Cancer, 21*(11), 3071-3077. doi:10.1007/s00520-013-1878-4

Sun, L., Quan, X. Q., & Yu, S. (2015). An Epidemiological Survey of Cachexia in Advanced Cancer Patients and Analysis on Its Diagnostic and Treatment Status. *Nutr Cancer, 67*(7), 1056-1062. doi:10.1080/01635581.2015.1073753

Sun, S., Wang, R., Song, J., Guan, M., Li, N., Zhang, X., . . . Zhang, J. (2017). Blocking gp130 signaling suppresses autotaxin expression in adipocytes and improves insulin sensitivity in diet-induced obesity. *J Lipid Res, 58*(11), 2102-2113. doi:10.1194/jlr.M075655

Sutton, R. B., Davletov, B. A., Berghuis, A. M., Sudhof, T. C., & Sprang, S. R. (1995). Structure of the first C2 domain of synaptotagmin I: a novel Ca2+/phospholipid-binding fold. *Cell, 80*(6), 929-938. doi:10.1016/0092-8674(95)90296-1

Szendroedi, J., Yoshimura, T., Phielix, E., Koliaki, C., Marcucci, M., Zhang, D., . . . Roden, M. (2014). Role of diacylglycerol activation of PKCtheta in lipid-induced muscle insulin resistance in humans. *Proc Natl Acad Sci U S A, 111*(26), 9597-9602. doi:10.1073/pnas.1409229111

Szychlinska, M. A., Castrogiovanni, P., Trovato, F. M., Nsir, H., Zarrouk, M., Lo Furno, D., . . . Musumeci, G. (2019). Physical activity and Mediterranean diet based on olive tree phenolic compounds from two different geographical areas have protective effects on early osteoarthritis, muscle atrophy and hepatic steatosis. *Eur J Nutr, 58*(2), 565-581. doi:10.1007/s00394-018-1632-2

Takai, Y., Kishimoto, A., Iwasa, Y., Kawahara, Y., Mori, T., & Nishizuka, Y. (1979). Calcium-dependent activation of a multifunctional protein kinase by membrane phospholipids. *J Biol Chem, 254*(10), 3692-3695. Retrieved from https://www.ncbi.nlm.nih.gov/pubmed/438153

Takayama, Y., Kusamori, K., & Nishikawa, M. (2019). Click Chemistry as a Tool for Cell Engineering and Drug Delivery. *Molecules, 24*(1). doi:10.3390/molecules24010172

Talbert, E. E., Lewis, H. L., Farren, M. R., Ramsey, M. L., Chakedis, J. M., Rajasekera, P., . . . Guttridge, D. C. (2018). Circulating monocyte chemoattractant protein-1 (MCP-1) is associated with cachexia in treatment-naive pancreatic cancer patients. *J Cachexia Sarcopenia Muscle, 9*(2), 358-368. doi:10.1002/jcsm.12251

Tang, Y., Luo, Y., Jiang, Z., Ma, Y., Lin, C. J., Kim, C., . . . Tian, X. C. (2012). Jak/Stat3 signaling promotes somatic cell reprogramming by epigenetic regulation. *Stem Cells, 30*(12), 2645-2656. doi:10.1002/stem.1225

Taniguchi, K., & Karin, M. (2014). IL-6 and related cytokines as the critical lynchpins between inflammation and cancer. *Semin Immunol, 26*(1), 54-74. doi:10.1016/j.smim.2014.01.001

Tapscott, S. J. (2005). The circuitry of a master switch: Myod and the regulation of skeletal muscle gene transcription. *Development, 132*(12), 2685-2695. doi:10.1242/dev.01874

Tierney, M. T., Aydogdu, T., Sala, D., Malecova, B., Gatto, S., Puri, P. L., . . . Sacco, A. (2014). STAT3 signaling controls satellite cell expansion and skeletal muscle repair. *Nat Med, 20*(10), 1182-1186. doi:10.1038/nm.3656

Toniolo, L., Maccatrozzo, L., Patruno, M., Caliaro, F., Mascarello, F., & Reggiani, C. (2005). Expression of eight distinct MHC isoforms in bovine striated muscles: evidence for MHC-2B presence only in extraocular muscles. *J Exp Biol, 208*(Pt 22), 4243-4253. doi:10.1242/jeb.01904

Toth, K. G., McKay, B. R., De Lisio, M., Little, J. P., Tarnopolsky, M. A., & Parise, G. (2011). IL-6 induced STAT3 signalling is associated with the proliferation of human muscle satellite cells following acute muscle damage. *PLoS One, 6*(3), e17392. doi:10.1371/journal.pone.0017392

Trujillo, M. E., Sullivan, S., Harten, I., Schneider, S. H., Greenberg, A. S., & Fried, S. K. (2004). Interleukin-6 regulates human adipose tissue lipid metabolism and leptin production in vitro. *J Clin Endocrinol Metab, 89*(11), 5577-5582. doi:10.1210/jc.2004-0603

Tsoli, M., Swarbrick, M. M., & Robertson, G. R. (2016). Lipolytic and thermogenic depletion of adipose tissue in cancer cachexia. *Semin Cell Dev Biol, 54*, 68-81. doi:10.1016/j.semcdb.2015.10.039

Tsubaki, M., Takeda, T., Tani, T., Shimaoka, H., Suzuyama, N., Sakamoto, K., . . . Nishida, S. (2015). PKC/MEK inhibitors suppress oxaliplatin-induced neuropathy and potentiate the antitumor effects. *Int J Cancer, 137*(1), 243-250. doi:10.1002/ijc.29367

Tsujinaka, T., Fujita, J., Ebisui, C., Yano, M., Kominami, E., Suzuki, K., . . . Monden, M. (1996). Interleukin 6 receptor antibody inhibits muscle atrophy and modulates proteolytic systems in interleukin 6 transgenic mice. *J Clin Invest, 97*(1), 244-249. doi:10.1172/JCI118398

Turcotte, L. P., Swenberger, J. R., Tucker, M. Z., Yee, A. J., Trump, G., Luiken, J. J., & Bonen, A. (2000). Muscle palmitate uptake and binding are saturable and inhibited by antibodies to FABP(PM). *Mol Cell Biochem, 210*(1-2), 53-63. doi:10.1023/a:1007046929776

Upadhya, S. C., Ding, L., Smith, T. K., & Hegde, A. N. (2006). Differential regulation of proteasome activity in the nucleus and the synaptic terminals. *Neurochem Int, 48*(4), 296-305. doi:10.1016/j.neuint.2005.11.003

VanderVeen, B. N., Fix, D. K., & Carson, J. A. (2017). Disrupted Skeletal Muscle Mitochondrial Dynamics, Mitophagy, and Biogenesis during Cancer Cachexia: A Role for Inflammation. *Oxid Med Cell Longev, 2017*, 3292087. doi:10.1155/2017/3292087

Verstovsek, S., Kantarjian, H., Mesa, R. A., Pardanani, A. D., Cortes-Franco, J., Thomas, D. A., . . . Tefferi, A. (2010). Safety and efficacy of INCB018424, a JAK1 and JAK2 inhibitor, in myelofibrosis. *N Engl J Med, 363*(12), 1117-1127. doi:10.1056/NEJMoa1002028

von Haehling, S., Anker, M. S., & Anker, S. D. (2016). Prevalence and clinical impact of cachexia in chronic illness in Europe, USA, and Japan: facts and numbers update 2016. *J Cachexia Sarcopenia Muscle, 7*(5), 507-509. doi:10.1002/jcsm.12167

Wang, K., Wang, C., Xiao, F., Wang, H., & Wu, Z. (2008). JAK2/STAT2/STAT3 are required for myogenic differentiation. *J Biol Chem, 283*(49), 34029-34036. doi:10.1074/jbc.M803012200

Wang, X., Chuang, H. C., Li, J. P., & Tan, T. H. (2012). Regulation of PKC-theta function by phosphorylation in T cell receptor signaling. *Front Immunol, 3*, 197. doi:10.3389/fimmu.2012.00197

Wang, Y., Fouret, G., Bonafos, B., Blachnio-Zabielska, A., Leroy, T., Crouzier, D., . . . Feillet-Coudray, C. (2019). Long-term follow-up of muscle lipid accumulation, mitochondrial activity and oxidative stress and their relationship with impaired glucose homeostasis in high fat high fructose

diet-fed rats. *J Nutr Biochem, 64*, 182-197. doi:10.1016/j.jnutbio.2018.10.021

Washington, T. A., White, J. P., Davis, J. M., Wilson, L. B., Lowe, L. L., Sato, S., & Carson, J. A. (2011). Skeletal muscle mass recovery from atrophy in IL-6 knockout mice. *Acta Physiol (Oxf), 202*(4), 657-669. doi:10.1111/j.1748-1716.2011.02281.x

Woodworth-Hobbs, M. E., Perry, B. D., Rahnert, J. A., Hudson, M. B., Zheng, B., & Russ Price, S. (2017). Docosahexaenoic acid counteracts palmitate-induced endoplasmic reticulum stress in C2C12 myotubes: Impact on muscle atrophy. *Physiol Rep, 5*(23). doi:10.14814/phy2.13530

Wu, C., Tang, L., Ni, X., Xu, T., Fang, Q., Xu, L., . . . Sun, H. (2019). Salidroside Attenuates Denervation-Induced Skeletal Muscle Atrophy Through Negative Regulation of Pro-inflammatory Cytokine. *Front Physiol, 10*, 665. doi:10.3389/fphys.2019.00665

Wu, J., Liu, S., Fan, Z., Zhang, L., Tian, Y., & Yang, R. (2016). A novel and selective inhibitor of PKC zeta potently inhibits human breast cancer metastasis in vitro and in mice. *Tumour Biol, 37*(6), 8391-8401. doi:10.1007/s13277-015-4744-9

Yaffe, D. (1969). Cellular aspects of muscle differentiation in vitro. *Curr Top Dev Biol, 4*, 37-77. doi:10.1016/s0070-2153(08)60480-9

Yaffe, D., & Saxel, O. (1977). A myogenic cell line with altered serum requirements for differentiation. *Differentiation, 7*(3), 159-166. doi:10.1111/j.1432-0436.1977.tb01507.x

Yang, Y., Xu, Y., Li, W., Wang, G., Song, Y., Yang, G., . . . Ma, K. (2009). STAT3 induces muscle stem cell differentiation by interaction with myoD. *Cytokine, 46*(1), 137-141. doi:10.1016/j.cyto.2008.12.015

Yao, M., Fang, W., Smart, C., Hu, Q., Huang, S., Alvarez, N., . . . Cheng, N. (2019). CCR2 Chemokine Receptors Enhance Growth and Cell-Cycle Progression of Breast Cancer Cells through SRC and PKC Activation. *Mol Cancer Res, 17*(2), 604-617. doi:10.1158/1541-7786.MCR-18-0750

Yaspelkis, B. B., 3rd, Kvasha, I. A., & Figueroa, T. Y. (2009). High-fat feeding increases insulin receptor and IRS-1 coimmunoprecipitation with SOCS-3, IKKalpha/beta phosphorylation and decreases PI-3 kinase activity in muscle. *Am J Physiol Regul Integr Comp Physiol, 296*(6), R1709-1715. doi:10.1152/ajpregu.00117.2009

Zagani, R., El-Assaad, W., Gamache, I., & Teodoro, J. G. (2015). Inhibition of adipose triglyceride lipase (ATGL) by the putative tumor suppressor G0S2 or a small molecule inhibitor attenuates the growth of cancer cells. *Oncotarget, 6*(29), 28282-28295. doi:10.18632/oncotarget.5061

Zammit, P. S., Partridge, T. A., & Yablonka-Reuveni, Z. (2006). The skeletal muscle satellite cell: the stem cell that came in from the cold. *J Histochem Cytochem, 54*(11), 1177-1191. doi:10.1369/jhc.6R6995.2006

Zechner, R., Zimmermann, R., Eichmann, T. O., Kohlwein, S. D., Haemmerle, G., Lass, A., & Madeo, F. (2012). FAT SIGNALS--lipases and lipolysis in lipid metabolism and signaling. *Cell Metab, 15*(3), 279-291. doi:10.1016/j.cmet.2011.12.018

Zhang, G., Kazanietz, M. G., Blumberg, P. M., & Hurley, J. H. (1995). Crystal structure of the cys2 activator-binding domain of protein kinase C delta in complex with phorbol ester. *Cell, 81*(6), 917-924. doi:10.1016/0092-8674(95)90011-x

Zhang, L., Du, J., Hu, Z., Han, G., Delafontaine, P., Garcia, G., & Mitch, W. E. (2009). IL-6 and serum amyloid A synergy mediates angiotensin II-induced muscle wasting. *J Am Soc Nephrol, 20*(3), 604-612. doi:10.1681/ASN.2008060628

Zhang, M. Y., Zhang, W. J., & Medler, S. (2010). The continuum of hybrid IIX/IIB fibers in normal mouse muscles: MHC isoform proportions and spatial distribution within single fibers. *Am J Physiol Regul Integr Comp Physiol, 299*(6), R1582-1591. doi:10.1152/ajpregu.00402.2010

Zhang, Y., Yan, W., Collins, M. A., Bednar, F., Rakshit, S., Zetter, B. R., . . . di Magliano, M. P. (2013). Interleukin-6 is required for pancreatic cancer progression by promoting MAPK signaling activation and oxidative stress resistance. *Cancer Res, 73*(20), 6359-6374. doi:10.1158/0008-5472.CAN-13-1558-T

Zhu, X., Kny, M., Schmidt, F., Hahn, A., Wollersheim, T., Kleber, C., . . . Fielitz, J. (2017). Secreted Frizzled-Related Protein 2 and Inflammation-Induced Skeletal Muscle Atrophy. *Crit Care Med, 45*(2), e169-e183. doi:10.1097/CCM.0000000000002056

Zolotnik, I. A., Figueroa, T. Y., & Yaspelkis, B. B., 3rd. (2012). Insulin receptor and IRS-1 co-immunoprecipitation with SOCS-3, and IKKalpha/beta phosphorylation are increased in obese Zucker rat skeletal muscle. *Life Sci, 91*(15-16), 816-822. doi:10.1016/j.lfs.2012.08.038

CURRICULUM VITAE

JOSEPH EMIL RUPERT

EDUCATION

10/2020	Doctor of Philosophy earned at Indiana University-Purdue University Indianapolis
2013	Master of Science earned at Youngstown State University
2010	Bachelor of Science earned at Youngstown State University

PROFESSIONAL EXPERIENCE

2013-2014	Hourly Research Technician, Department of Anatomy and Cell Biology, Indiana University School of Medicine
2011-2013	Teaching Assistant, Department of Biological Sciences, Youngstown State University

HONORS & AWARDS

2016	3RD Place- Basic Science by Graduate Student. IU Simon Cancer Center Annual Research Day
2013	Who's Who Among Students In American Universities & Colleges
2013	Vitullo Travel Award

GRANTS & SCHOLARSHIPS

2017-2020	NIH 2017 T32 DK (Broxmeyer Hal, E.: Pelus Louis, M.) Regulation of Hematopoietic Cell Production
2013	The John C. Vitullo Travel Award ($500)
2012	Graduate Travel Grant, Youngstown State University ($800)
2012	Research Assistantship Award (RA), Youngstown State University ($1800)

PRESENTATIONS

Rupert JE, Bonetto A, Narasimhan A, O'Connell T, Koniaris LG, Zimmers TA. IL-6 trans-signaling among tumor, muscle and fat mediates pancreatic cancer cachexia. Department of Clinical and Biological Sciences, University of Turin. Turin, Italy: Dec 12, 2018.

Symposium: Terrestrial locomotion: where do we stand where are we going. Society for Integrative and Comparative Biology Annual Meeting, Austin, TX: Jan. 3, 2014

Analysis of myosin heavy chain isoforms in prehensile tails of Didelphid marsupials: muscle specializations for arboreal *versus* terrestrial locomotion. Texas Bio-Med Research Institute, 2012.

Rupert JE, Bonetto A, Narasimhan A, O'Connell T, Koniaris LG, Zimmers TA. IL-6 trans-signaling among tumor, muscle and fat mediates pancreatic cancer cachexia. 11th International SCWD Conference on Cachexia, Sarcopenia and Muscle Wasting. Maastricht, Netherlands: Dec 7-9, 2018.

Rupert JE, Jiang Y, Bonetto A, Koniaris LG, Zimmers TA. Understanding the Role of Tumor-Derived IL-6 in Muscle Wasting of Pancreatic Cancer Cachexia. 3RD Cancer Cachexia Conference, Washington, D.C.: Mar 23-25, 2016.

Rupert Joseph E, Yanlin, J, Bonetto A, Koniaris L, Zimmers T. Understanding the Role of IL-6 in Muscle Wasting of Pancreatic Cancer Cachexia. Poster Presentation: Advances in Skeletal Muscle Biology in Health and Disease Conference, Gainesville, FL: Jan 20-22, 2016.

Rupert Joseph E, Butcher MT. Prehensile tail use in didelphid marsupials: functional modifications for terrestrial species. Oral Presentation: Society for Integrative and Comparative Biology Annual Meeting, Austin, TX: Jan 3, 2014.

Rupert Joseph E, Butcher MT. Analysis of myosin heavy chain (MHC) isoforms in the prehensile tails of didelphid marsupials: functional differences in arboreal versus terrestrial opossums. *QUEST*, Youngstown State University; Youngstown, Ohio: April 2, 2013.

Rupert Joseph E, Butcher MT. Analysis of myosin heavy chain (MHC) isoforms in the prehensile tails of didelphid marsupials: functional differences in arboreal versus terrestrial opossums. Oral presentation: Society for Integrative and Comparative Biology Annual Meeting, San Francisco, CA: Jan. 5, 2013

Rupert Joseph E, Butcher MT. Analysis of myosin heavy chain isoforms in prehensile tails of didelphid marsupials: muscle specializations for arboreal versus terrestrial locomotion. Oral Presentation: QUEST, Youngstown State University; Youngstown, Ohio: April 3, 2012

ABSTRACTS

Polster NJ, Rupert JE, Young AR, Zimmers TA. Association between IL6R polymorphisms and cachexia phenotype in patients with pancreatic ductal adenocarcinoma. *Indiana Medical Student Program for Research and Scholarship Oral Presentations.* Indianapolis, IN. 2019.

Rupert JE, Bonetto A, Narasimhan A, Koniaris L, Zimmers TA. IL-6 trans-signaling amoung tumour, muscle, and fat mediates pancreatic cancer cachexia. *Journal of Cachexia, Sarcopenia and Muscle.* 11th International Conference on Cachexia, Sarcopenia and Muscle Wasting, Maastricht, The Netherlands. 2018.

Rupert JE, Au E**,** Bonetto A, Narasimhan A, Koniaris L, Zimmers TA. IL-6 trans-signaling amoung tumour, muscle, and fat mediates pancreatic cancer cachexia. *Journal of Cachexia, Sarcopenia and Muscle.* 4th Cancer Cachexia Conference, Philadelphia, PA. 2018.

Rupert JE, Jiang Y, Bonnetto A, Koniaris LG, Zimmers TA. Understanding the Role of Tumor-Derived IL-6 in Muscle Wasting of Pancreatic Cancer Cachexia. 2016 *3RD Cancer Cachexia Conference, Washington, D.C.*

Rupert JE, Zimmers TA. Tumor derived IL6 may promote skeletal muscle atrophy in Pancreatic Cancer. *2016 Advances in Skeletal Muscle Biology in Health and Disease Conference,* Gainesville, FL.

Rupert JE**,** Byron C, Condon K, Organ JM. Heirarchical analyses of bone and muscle structural, material, and metabolic properties improves our understanding of their integrated functions. *Am J Phys Anthropol.* 2014.

Rupert JE, Moriera A, Butcher MT. Analysis of myosin heavy chain (MHC) isoforms in the prehensile tails of didelphid marsupials: functional differences in arboreal versus terrestrial opossums. *Integr Comp Biol.* 53(suppl 1): E186.

Rupert JE, Butcher MT. Analysis of myosin heavy chain isoforms in prehensile tails of Didelphid marsupials: muscle specializations for arboreal *versus* terrestrial locomotion. *2012 QUEST,* YSU.

PUBLICATIONS

Rupert JE, Jengelley DH, Zimmers TA. In vitro, in vivo, and in silico methods for assessment of muscle size and muscle growth regulation. *Shock.* 53(5): 605-615. 2020.

Rupert JE, Koniaris LG, Zimmers TA. Multimodal action of Mas activation for systemic cancer cachexia therapy. *Cancer Res.* 79(4): 699-700. 2019.

Aguilar-Perez A, Pacheco-Costa R, Atkinson EG, Deosthale P, Davis HM, Essex AL, Dilley JE, Gomez L, Rupert JE, Zimmers TA, Thompson RJ, Allen MR, Plotkin LI. Age- and sex-dependent role of osteocytic pannexin1 on bone and muscle mass and strength. *Scientific Reports*. 9(3903). 2019.

Rupert J, Joll J, Elkhatib W, Organ J. Mouse hind limb skeletal muscle functional adaptation in a simulated fine branch arboreal habitat. *Anat Rec.* 301(3): 434-440. 2018.

Zimmers TA, Jiang Y, Wang M, Liang TW, Rupert JE, Au ED, Marino FE, Couch ME, Koniaris LG. Exogenous GDF11 induces cardiac and skeletal muscle dysfunction and wasting. *Basic Res Cardiol*. 2017 Sep;112(5):53. doi: 10.1007/s00395-017-0642-1.

Bonetto A, Rupert JE, Barreto R, Zimmers TA. The Colon-26 Carcinoma Tumor-bearing Mouse as a Model for the Study of Cancer Cachexia. *J Vis Exp*. 117. 2016.

Organ, J, Srisuwananukorn, A, Price, P, Joll, J, Biro, K, Rupert, JE, Chen, N, Avin, K, Moe, S, & Allen, M. Reduced skeletal muscle function is associated with decreased fiber cross-sectional area in the Cy/ rat model of progressive kidney disease*. Nephrol. Dial. Transplant. 31(2), 223-230.* 2015.

Rupert JE, Rose JA, Organ JM, Butcher MT. Forelimb muscle architecture and myosin isoform composition in the groundhog (*Marmota monax*). *J Exp Bio.* 2014.

Rupert JE, Moriera A, Cordero Schmidt E, VandeBerg JL, Rodriguez Herrera B, Butcher MT. Myosin heavy chain (MHC) isoform expression in the prehensile tails of didelphid marsupials: functional differences between arboreal and terrestrial opossums. *Anat Rec.* 2013.

TEACHING EXPERIENCE

Teaching assistant posts:
Youngstown State University, Labs Taught:

2012-13 Biol 3730: Human Physiology (Fall 2012 and Spring 2013)
AP 1551: Anatomy & Physiology (Fall 2012 and Spring 2013)

2011-12 Allied Health 1545: Anatomy & Physiology (Spring 2012)
AP 1552: Anatomy & Physiology II (Fall 2011 and Spring 2012)
AP 1551: Anatomy & Physiology I (Fall 2011)

PROFESSIONAL & PUBLIC SERVICE

Biological Sciences Group Leader

- YSU Crash Days (Oct. – Nov. 2012)

Mowhawk Elementary School

- Science Career Day (December 6, 2012)

PUBLIC DISSEMINATION OF RESEARCH

Print-digital media:
Telling *Tails*. By Ashley Luthern, *The Vindicator,* March 2013
http://www.vindy.com/news/2013/feb/26/telling-tails/

Student Success: In search of the Woolly Opossum. *YSU Update,* October 2012
http://www.ysunews.com/woolly-opossum-research-ysu-student-success/

GRADUATE & POSTDOCTORAL ADVISORS

Teresa A. Zimmers, Pre-doctoral Thesis Advisor, Dept. of Biochemistry; Dept. of Surgery, Indiana University School of Medicine

Thesis Committee Members:

Hal E. Broxmeyer, Dept. of Microbiology and Immunology, Indiana University School of Medicine

Lawrence A. Quilliam, Dept. of Biochemistry and Molecular Biology, Indiana University School of Medicine

Mark G. Goebl, Dept of Biochemistry and Molecular Biology, Indiana University School of Medicine

Thomas O'Connell, Dept of Department of Otolaryngology-Head and Neck Surgery, Indiana University School of Medicine